

PL-TR-95-2156

**STATISTICAL METHODOLOGY AND
ASSESSMENT OF SEISMIC EVENT
CHARACTERIZATION CAPABILITY**

**Mark D. Fisk
Henry L. Gray
Gary D. McCartor**

**Mission Research Corporation
735 State Street
P.O. Drawer 719
Santa Barbara, CA 93102**

31 October 1995

**Final Report
2 June 1993 – 2 September 1995**

19960320 078

Approved for public release; distribution unlimited



**PHILLIPS LABORATORY
Directorate of Geophysics
AIR FORCE MATERIEL COMMAND
HANSCOM AFB, MA 01731-3010**

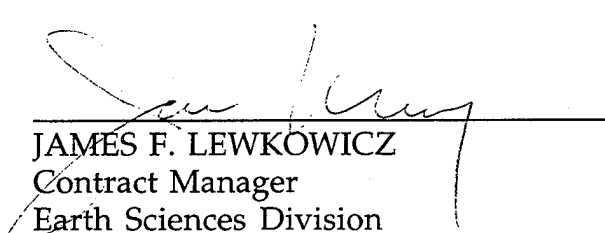
DTIC QUALITY INSPECTED 1

SPONSORED BY
Advanced Research Projects Agency (DoD)
Nuclear Monitoring Research Office
ARPA ORDER No. A-128

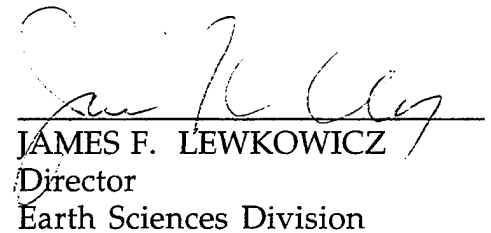
MONITORED BY
Phillips Laboratory
CONTRACT No. F19628-93-C-0117

The views and conclusions contained in this document are those of the authors and should not be interpreted as representing the official policies, either express or implied, of the Air Force or the U.S. Government.

This technical report has been reviewed and is approved for publication.



JAMES F. LEWKOWICZ
Contract Manager
Earth Sciences Division



JAMES F. LEWKOWICZ
Director
Earth Sciences Division

This report has been reviewed by the ESC Public Affairs Office (PA) and is releasable to the National Technical Information Service (NTIS).

Qualified requestors may obtain additional copies from the Defense Technical Information Center. All others should apply to the National Technical Information Service.

If your address has changed, or if you wish to be removed from the mailing list, or if the addressee is no longer employed by your organization, please notify PL/IM, 29 Randolph Road, Hanscom AFB, MA 01731-3010. This will assist us in maintaining a current mailing list.

Do not return copies of this report unless contractual obligations or notices on a specific document requires that it be returned.

REPORT DOCUMENTATION PAGE			<i>Form Approved</i> <i>OMB NO. 0704.0188</i>	
Public reporting burden for this collection of information is estimated to average 1 hour per response, including the time for reviewing instructions, searching existing data sources, gathering and maintaining the data needed, and completing and reviewing the collection of information. Send comments regarding this burden estimate or any other aspect of the collection of information, including suggestions for reducing this burden, to Washington Headquarters Services, Directorate for Information Operations and Reports, 1215 Jefferson Davis Highway, suite 1204, Arlington, VA 22202-4302, and to the Office of Management and Budget, Paperwork Reduction Project (0704-0188), Washington, DC 20503.				
1. AGENCY USE ONLY (Leave Blank)		2. REPORT DATE 31 Oct 1995	3. REPORT TYPE AND DATES COVERED Final Report 2 Jun 1993 to 2 Sep 1995	
4. TITLE AND SUBTITLE Statistical Methodology and Assessment of Seismic Event Characterization Capability			5. FUNDING NUMBERS PE62301E	
6. AUTHOR(s) Mark D. Fisk Henry L. Gray* Gary D. McCartor*			PR NM93 TA GM WU AL Contract F19628-93-C-0117	
7. PERFORMING ORGANIZATION NAME(S) AND ADDRESS(ES) Mission Research Corporation 735 State Street, P.O. Drawer 719 Santa Barbara, CA 93102-0719			8. PERFORMING ORGANIZATION REPORT NUMBER MRC-R-1509	
9. SPONSORING/MONITORING AGENCY NAME(S) AND ADDRESS(ES) Phillips Laboratory 29 Randolph Road Hanscom Air Force Base, MA 01731-3010 Contract Manager: James Lewkowicz/GPEH			10. SPONSORING/MONITORING AGENCY REPORT NUMBER PL-TR-95-2156	
11. SUPPLEMENTARY NOTES * Southern Methodist University, Dallas, TX				
12a. DISTRIBUTION/AVAILABILITY STATEMENT Approved for public release; distribution unlimited			12b. DISTRIBUTION CODE	
13. ABSTRACT (Maximum 200 words) This project has focused on developing and applying statistical methods to perform seismic event characterization/identification and on quantifying capabilities with regard to monitoring of a Comprehensive Test Ban. The report is divided into four separate but related sections. First, an automated procedure is described to categorize seismic events, based on multivariate analysis of features derived from seismic waveforms. The procedure is intended to aid CMR subscribers in focussing upon events of interest. Second, preliminary event identification results are presented for a seismic event which occurred on 5 January 1995 in the Southern Ural Mountains region. This was a shallow event which occurred in an area of low seismicity and near where several PNEs had been conducted. Third, various statistics are compiled regarding 1786 seismic events which occurred between 11 January 1995 and 12 February 1995 and were detected by a set of 30 GSETT-3 Alpha stations. The objective of this study is to determine how many events can be screened with high confidence as due to natural seismicity, based on teleseismic measures of depth, Ms:mb and location (offshore/onshore). Of the remaining events, the number with useful regional discriminants is quantified. Last, we evaluate the number of remaining ambiguous events lacking adequate event characterization data to identify them, based on the Alpha network which existed at the time of this study. Fourth, a fundamental problem is addressed of how to utilize multivariate discriminant data from a multi-station network in order to optimize the power of the outlier test for fixed false alarm rate. Analytic expressions for the power of three outlier tests are derived and a parametric study is presented in order to determine conditions for which a particular test is favored over the others.				
14. SUBJECT TERMS Seismic Event Characterization Comprehensive Test Ban Outlier Analysis Regional Discriminants GSETT-3 Alpha Network			15. NUMBER OF PAGES 90	
			16. PRICE CODE	
17. Security CLASSIFICATION OF REPORT UNCLASSIFIED	18. Security CLASSIFICATION OF THIS PAGE UNCLASSIFIED	19. Security CLASSIFICATION OF ABSTRACT UNCLASSIFIED	20. LIMITATION OF ABSTRACT SAR	

UNCLASSIFIED

SECURITY CLASSIFICATION OF THIS PAGE

CLASSIFIED BY:

DECLASSIFY ON:

SECURITY CLASSIFICATION OF THIS PAGE

UNCLASSIFIED

Table of Contents

Executive Summary	ix
Bibliography of Publications Sponsored by Contract	xii
1. A Statistical Procedure for Categorizing Seismic Events	1
1.1. Introduction	1
1.2. Overview of Technical Approach	3
1.2.1. Event Screening	3
1.2.2. Population Analysis	5
1.3. Definition of Event Categories	7
1.4. Examples of Event Categorization	8
1.4.1. Categorization Results for WMQ Events	11
1.4.2. Categorization Results for ARCESS Events	14
1.4.3. Categorization Results for KNB and MNV Events	16
1.5. Summary	19
2. Preliminary Identification Analysis of the 950105 Urals Event	20
2.1. Introduction	20
2.2. Data	21
2.2.1. Amplitude Ratios Prior to Applying Distance Corrections	22
2.2.2. Amplitude Ratios After Applying Distance Corrections	24
2.3. Categorization Results for the 950105 Event	28
2.4. Conclusions and Future Plans	28
3. Assessment of Current Event Characterization Capability using GSETT-3 Alpha	
Network Data	30
3.1. Introduction	30
3.2. GSETT-3 Data	31
3.2.1. Events Per Alpha Station	31
3.2.2. Events Versus Location and Location Uncertainty	33
3.2.3. Events Versus Depth and Detected Depth Phases	35
3.2.4. Events Versus Magnitude	37
3.2.5. Regional High-Frequency Amplitude Ratios	39
3.3. Utility of Event Characterization Parameters	51
3.4. Conclusions and Recommendations	55

4. Optimizing Multivariate Network Evidence for Outlier Detection	57
4.1. Introduction	57
4.2. Technical Approach	57
4.3. Parametric Power Comparison	59
4.4. Conclusions and Recommendations	70

List of Figures

1. Schematic of first-cut event screening.	4
2. Relationship of Categories 3-10 to the cumulative probability of the log likelihood ratio when the null hypothesis is true.	9
3. Locations of ARCESS, CDSN station WMQ, LNN stations KNB and MNV, and the seismic events used in this study.	10
4. Locations of CDSN station WMQ, 16 nuclear explosions in Kazakhstan, the 880929 nuclear explosion at Lop Nor and 23 earthquakes in China and nearby countries.	11
5. Distance-Corrected Pn/Lg in nine frequency bands for 23 earthquakes and 17 nuclear explosions recorded by WMQ.	12
6. Categorization results for events recorded by station WMQ.	13
7. Outlier test results for events recorded by station WMQ.	13
8. Locations of the ARCESS array, 3 nuclear explosions on Novaya Zemlya, 5 Spitsbergen and 24 Steigen earthquakes.	14
9. Distance-corrected Pn/Sn measurements in six frequency bands for events recorded by ARCESS.	15
10. Categorization results for events recorded by ARCESS.	15
11. Locations of LNN stations KNB and MNV (among others) relative to NTS. On the left is an enlarged map of NTS showing epicenters of the nuclear explosions and earthquakes.	16
12. Pn/Lg measurements in the 6-8 Hz band versus ML(coda) for events recorded by KNB.	17
13. Pn/Lg measurements in the 6-8 Hz band versus ML(coda) for events recorded by MNV.	18
14. Categorization results for events recorded by KNB and MNV.	18
15. Locations of seismic stations, arrays and events used in our analysis of the 950105 Southern Urals event (ORID=273228).	21
16. Uncorrected Pn/Lg in the 6-8 Hz band versus distance for earthquakes, nuclear explosions, and the 950105 Urals event.	23
17. Uncorrected Pn/Sn in the 6-8 Hz band versus distance for earthquakes, nuclear explosions, and the 950105 Urals event.	23

18. Uncorrected Pn/Sn measurements in nine frequency bands for 3 Novaya Zemlya nuclear explosions, 24 Steigen earthquakes and the 950105 event recorded by ARCESS.	24
19. Uncorrected Pn/Lg measurements in eight frequency bands for the 950105 event recorded by ARU and OBN and earthquakes and nuclear explosions recorded by WMQ.	25
20. Same as Figure 19, but for uncorrected Pn/Sn.	25
21. Distance-corrected Pn/Sn values in nine frequency bands for events recorded by ARCESS.	26
22. Distance-corrected Pn/Lg measurements in eight frequency bands for the 950105 event recorded by OBN and earthquakes and nuclear explosions recorded by WMQ.	27
23. Same as Figure 22, but for distance-corrected Pn/Sn.	27
24. Categorization results for the 950105 event, 29 earthquakes in the Steigen and Spitsbergen regions, and 3 nuclear explosions at the Novaya Zemlya test site.	29
25. Locations of 30 Alpha stations and 1786 seismic events recorded by them between 11 January and 12 February 1995.	31
26. Number of overall and regional events per Alpha station.	33
27. Distribution of events versus 90% confidence location error ellipse area.	34
28. Scatter plot of 90% confidence location error ellipse area versus mb.	34
29. Distribution of events vs. hypocentral depth estimate.	35
30. Distribution of events vs. number of depth phases per event.	36
31. Cumulative distribution of events, with or without one or more detected depth phases, versus the upper bound of the 95% confidence interval for depth.	36
32. Distributions of events versus mb, M_S and M_L	37
33. Scatter plot of M_S versus mb.	38
34. Scatter plot of M_L versus mb.	38
35. Number of regional events per Alpha station.	40
36. Distribution of regional events versus the number of stations per event.	41
37. Pn/Sn in 4 frequency bands versus Alpha station. Circles indicate $SNR < 2$ for either numerator or denominator, while asterisks indicate $SNR > 2$ for both numerator and denominator.	42
38. Same as Figure 37, but for Pn/Lg.	43

39. Same as Figure 37, but for Pg/Sn.	44
40. Same as Figure 37, but for Pg/Lg.	45
41. Pn/Sn in 4 frequency bands versus distance. Markers are defined as in Figure 37. ..	46
42. Same as Figure 41, but for Pn/Lg.	47
43. Seismic waveforms for a Gulf of California event which was recorded by the Pinedale array. Large amplitude noise spikes were present on two of the channels.	49
44. Sn travel times versus distance (stars) based on phase picks by seismic analysts for the one-month data set. Also plotted are the IASPEI91 Sn travel time curve (solid line) and the theoretical velocity window (dashed lines) used to make automated Sn measurements.	50
45. Distribution of events with various available discriminants.....	52
46. Locations of events which can be classified as deep, offshore, with $mb-M_S < 1.2$, or with at least one high-frequency regional amplitude ratio. Markers are coded by category.	53
47. Locations of events for which none of the considered teleseismic and regional discriminants are available.	54
48. Power comparison of the three tests for $\sigma_1 = \sigma_2 = 1$	61
49. Power comparison of the three tests for $\sigma_1 = 1$ and $\sigma_2 = 2$	62
50. Power of Tests 1 (solid), 2 (dashed) and 3 (dotted) versus ρ for $\sigma_1 = \sigma_2 = 1$ and various values of $\Delta\mu_1$ and $\Delta\mu_2$ from 0 to 3.	63
51. Same as Figure 50, except that $\sigma_2 = 2$	64
52. Difference in the power of Test 2 and Test 1 versus correlation for various values of $\Delta\mu_1$ and $\Delta\mu_2$ from 0 to 4.	65
53. Difference in the power of Test 3 and Test 1 versus correlation for various values of $\Delta\mu_1$ and $\Delta\mu_2$ from 0 to 4.	66
54. Power of Tests 2 (solid), 4 (dashed) and 5 (dotted) versus ρ for $\sigma_1 = 1$, $\sigma_2 = 2$ and various values of $\Delta\mu_1$ and $\Delta\mu_2$ from 0 to 3.	68
55. Difference in the power of Test 4 and Test 2 versus correlation for various values of $\Delta\mu_1$ and $\Delta\mu_2$ from 0 to 4.	69
56. Difference in the power of Test 5 and Test 2 versus correlation for various values of $\Delta\mu_1$ and $\Delta\mu_2$ from 0 to 4.	70

List of Tables

1. Summary of Event Category Definitions.	8
2. Summary of seismic data sets used in this study.	10
3. Summary of seismic data sets used in the analysis of the 950105 Urals Event.	22
4. Alpha station names, operation start dates, locations, and types.	32
5. Description of regional phase amplitude measurements.	39

Executive Summary

This effort has focused on developing and applying statistical methods to perform seismic event characterization/identification and on quantifying identification capabilities with regard to seismic monitoring of a Comprehensive Test Ban Treaty (CTBT). Difficulties associated with seismic event identification, within the context of CTBT verification, include the fact that small events are seen at fewer stations or arrays, possibly, at only a single station. In addition, there are many thousands of competing earthquakes, mining blasts and other mining-induced events worldwide per year. Thus, robust automated methods are needed to utilize potentially limited information and to reduce the workload of human analysts to a manageable level.

While useful discriminants such as $M_S:mb$ and determination of focal depth can be measured and provide robust discrimination, typically for large events ($mb > 4.5$) seen at teleseismic distances by many stations, useful measurements of these discriminants cannot currently be obtained for small events seen only at regional distances by a small number of stations. Furthermore, seismic signals seen at regional distances from small sources are generally quite complicated and exhibit dramatic dependence on regional geophysics; even the most promising regional discriminants can vary widely in different regions. Hence, region-specific information regarding seismic discriminants is vital in distinguishing nuclear explosions from other events. Unfortunately, relevant ground-truth data, particularly for small underground nuclear explosions, do not exist for most regions. In addition, it has yet to be shown that a discrimination rule, established in a region for which data exist, can be transported effectively to a new region. Thus, for many cases, seismic event identification, within the context of CTBT or NPT (Non-Proliferation Treaty) monitoring, is a problem of identifying unusual events, i.e., outliers.

This report is divided into four separate but related sections. In Section 1, we describe a technical approach to categorize seismic events with these and other considerations in mind. Our objective is to provide an automated procedure to categorize events, based on multivariate analysis of features derived from seismic waveforms, and to make this information available in a database at the Center for Monitoring Research (CMR). Subscribers will be able to obtain this information, to aid in focussing upon events of particular interest.

Since there are only a small number of mining blasts that occur annually above magnitude 3, our primary concern for monitoring above this threshold is to be able to distinguish nuclear explosions from earthquakes. Thus, we focus on this case here. Monitoring below this threshold poses greater difficulty and will be addressed in a subsequent report under a new ARPA contract.

We describe an approach which first determines those events that are of natural seismic origin, based on confidence intervals for depth, location (offshore versus onshore) and $M_S:mb$. This analysis applies to only those events for which these parameters can be estimated, currently those observed at teleseismic distances by many stations. Further analysis is then performed, using a multivariate population (i.e., outlier) analysis for remaining regional events. The outlier method has sufficient generality to utilize any combination of teleseismic and regional discriminants seen at single or multiple stations. The procedure may be fully automated to categorize events and to test all appropriate assumptions to ensure validity of the results. Fisk et al. (1993, 1994) describe the methodology in detail and provide numerous results of applications to seismic data.

Although the method can be used to perform a hypothesis test with a controlled false alarm rate (e.g., Fisk et al., 1994), our focus here is to use the population analysis to categorize events rather than providing a "yes/no" decision. We define event categories based on the discriminant analysis described below. Categories are intentionally defined in a non-judgemental manner, but with a statistically rigorous interpretation. We present examples of the categorization procedure to regional data sets consisting of earthquakes and underground nuclear explosions recorded by the ARCESS array, CDSN station WMQ, and LNN stations KNB and MNV.

In Section 2, we present preliminary event identification results for a seismic event which occurred on 5 January 1995 in the Southern Ural Mountains region. This was a shallow event which occurred in an area of low seismicity and near where several PNEs had been conducted. Of further interest was the fact that its relatively small value of $M_S:mb$ was considered inconsistent with identification as a shallow earthquake. A press release by the Moscow ITAR-TASS World Service, 6 January 1995, reported a statement by the Russian Federation's State Technical Inspectorate that this event was a tectonic shock at Pit Number 2 of the Silvinit Joint-Stock Company, caused by an earthquake with its epicenter near the settlement of Chashkino in Perm Oblast. The announcement also indicates that the tectonic shock led to the destruction of ventilation systems at the mine and to considerable emissions of explosive gases - methane and hydrogen - which subsequently ignited and exploded.

The objective of our analysis is to independently assess the identification of this event by comparing its seismic data, recorded by the ARCESS and KVAR arrays and stations ARU and OBN, to that of previous earthquakes and nuclear explosions. Since the 950105 event had a magnitude of mb 4.35, considerably larger than would be produced by a large mining blast, we focus here on characterizing this event as either an earthquake, a nuclear explosion or neither. (Walter, 1995, and others have explicitly considered other alternatives such as a mine collapse.)

In Section 3, we compile various statistics regarding 1786 seismic events which occurred between 11 January 1995 and 12 February 1995 and were detected by a set of 30 Alpha stations as part of GSETT-3 (Group of Scientific Experts Technical Test-3). Seismic data from these stations were transmitted to the CMR where the records were analyzed. The objective of this study is to assess the numbers and characteristics of events that can be expected to be observed by the Alpha stations during a given period, including the availability and utility of event characterization parameters that can be used to identify them. High-frequency regional phase amplitudes and M_S were computed for the events during this period, as well as location, depth and mb parameters.

We examine how many events can be screened with high confidence as due to natural seismicity, based on teleseismic measures of depth, location and M_S :mb. Of the remaining events, we examine how many have useful regional discriminants such that they could potentially be identified, considering primarily high-frequency regional P/Sn and P/Lg amplitude ratios. We also assess their utility with respect to signal-to-noise ratios. Last, we evaluate the number of remaining ambiguous events lacking adequate event characterization data to identify them, based on the Alpha network which existed at the time of this study.

In Section 4, we address a fundamental problem of how to utilize multivariate discriminant data from a multi-station network in order to optimize the power of the outlier test for fixed false alarm rate. In general, there are numerous types of regional measurements that can be used as discriminants, which may be available at multiple (e.g., 2 to 5) Alpha stations and it is not clear from the outset how to best combine this information in a test for outliers. We present three approaches to this problem. The first is to simply insert all available features that are thought to discriminate into the likelihood ratio. The second is to perform an optimal weighting of some or all of the discriminants first and then insert the weighted combinations into the likelihood ratio. The third is to perform separate tests, based on the likelihood ratio and subsets of discriminants, calling an event an outlier if it is found to be an outlier by any of the individual tests. The significance levels of the individual tests, in this case, must be appropriately modified to maintain the overall false alarm rate of the combined results.

We derive analytic expressions for the power of each of these three tests. We then present a parametric study in which the power of the three tests are compared in order to determine conditions for which a particular test is favored over the others. Last, we provide some conclusions and recommendations for operational application to seismic monitoring.

Bibliography of Publications Sponsored by Contract

- Fisk, M.D., H.L. Gray and G.D. McCartor (1995). Regional event discrimination without transporting thresholds, submitted to *Bull. Seis. Soc. Am.*
- Fisk, M.D., H.L. Gray and G.D. McCartor (1995). Statistical Framework for Seismic Event Identification and Preliminary Assessment of Seismic CTBT Monitoring Capability, Proceedings of the *17th Annual Seismic Research Symposium*, 12-15 September 1995, Scottsdale, AZ, PL-TR-95-2108, Phillips Laboratory, Hanscom AFB, MA.
- Fisk, M.D., H.L. Gray and G.D. McCartor (1995). Preliminary Look at the Event Identification Problem through Analysis of GSETT-3 Data, Proceedings of the *ARPA CTBT Monitoring Technologies Conference*, 15-18 May 1995, Chantilly, VA.
- Fisk, M.D. (1994). Identification and Event Characterization - Getting Down to the Outliers, Proceedings of the *ARPA CTBT Monitoring Technologies Conference*, 26-29 September 1994, San Diego, CA.
- Fisk, M.D., H.L. Gray and G.D. McCartor (1995). Preliminary Assessment of Seismic CTBT/NPT Monitoring Capability, Proceedings of the *16th Annual Seismic Research Symposium*, 7-9 September 1994, Thornwood, NY, PL-TR-94-2217, Phillips Laboratory, Hanscom AFB, MA. **ADA284667**
- Fisk, M.D., H.L. Gray and G.D. McCartor (1994). Preliminary Assessment of Seismic CTBT/NPT Monitoring Capability, PL-TR-94-2300, Phillips Laboratory, Hanscom AFB, MA. **ADA293188**
- Ryall, A.S., D.R. Baumgardt, M.D. Fisk and F. Riviere-Barbier (1994). Resolving Regional Discrimination Problems: Some Case Histories, Proceedings of the *NATO Conference on Disarmament*, Lisbon, Portugal, December, 1994.

1. A Statistical Procedure for Categorizing Seismic Events

1.1. Introduction

Objectives for an international CTBT (Comprehensive Test Ban Treaty) monitoring system, stated in the United States Working Paper for the Committee on Disarmament (May 18, 1994), are detection and identification of nuclear explosions down to a few kilotons or less. Difficulties associated with seismic event identification down to this level include the fact that small events are seen at fewer stations or arrays, possibly, at only a single station. In addition, there are many thousands of competing earthquakes, mining blasts and other mining-induced events worldwide per year (Ringdal, 1984; Lilwall and Douglas, 1985). While useful discriminants such as M_s - m_b and determination of focal depth can be measured and provide robust discrimination, typically for large events ($m_b > 4.5$) seen at teleseismic distances by many stations (e.g., Blandford et al., 1992), useful measurements of these discriminants cannot be obtained currently for small events seen only at regional distances by a small number of stations. Thus, robust automated methods are needed to utilize potentially limited information and to reduce the workload of human analysts to a manageable level.

Furthermore, seismic signals seen at regional distances from small sources are generally quite complicated and exhibit dramatic dependence on regional geophysics; even the most promising regional discriminants can vary widely in different regions (Fisk et al., 1994). Hence, region-specific information regarding seismic discriminants is vital in distinguishing nuclear explosions from other events. Unfortunately, relevant ground-truth data, particularly for small underground nuclear explosions, do not exist for most regions. In addition, it has yet to be shown that a discrimination rule, established in a region for which data exist, can be transported effectively to a new region. Thus, in most cases, seismic event identification, within the context of CTBT or NPT (Non-Proliferation Treaty) monitoring, is a problem of identifying unusual events, i.e., outliers.

Here we describe a technical approach to categorize seismic events with these and other considerations in mind. Our objective is to provide an automated procedure to categorize events, based on multivariate analysis of features derived from seismic waveforms, and to make this information available in a database at the Center for Monitoring Research (CMR). Subscribers will be able to obtain this information, to aid in focussing upon events of particular interest.

Since there are only a small number of mining blasts that occur annually above magnitude 3, our primary concern for monitoring above this threshold is to be able to distinguish nuclear explosions from earthquakes. Thus, we focus on this case here. Monitoring below this threshold poses greater difficulty and will be addressed in a subsequent report.

In Section 1.2, we describe our approach which first determines those events that are of natural seismic origin, based on their depth, location and M_s - m_b . This analysis applies to only those events for which these parameters can be estimated, currently those observed at teleseismic distances by many stations. Further analysis is then performed, using a multivariate statistical method for outlier detection, on those events which cannot be determined to be of natural seismic origin based on depth, location and M_s - m_b . The outlier method has sufficient generality to utilize any combination of teleseismic and regional discriminants seen at single or multiple stations. The procedure may be fully automated to categorize events and to test all appropriate assumptions to ensure validity of the results. Fisk et al. (1993, 1994) describe the methodology in detail and provide numerous results of applications to seismic data. Gray et al. (1994) have extended the methodology to treat data values which are commonly missing due to a variety of physical causes.

The method can be used to perform a hypothesis test, with a controlled false alarm rate, as to whether an event is an outlier or not. Fisk et al. (1994) applied this approach to seismic events in diverse geological regions, recorded by the ARCESS and GERESS arrays in Norway and Germany, CDSN (Chinese Digital Seismic Network) station WMQ in China, and LNN (Livermore NTS Network) stations KNB and MNV in the western U.S. Results show that useful monitoring can be performed with the outlier-detection approach, currently down to magnitude 3, for regions that are well-covered by at least one seismic station or array. Overall, 264 of 290 (91%) explosions were identified as outliers and there were 3 false alarms out of 158 earthquakes (1.9%), slightly higher than the target rate of 1%. In addition to the diversity of the regions, these results were obtained for events with a wide range of epicentral distances and magnitudes.

Although the method can be used to perform a hypothesis test, our focus here is to use the outlier method to categorize events rather than providing a “yes/no” decision. In Section 1.3, we define event categories based on the discriminant analysis described in Section 1.2. Categories are intentionally defined in a non-judgemental manner, but with a statistically rigorous interpretation. In Section 1.4, we describe the data sets used and present examples of the categorization procedure to regional data sets of earthquakes and underground nuclear explosions recorded by the ARCESS array, CDSN station WMQ, and LNN stations KNB and MNV.

1.2. Overview of Technical Approach

Here we describe our approach which is divided into two distinct steps. The objective of the first step is to screen large events of natural seismicity, based on the context in which the event occurred, namely, event depth and location. We also use M_s - m_b in this step to screen earthquakes for which long-period (20 second) surface waves and teleseismic P waves are measured. Events that are determined to be of natural seismicity at a particular confidence level are not processed further. The objective of the second step is to categorize the remaining events using a multivariate statistical outlier method (or population analysis) which measures how similar or different the event being tested is to other events seen by the same set of stations or arrays. Details of these steps are presented in the remainder of this section.

1.2.1. Event Screening

The analysis in this step is based on the physical argument that events that are deep (e.g., deeper than 10 km) cannot be of man-made origin. M_s - m_b provides a robust indicator of earthquakes, provided they are not too deep, for events above m_b 4.5. Thus, this analysis identifies natural events that are either deep or shallow but with M_s - m_b indicating an earthquake. Events located offshore are also screened and can be investigated more reliably using hydroacoustic techniques. Since there are uncertainties in these measurements, the thresholds in this screening process are set conservatively to maintain a high level of confidence, so as not to discard events of possible man-made origin from further processing.

Figure 1 illustrates this screening process. Event parameters required to perform the analysis steps will be retrieved from REB (Reviewed Event Bulletin) database at the CMR. These parameters will include an estimate of event depth and parameters to compute its confidence interval, the number of depth phases (e.g., pP) detected, an estimate of epicentral location and parameters to compute its error ellipse, and measurements of M_s and m_b . (Once available, hydroacoustic parameters will also be retrieved for offshore events.) Parameters such as signal-to-noise (SNR), the number of reporting stations, and quadrant coverage will also be retrieved from the database to assess the quality of information. The analysis then proceeds in the following stages in terms of these parameters, provided they could be measured and are available in the database.

A) Depth Analysis. The first step is to determine whether the entire 95% confidence interval for depth is deeper than 10 km. If it is and at least one depth phase (e.g., pP) was detected, the event is categorized as a deep natural event. If these criteria are not met, the event is processed further. (Differences in P and S travel times, once computed by the CMR, may also be used to better constrain focal depth.)

B) Location Analysis. The second step is to determine whether the 95% confidence error ellipse of epicentral location is entirely onshore, entirely offshore or overlapping. If the error ellipse is entirely offshore and no hydroacoustic bubble pulse is detected, the event is categorized as a natural offshore event. If the error ellipse is either entirely or partially offshore and a bubble pulse is detected, the event is categorized as a offshore explosion of unknown (i.e., chemical or nuclear) source. Remaining events are processed further.

B) Ms-mb Analysis. The third step is to assess whether the 99% Ms-mb confidence interval is entirely outside the nuclear explosion population, based on previous teleseismic recordings of known nuclear explosions. Events must also satisfy the conditions that SNR of the long period surface waves and the teleseismic P waves are both greater than 4 and that the event was recorded by stations in all four quadrants. Events which satisfy these criteria are categorized as earthquakes. The remainder are processed further.

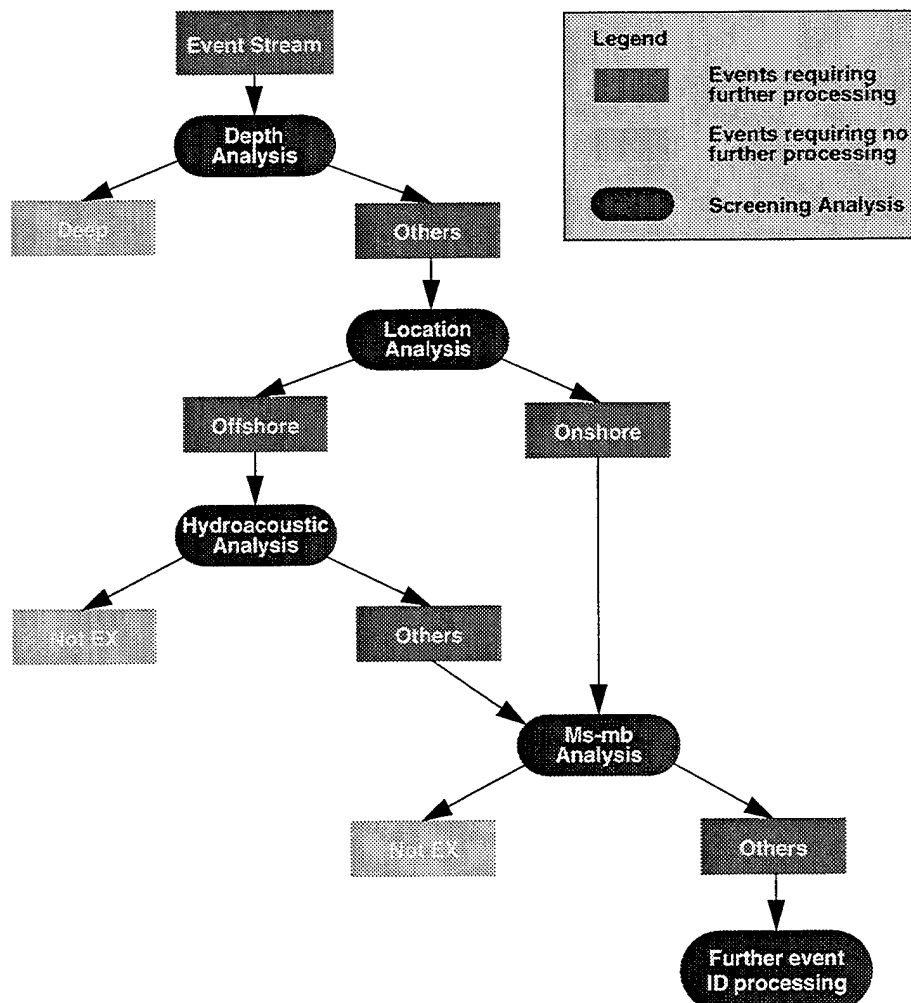


Figure 1. Schematic of first-cut event screening.

Note that the criteria stated above in terms of confidence levels, SNR thresholds and quadrant coverage of reporting stations are currently set with very conservative values so as to categorize natural events with very high confidence, while performing further analysis on remaining events. Criteria in terms of these parameters can be modified as necessary or desired.

1.2.2. Population Analysis

Due to current limitations in estimating depth, location and M_s - m_b for events below m_b 4.5, the remaining events will be predominantly small. (There will likely also be some large events which are not necessarily deep, not necessarily offshore, and lacking high confidence evidence regarding M_s - m_b .) Analysis of the remaining events will thus be based, at least in part, on high-frequency regional discriminants which include P_n/L_g and P_n/S_n . Due to regional variations of these discriminants and the lack of calibration data for nuclear explosions in most regions, we have adopted an outlier procedure to characterize events observed in various regions.

In the population (i.e., outlier) analysis, an event being tested is compared to other events seen at the same set of stations or arrays. To make a meaningful comparison, the new event is compared to events seen in the same region (defined by distance and azimuth relative to the station) when high-frequency regional discriminants are used. In most practical situations, we will not know the identifications of these events, a priori. Thus, an assumption is made that the number of new nuclear tests in a region will be relatively small compared to the number of earthquakes, mining blasts or mine tremors. If this assumption fails, i.e., if a region is aseismic and with no mining activity, then any new event would be suspicious, warranting further investigation. Since there are only a small number of mining blasts that occur annually above m_b 3, our primary concern for monitoring above this threshold is to distinguish nuclear explosions from earthquakes.

A standard set of discriminants is used, unless we have information about particular ones that work best for a given region. For the examples given in Section 1.4, we focus on P_n/L_g and P_n/S_n in the 3-5, 4-6, 5-7 and 6-8 Hz bands, provided measurements are available for the events. In general, the outlier method can rigorously include any discrete or continuous discriminant. Regional discriminants are corrected for attenuation as functions of type, distance and frequency.

The likelihood ratio is then computed for each event and categorized in terms of its value relative to the distribution of the likelihood ratio for the remaining events. (Technical details of the outlier test and previous applications are provided by Baek et al., 1992; Fisk et al., 1993, 1994; Fisk and Gray, 1993; Fisk, 1993.)

The likelihood ratio is given by

$$\lambda = \frac{\max L(\text{parameters} \mid \text{data}; \text{under null hypothesis})}{\max L(\text{parameters} \mid \text{data}; \text{under alternative hypothesis})},$$

where the numerator is computed under the null hypothesis being tested, given the data, and the denominator is computed under the alternative hypothesis. For the outlier test, the null hypothesis is that the event being tested belongs to the same population as the remainder of the events. The alternative hypothesis is that it is not a member. Since the true parameters (e.g., the mean and covariance matrix of the discriminants) of the likelihood functions are unknown, maximum likelihood estimates are computed from the data, subject to the particular hypothesis, and inserted into the likelihood functions. This yields the ratio of maximized likelihoods. The resulting expression for λ combines multivariate discriminant data for the event being tested and the reference events into a univariate expression. This provides a straightforward metric with which to perform a hypothesis test, to rank and/or categorize events.

Small values of λ indicate that the null hypothesis should be rejected. To quantify what is meant by “small,” the distribution of λ is needed. Under the assumption that the discriminants are multivariate normal, the distribution of λ may be obtained in closed form in terms of Hotelling’s T^2 -distribution or, equivalently, the F-distribution. In general, the distribution of λ is quite complicated, often with no closed form expression, depending on the multivariate discriminant distribution. To estimate it empirically under more general assumptions, we use the bootstrap technique (Efron, 1979) to generate random samples from the distribution of discriminants for the reference events, and insert bootstrapped data in the likelihood ratio for many samples. From this distribution of λ , a threshold, λ_α , may be set so that the test has a specified false alarm rate. That is, λ_α is set such that $P[\lambda \leq \lambda_\alpha \mid H_0] = \alpha$, where α is the significance level. Events whose likelihood ratio are less than λ_α are considered outliers at the specified significance level.

To formulate the results in terms of event categories rather than providing a rigid “yes/no” judgement, we define the categories in terms of thresholds for various significance levels. That is, we define the categories in terms of a range of probabilities, based on the distribution of λ , that an earthquake in a particular region would fall in a given category. Thus an event is placed in the i th category if its value of the likelihood ratio, λ_0 , satisfies $\lambda_{\alpha_{i+1}} < \lambda_0 \leq \lambda_{\alpha_i}$, where λ_{α_i} is set such that $P[\lambda \leq \lambda_{\alpha_i} \mid H_0] = \alpha_i$. Equivalently, an event falls in the i th category if $\alpha_{i+1} < P_{\lambda_0} \leq \alpha_i$, where $P_{\lambda_0} = P[\lambda \leq \lambda_0 \mid H_0]$ is the probability that an earthquake would have a value of λ less than the value for the event being tested. If an event falls in a category corresponding to a small value of α_i , the probability that this event is an earthquake is likewise small. In Section 1.3 we define event categories in terms of the α_i and provide further interpretation.

Note that if the value of the likelihood ratio for an event being tested is one, discriminant values for this event are identical to the sample discriminant means based on the other events. Thus, in this case, the event being tested is entirely consistent with the remaining population. Any departure of the discriminant values from the sample means leads to smaller values of λ . The likelihood ratio does not differentiate between events that have abnormally small versus large discriminant values. It is a measure of the absolute distance of the discriminant values for the new event from the means, based on the other events, as compared to the covariance matrix. This allows for cases in which an event could rightfully be called an outlier, but with discriminant values that are even more inconsistent with explosions than with earthquakes. While it is useful to flag such peculiar events for analyst review, this could lead to confusion in an automated setting. To alleviate potential confusion, we define in the following section a category which corresponds to events for which all discriminant values are on the side of the discriminant means, based on the remaining events, away from values for explosions.

1.3. Definition of Event Categories

Based on the approach just described, we now define ten event categories. Category 1 corresponds to events which are determined to be of natural seismic origin based on depth and detection of at least one depth phase, location and lack of a hydroacoustic bubble pulse (for events offshore), and/or Ms-mb. Category 2 is defined by events whose Pn/Lg and Pn/Sn values are all less than the means, based on the reference events. Categories 3-10 are defined in terms of probabilities, α_i , which set the criteria $\lambda_{\alpha_{i+1}} < \lambda \leq \lambda_{\alpha_i}$. The probability that an event would fall in the i th category if it was an earthquake is $\text{Prob}[i] = P[\lambda_{\alpha_{i+1}} < \lambda \leq \lambda_{\alpha_i} | H_0] = \alpha_i - \alpha_{i+1}$. (Note that for a fixed set of α_i , the λ_{α_i} depend on the multivariate distribution of the discriminants for events in various regions, as well as on the sample size of reference events. The outlier methodology automatically adapts the category thresholds to the quality and quantity of data in a given region to maintain a rigorous interpretation in terms of probabilities that an earthquake fall in a particular category.) Table 1 summarizes definitions of the event categories.

Figure 2 shows how Categories 3-10 are defined in terms of the cumulative distribution function (cdf) of the log likelihood ratio, under the null hypothesis that the event being tested belongs to the same group as the reference events. The categories are defined by the lines which intersect the cdf at particular values, namely, 0.5, 0.1, 0.01, 0.001, 0.0001, 0.00001, 0.000001. Category 3, for example, contains 50% of the earthquakes which occur in a given region and are also the most typical of the events recorded there. Events that fall in the other categories are progressively less consistent with the earthquake population in the region. Events that fall in Category 10, for example, have a probability less than or equal to 0.000001 of being an earthquake in this region.

Table 1. Summary of Event Category Definitions.

Category	Description
Category 1:	Very high confidence natural event (based on event context and Ms-mb)
Category 1(a)	• 95% depth confidence interval > 5 km and depth phase pP detected
Category 1(b)	• 95% location error ellipse entirely offshore and no bubble pulse detected
Category 1(c)	• 99% Ms-mb confidence interval is entirely outside explosion population
Category 2	Events with Pn/Lg & Pn/Sn < means, based on the remaining events in the region
Category 3	$0.5 < P_{\lambda_0} \leq 1.0$; Prob = 0.5 that an earthquake will fall in this category
Category 4	$0.1 < P_{\lambda_0} \leq 0.5$; Prob = 0.4 that an earthquake will fall in this category
Category 5	$0.01 < P_{\lambda_0} \leq 0.1$; Prob = 0.09 that an earthquake will fall in this category
Category 6	$0.001 < P_{\lambda_0} \leq 0.01$; Prob = 0.009 that an earthquake will fall in this category
Category 7	$0.0001 < P_{\lambda_0} \leq 0.001$; Prob = 0.0009 that an earthquake will fall in this category
Category 8	$0.00001 < P_{\lambda_0} \leq 0.0001$; Prob = 0.00009 that an earthquake will fall in this category
Category 9	$0.000001 < P_{\lambda_0} \leq 0.000001$; Prob = 0.000009 that an earthquake will fall in this category
Category 10	$P_{\lambda_0} \leq 0.000001$; Prob = 0.000001 that an earthquake will fall in this category

1.4. Examples of Event Categorization

To illustrate the categorization procedure, we applied it to earthquakes and nuclear explosions recorded by the ARCESS array, CDSN station WMQ, and LNN stations KNB and MNV. ARCESS events include 24 earthquakes near Steigen, Norway, 5 earthquakes near Spitsbergen, and 3 underground nuclear explosions at the Novaya Zemlya test site. WMQ events include 23 earthquakes in China and nearby countries, 16 nuclear explosions in Kazakhstan, and 1 nuclear explosion at the Lop Nor test site in China. Data for these events were provided by Baumgardt (1993). Patton and Walter (1994) also provided us with seismic data from stations KNB and MNV for a total of 76 earthquakes, 141 nuclear explosions, and 1 contained 1 kt chemical explosion at NTS. The chemical explosion was the September 1993 Non-Proliferation Experiment (NPE). Due to SNR limitations for some events, Pn/Lg measurements were computed for 59 earthquakes and 89 explosions of those detected by KNB. Similar measurements were computed for 37 earthquakes and 78 explosions of those detected by MNV.

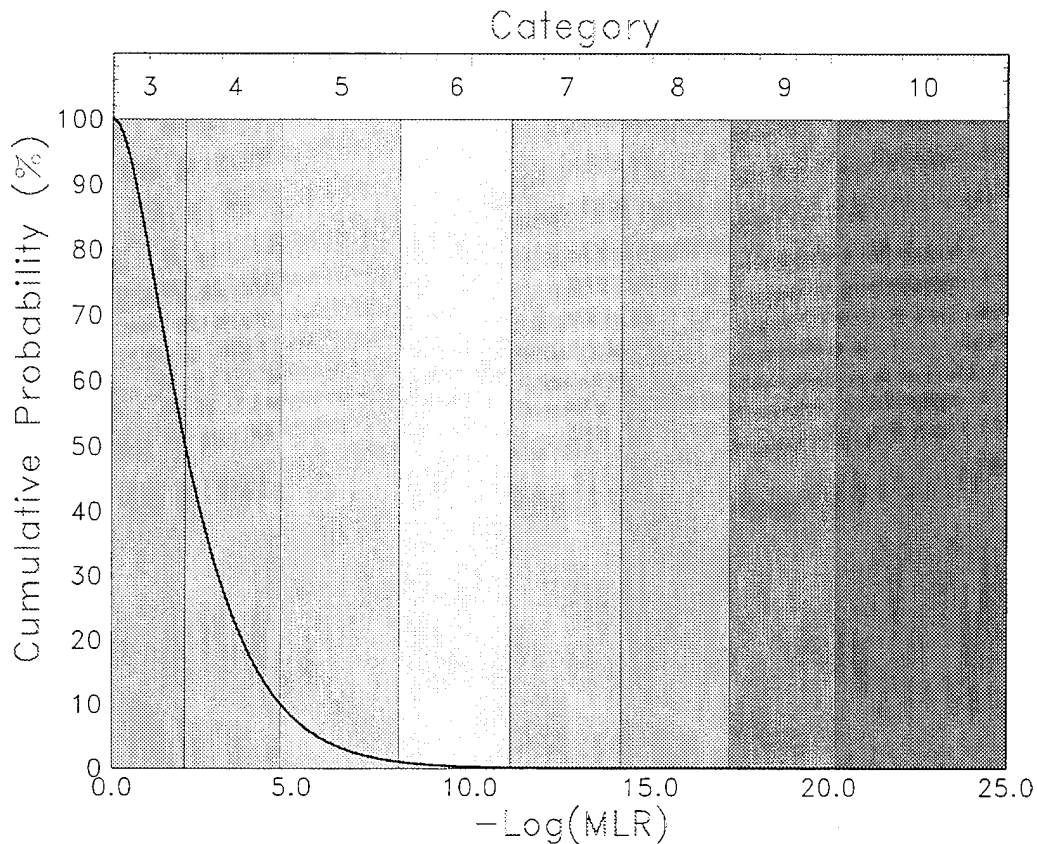


Figure 2. Relationship of Categories 3-10 to the cumulative probability of the log likelihood ratio when the null hypothesis is true.

Table 2 summarizes the events, their epicentral distances and magnitudes. Figure 3 depicts locations of the seismic stations, arrays, and events considered in this study (as well as others that were not considered here). The combined data set represents events in diverse geological regions, seen at a wide range of regional distances (100 to 1300 km), and with a wide range of magnitudes (1.0 to 6.1). Fisk et al. (1994) provide a more detailed discussion of these data sets.

Discriminants used in this study include Pn/Lg and Pn/Sn in 3-5, 4-6, 5-7, 6-8 Hz bands. Of these, only Pn/Lg measurements in the 6-8 Hz band were provided for events recorded by KNB and MNV. Also, Sn was measured for only 2 of 17 explosions recorded by WMQ. Thus, only Pn/Lg in the listed frequency bands was used for this station. Baumgardt et al. (1992) describe how these discriminants are computed from seismic waveforms for the ARCESS and WMQ data sets, while Walter et al. (1994) provide similar descriptions for the KNB and MNV data sets. We did not receive depth or Ms-mb measurements for these events and none had location error ellipses entirely offshore. Thus, none of these events could be placed in Category 1.

Table 2. Summary of seismic data sets used in this study.

Array/Station	Events	Distance (km)	Magnitude
ARCESS	24 Steigen EQs	385-480	1.0-3.2
	5 Spitsbergen EQs	795-1320	1.5-2.9
	3 NZ EXs	1100	>3.9
WMQ	23 EQs	100-1100	4.2-5.9
	16 Kazakh EXs	950	4.8-6.1
	1 Lop Nor EX	240	4.7
KNB	59 NTS EQs	295-310	2.1-5.9
	89 NTS EXs	280-315	2.4-5.5
MNV	37 NTS EQs	250-260	2.2-5.9
	78 NTS EXs	190-245	2.6-5.5

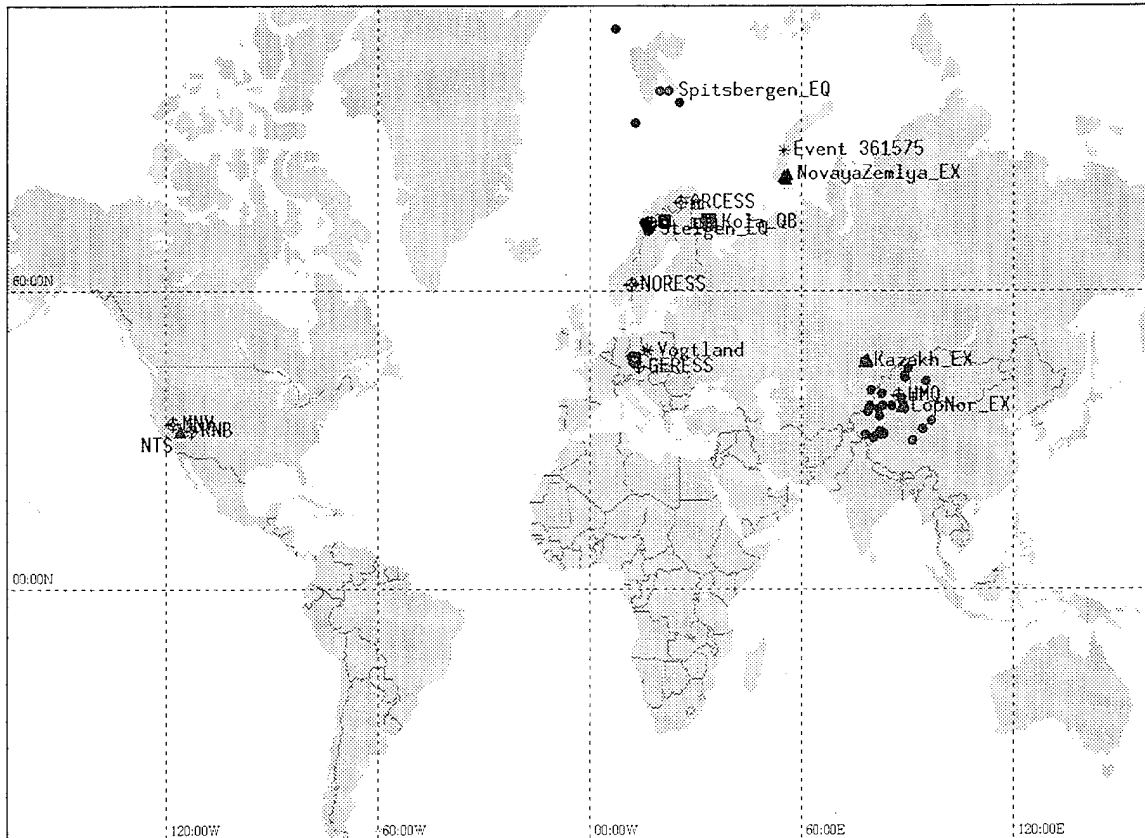


Figure 3. Locations of ARCESS, CDSN station WMQ, LNN stations KNB and MNV, and the seismic events used in this study.

1.4.1. Categorization Results for WMQ Events

Figure 4 shows locations of CDSN station WMQ, 16 nuclear explosions at the Balapan test site in Kazakhstan, the 29 September 1988 (880929) nuclear explosion at the Lop Nor test site in China, and 23 earthquakes scattered mostly around the northwest portion of China and western Mongolia. These events ranged in distance from 100 to 1100 km and from magnitude 4.2 to 6.1. Figure 5 shows distance-corrected Pn/Lg values in nine frequency bands from 0.5 to 16 Hz. Of these, the 3-5, 4-6, 5-7, and 6-8 Hz bands were used in the outlier analysis.

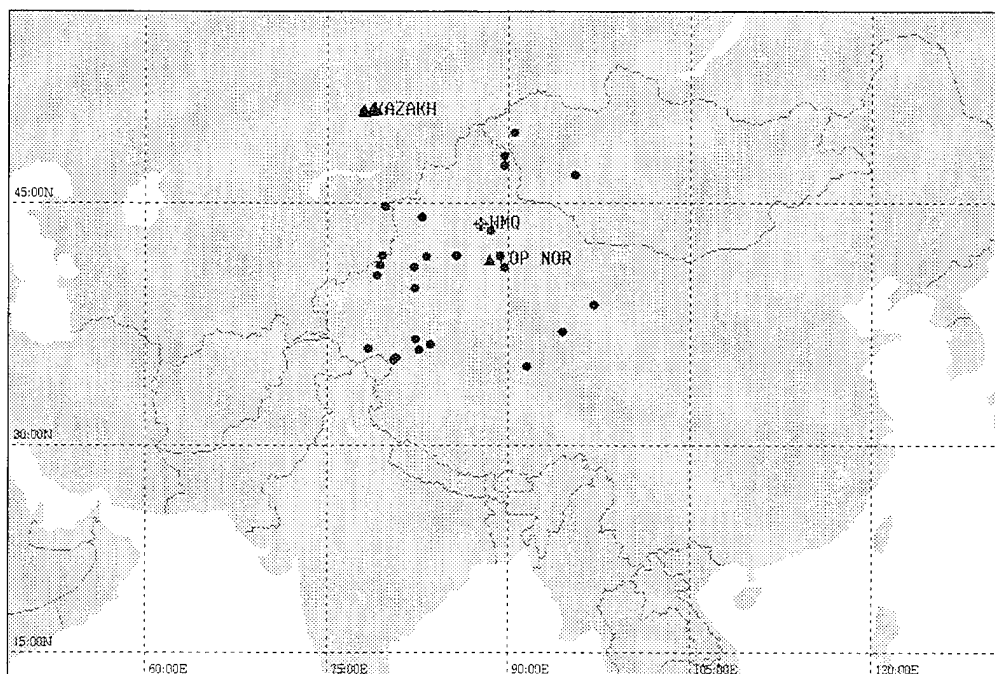


Figure 4. Locations of CDSN station WMQ, 16 nuclear explosions in Kazakhstan, the 880929 nuclear explosion at Lop Nor and 23 earthquakes in China and nearby countries.

Figure 6 shows categorization results for the 23 earthquakes and 17 nuclear explosions recorded by station WMQ. The categorized events are labelled by their origin identification (ORID) numbers. ORIDs shown in white correspond to actual earthquakes, while those shown in black correspond to underground nuclear detonations. For this case all 17 nuclear explosions fall in Category 10. There are 7 earthquakes in Category 2 with Pn/Lg values in all four bands less than the corresponding means computed from the remaining earthquakes. Seven other earthquakes fall in Category 3, 5 in Category 4, 3 in Category 5 and 1 in Category 6.

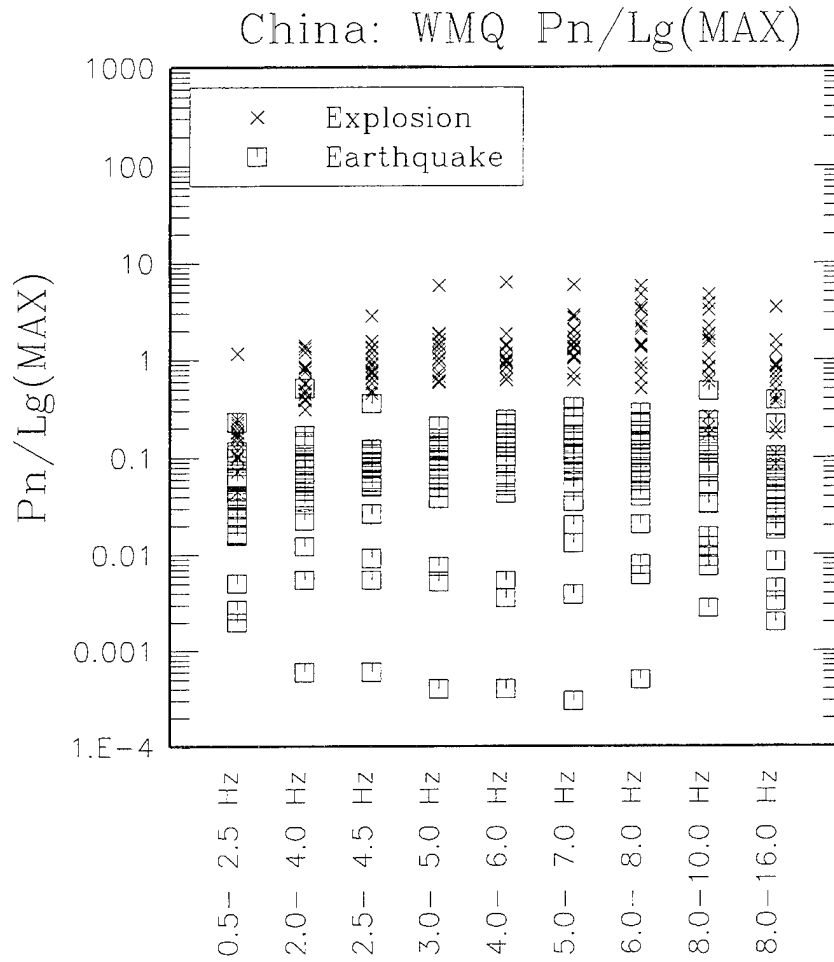


Figure 5. Distance-Corrected Pn/Lg in nine frequency bands for 23 earthquakes and 17 nuclear explosions recorded by WMQ.

For comparison, Figure 7 shows results of the outlier hypothesis test for the same events. The curve shown is of the probability density function (pdf) of the log likelihood ratio when the event being tested is from the same group as the earthquake training set. The vertical line represents the threshold of the test for the significance level listed in the lowest legend. Events whose likelihood ratio are less than the threshold are identified as outliers at the corresponding significance level. The triangles and circles depict values of the likelihood ratio for the explosions and earthquakes being individually tested, respectively. Figure 7 shows that all 17 nuclear explosions are flagged as outliers of the earthquake group at 0.01 significance level. There was one false alarm out of the 23 earthquakes. This earthquake corresponds to ORID=393656 shown in Category 6 of Figure 6.

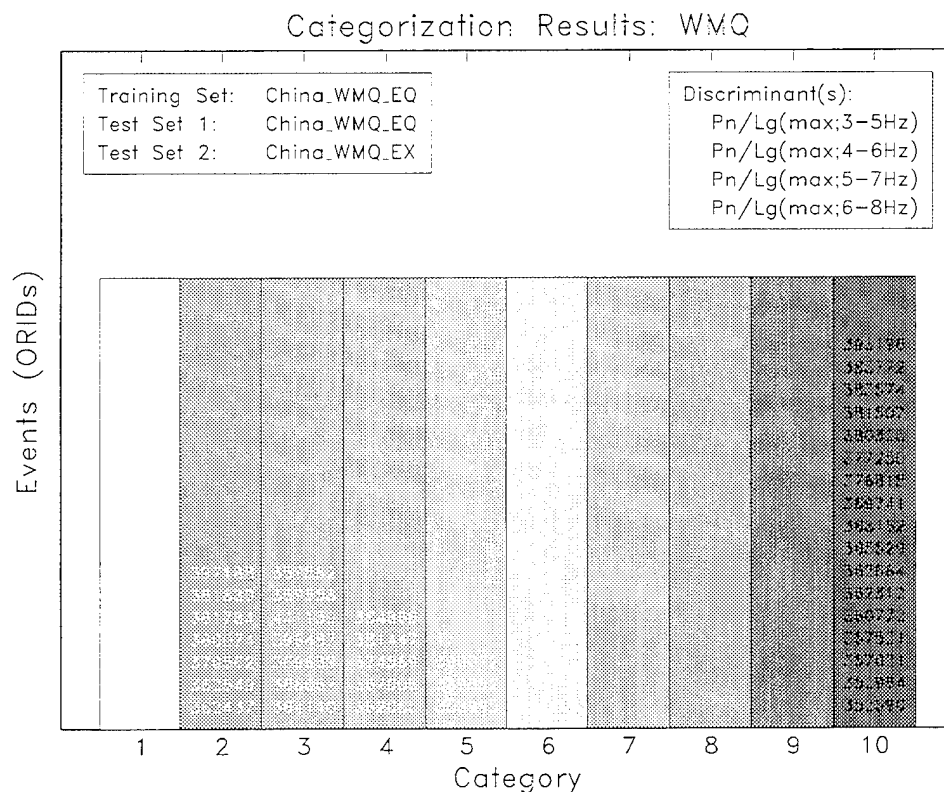


Figure 6. Categorization results for events recorded by station WMQ.

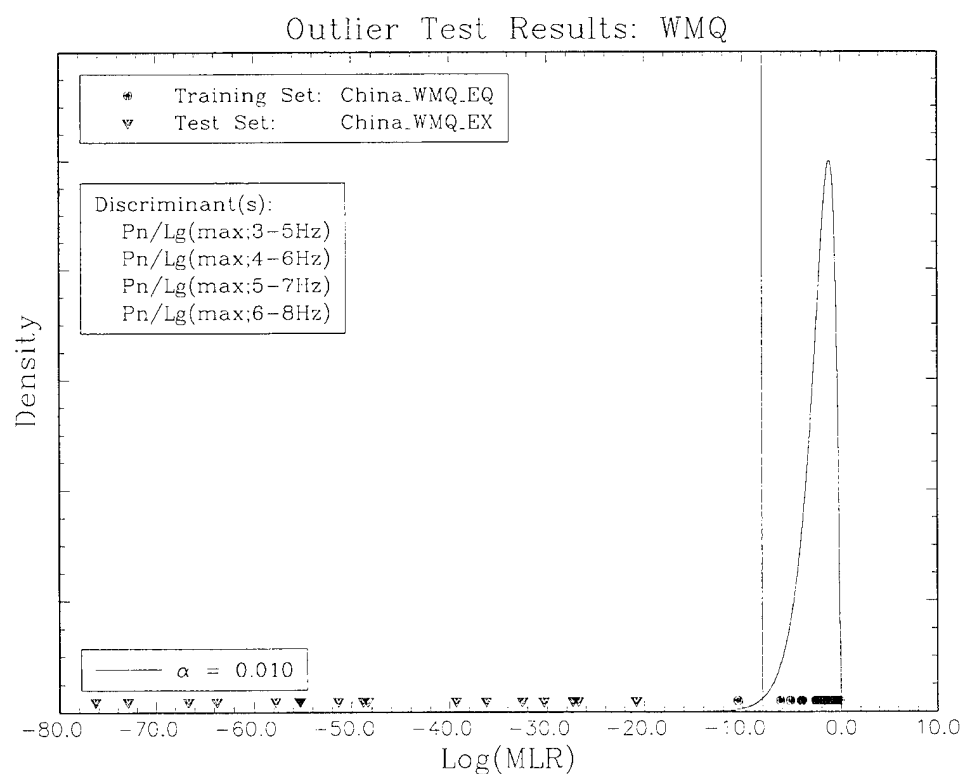


Figure 7. Outlier test results for events recorded by station WMQ.

1.4.2. Categorization Results for ARCESS Events

Events considered for ARCESS include 3 nuclear explosions at the Novaya Zemlya test site, 24 earthquakes near Steigen, Norway, and 5 earthquakes near Spitsbergen. Figure 8 shows the locations of these events (as well as quarry blasts on the Kola Peninsula, not considered here) and the ARCESS array. Table 2 summarizes magnitude and distance information for these events.

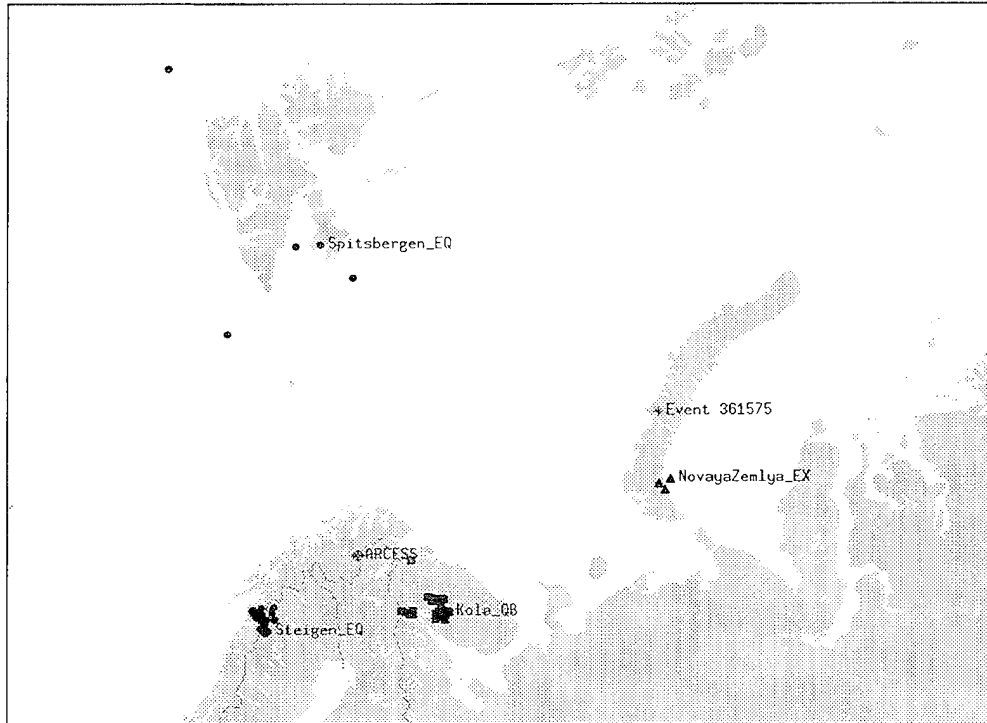


Figure 8. Locations of the ARCESS array, 3 nuclear explosions on Novaya Zemlya, 5 Spitsbergen and 24 Steigen earthquakes.

Figure 9 shows scatter plots of Pn/Sn measurements in six frequency bands for these and other events after applying distance corrections. The upper legend associates the marker type with the event type. This plot shows that there is good separation between the earthquake and nuclear explosion groups in the bands above 4 Hz. Pn/Lg measurements were not available for the Novaya Zemlya events, nor the 5 earthquakes near Spitsbergen, since Lg does not propagate efficiently beneath the Barents Sea.

Figure 10 shows categorization results for the 29 earthquakes and 3 Novaya Zemlya nuclear explosions, based on Pn/Sn recordings at the ARCESS array. Figure 10 shows that all 3 nuclear explosions fall in Category 10. Applying the outlier hypothesis test, Fisk et al. (1994) found that, at 0.01 significance level, the 3 Novaya Zemlya explosions were identified as outliers of the Steigen/Spitsbergen earthquake group and there were no false alarms.

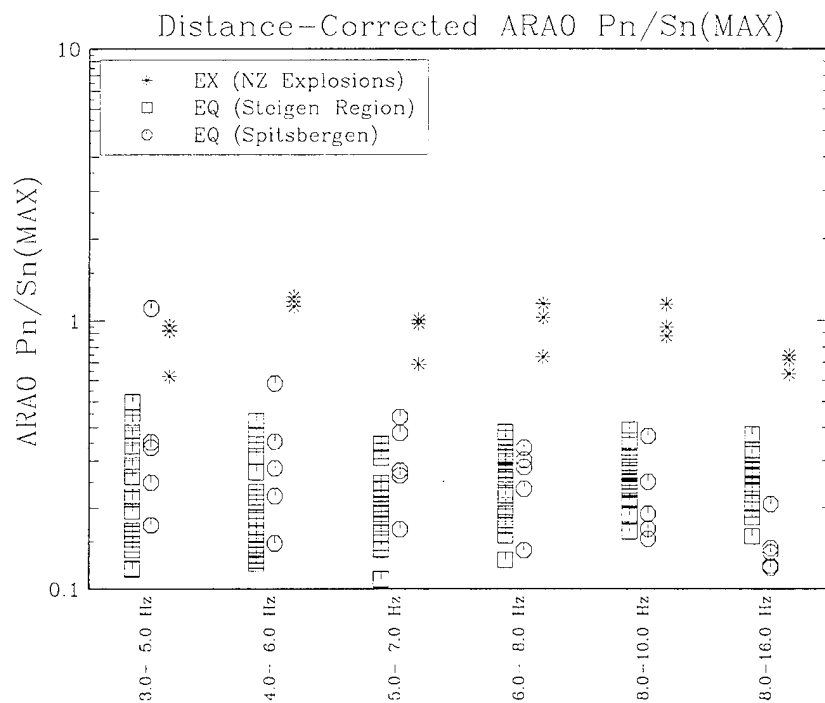


Figure 9. Distance-corrected Pn/Sn measurements in six frequency bands for events recorded by ARCESS.

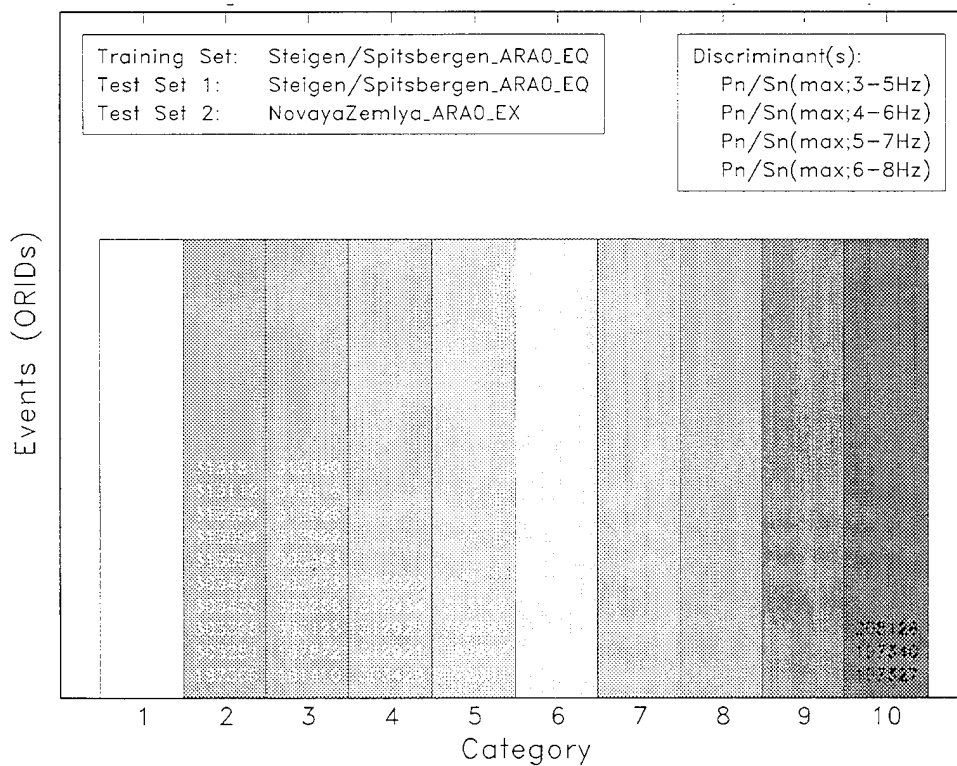


Figure 10. Categorization results for events recorded by ARCESS.

1.4.3. Categorization Results for KNB and MNV Events

To illustrate how the categorization procedure applies to events detected by more than one station, we use data from both KNB and MNV to categorize the earthquakes and explosions which occurred at the Nevada Test Site (NTS). Figure 11 shows a map of the southwestern U.S. depicting locations of LNN stations KNB and MNV relative to NTS. On the left is an enlarged map of NTS showing epicenters of the nuclear explosions and earthquakes used in this study. The earthquakes, ranging from magnitude (ML) 2.1 to 5.9, were clustered in three main locations: Little Skull Mountain, Rock Valley, and one at Massachusetts Mountain. The explosions ranged in magnitude from ML 2.4 to 5.5 and in depth from 200 to nearly 700 meters, in media with a relatively wide range of properties. To conform more closely to the event definition currently adopted by the CMR for GSETT-3, we consider only those events for which a P phase was detected at both stations. This definition is satisfied by 35 earthquakes and 69 nuclear explosions.

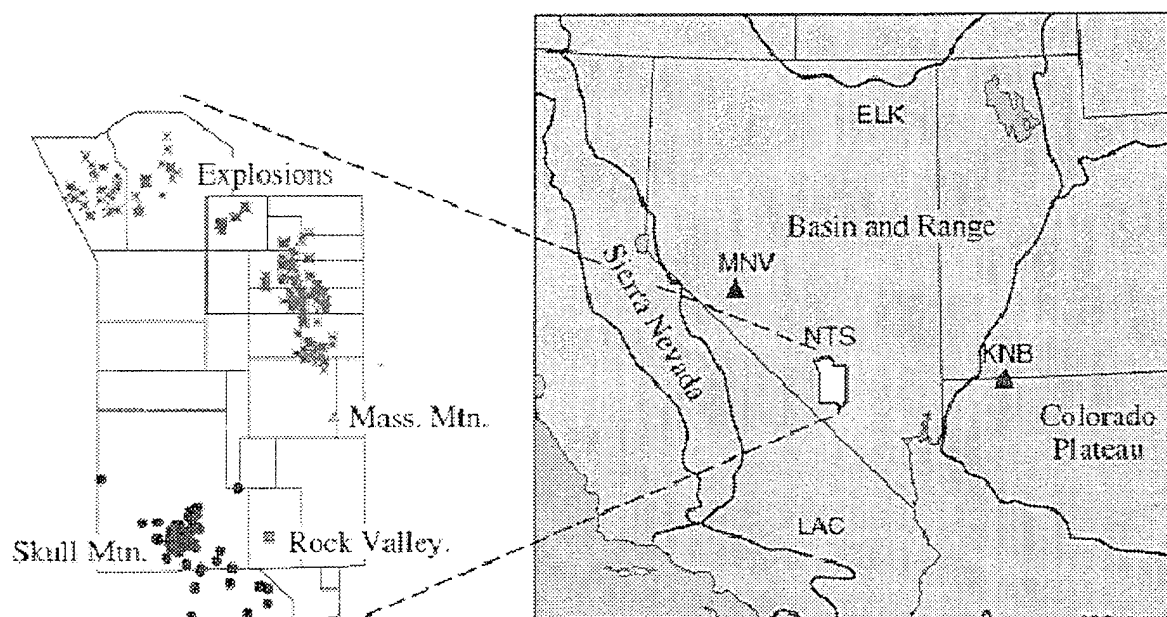


Figure 11. Locations of LNN stations KNB and MNV (among others) relative to NTS. On the left is an enlarged map of NTS showing epicenters of the nuclear explosions and earthquakes.

Figures 12 and 13 show Pn/Lg measurements in the 6-8 Hz band versus ML(coda) for the events recorded by KNB and MNV, respectively. (Note that Sn measurements were not available since Sn does not propagate efficiently in the western U.S.) The explosions are separated by those which were detonated in media with high versus low gas porosity (GP) and the earthquakes are separated into subregions in which they occurred. The legend associates the marker types with the

various events. Pn/Lg at MNV provides the best discrimination of earthquakes and explosions in this region, while there is more overlap at KNB, particularly for the shallow (1-3 km deep) Rock Valley earthquakes. Walter et al. (1994) noted that Pn/Lg exhibits differing values for shallow than for deeper earthquakes at KNB, possibly due to radiation pattern or path effects. There is no significant difference between Pn/Lg values for explosions in media of high versus low gas porosity. Figures 12 and 13 show that Pn/Lg in the 6-8 Hz band exhibits some dependence on magnitude, ML(coda), at both stations, although this is actually a signal-to-noise effect.

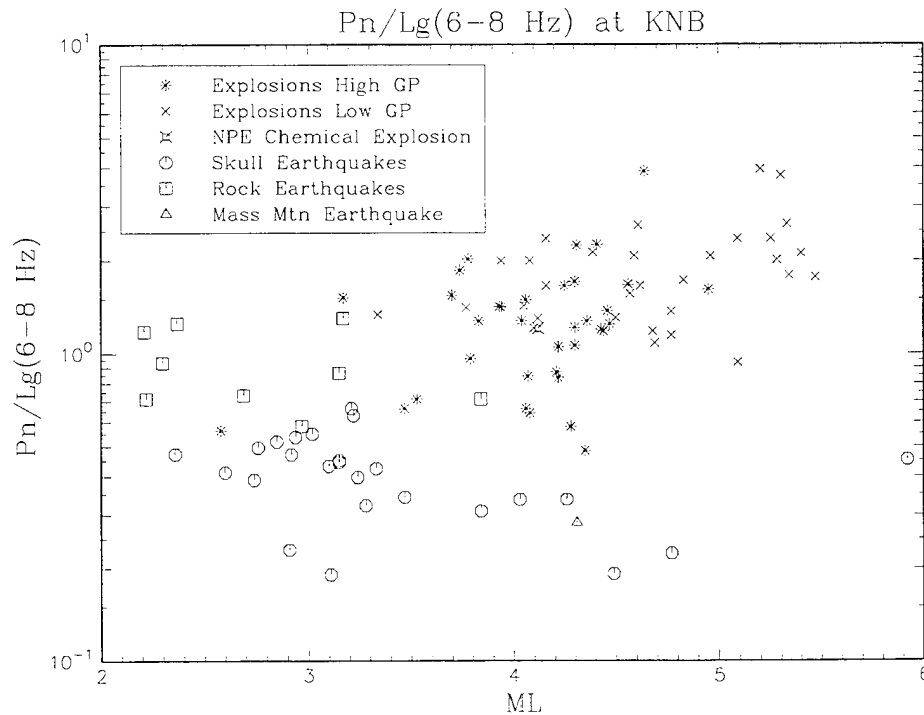


Figure 12. Pn/Lg measurements in the 6-8 Hz band versus ML(coda) for events recorded by KNB.

Figure 14 shows categorization results for these events using Pn/Lg(6-8 Hz) measurements at both stations. Performance at these stations is significantly worse than at either ARCESS or WMQ, where more discriminants are available. Note that for the outlier hypothesis test at 0.01 significance level, 59 of 69 (86%) explosions are identified as outliers and there are no false alarms. Events in Categories 6-10 are those identified as outliers by the hypothesis test at 0.01 significance level. Using Pn/Lg(6-8 Hz) for the same set of events at the individual stations, 63 of 69 (91%) explosions are identified as outliers at MNV and 20 of 69 (29%) explosions are identified as outliers at KNB and there are no false alarms at either station. Thus, combining evidence from the two stations is almost as effective as only using the best station (MNV) and is significantly better than only using the worst station (KNB). Note that in most practical monitoring situations we will not necessarily know which station provides better discrimination.

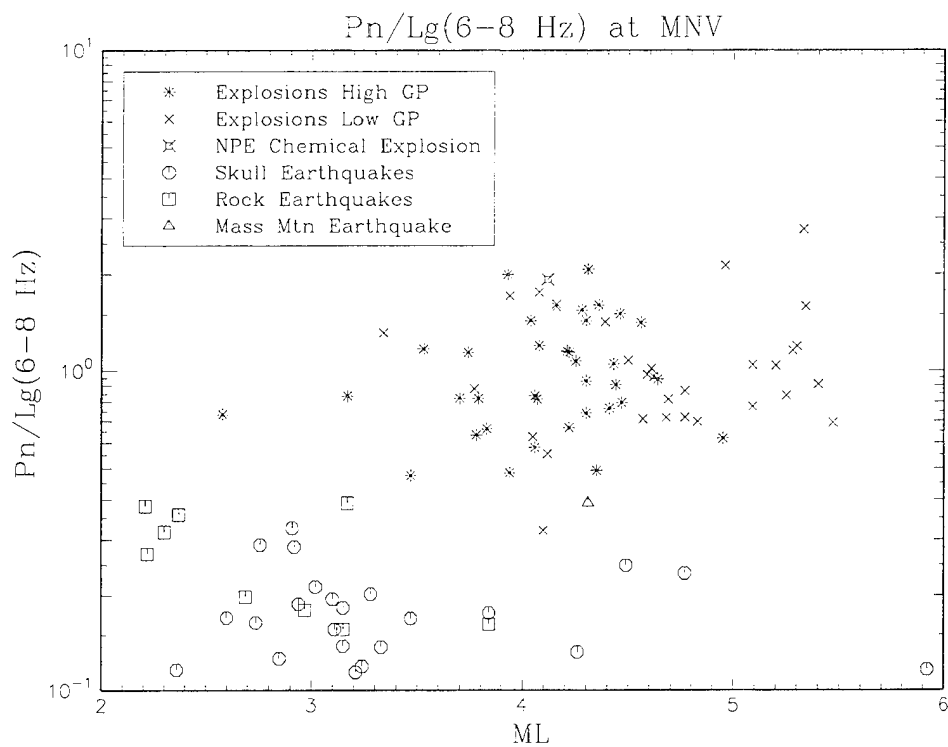


Figure 13. Pn/Lg measurements in the 6-8 Hz band versus ML(coda) for events recorded by MNV.

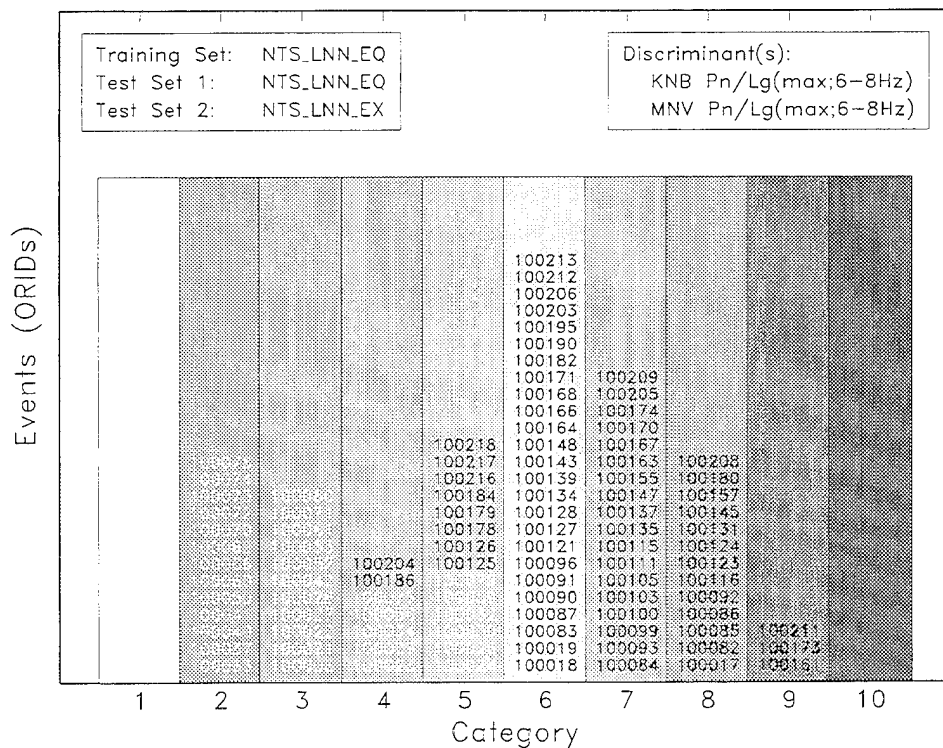


Figure 14. Categorization results for events recorded by KNB and MNV.

These results also show that additional discriminants are needed, for this region in particular. In a previous study, Fisk et al. (1994) used a spectral ratio of Lg coda, in addition to Pn/Lg(6-8 Hz), at the individual stations. They found that 95% and 80% of the explosions were identified as outliers at MNV and KNB, respectively, as compared to 91% and 29% using only Pn/Lg. Although Lg spectral ratios discriminate in some regions (e.g., the western U.S. and Germany), they do not in others (e.g., Scandinavia and Eurasia) (Fisk et al., 1994). Thus, we are hesitant to use them until further physical understanding of where and why they discriminate is obtained. Also, Fisk et al. (1995) included Pg/Lg(6-8 Hz) in the outlier analysis and found further improvement.

1.5. Summary

We have provided an event categorization procedure that focussed here on categorizing events which satisfy the event definition currently used at the CMR in terms of a minimum number of phase detections at the Alpha stations. This definition effectively restricts analysis to events above mb 3, possibly above mb 3.5 (Carter, 1995), for which the primary concern is distinguishing underground nuclear explosions from earthquakes.

Confidence intervals for universal discriminants (such as depth, location and Ms-mb) are used to categorize events when such measurements can be obtained. These rules define Category 1 which consist of high confidence natural events, typically those above mb 4.5. Events, for which regionally-varying discriminants such as Pn/Lg and Pn/Sn are used, are categorized using a multivariate population (i.e., outlier) analysis which compares new events to others seen in the same region by the same set of stations or arrays. It is assumed that the number of new nuclear tests in a region will be small compared to the number of earthquakes in that region. Using the distribution of the likelihood ratio, Categories 3-10 are defined in terms of the cumulative probability that an earthquake in a given region would fall in a particular category. Since the likelihood ratio does not differentiate between events with discriminant values that are higher or lower than the discriminant means, Category 2 is reserved for those events with all of their discriminant values on the side of the means away from values for explosions.

The examples in Section 1.4 show that all nuclear explosions recorded by either station WMQ or the ARCESS array fall in Category 10. Using a single discriminant, Pn/Lg(6-8 Hz), measured at both KNB and MNV, there were no Category 10 events, although 59 of 69 (89%) explosions were in Category 6 or higher. This case illustrates how evidence from multiple stations can be combined, as well as the need for additional discriminants, particularly in this region. To extend this categorization procedure to even smaller events (mb < 3), future effort will focus on investigating additional discriminants, techniques to discriminate single explosions from ripple-fired mining blasts, and on defining additional categories for mining blasts and mine tremors.

2. Preliminary Identification Analysis of the 950105 Urals Event

2.1. Introduction

Based on origin analysis at the CMR, a seismic event of mb 4.35 occurred at origin time 01/05/95 12:46:01 (GMT), latitude 59.52 and longitude 56.31 in the Southern Ural Mountains region. (We will refer to this as the 950105 event.) It was a shallow event which occurred in an area of low seismicity and near where several PNEs had been conducted. Of further interest was the fact that it had a relatively small M_s :mb value, inconsistent with typical values for shallow earthquakes.

A press release by the Moscow ITAR-TASS World Service, 6 January 1995, reported a statement by the Russian Federation's State Technical Inspectorate that this event was a tectonic shock at Pit Number 2 of the Silvinit Joint-Stock Company, caused by an earthquake with its epicenter near the settlement of Chashkino in Perm Oblast. The announcement also indicates that the tectonic shock led to the destruction of ventilation systems at the mine and to considerable emissions of explosive gases - methane and hydrogen - which subsequently ignited and exploded.

The objective of our analysis is to independently assess the identification of this event by comparing its seismic data, recorded by the ARCESS and KVAR arrays and stations ARU and OBN, to that of previous earthquakes and nuclear explosions. Since the 950105 event had a magnitude of mb 4.35, considerably larger than would be produced by a large mining blast, we focus here on identifying this event as either an earthquake or a nuclear explosion. (Walter, 1995, and others have considered other alternatives such as a mine collapse.)

In Section 2.2 we describe seismic data sets which are currently available to us, consisting of earthquakes and nuclear explosions in several regions, recorded by the ARCESS array in Norway and station WMQ in China. We compare high-frequency Pn/Lg and Pn/Sn measurements for the 950105 event to equivalent measurements for these reference data sets. Measurements are corrected for instrument response and distance effects. Since measurements for the 950105 event are not available for WMQ, comparisons to events recorded by WMQ are noted with the caveat that there may be significant path and station differences. Also, although the 950105 event was recorded at the ARCESS array, its propagation distance and azimuth are considerably different than for the ARCESS reference events. We provide conclusions regarding the identification of the 950105 event, based on these reference data sets, with these caveats in mind.

In Section 2.3 we categorize the 950105 event using our multivariate outlier analysis in which we compare high-frequency Pn/Sn measurements at ARCESS to those for earthquakes and nuclear explosions recorded by the same array. In Section 2.4 we provide preliminary conclusions regarding the identification of this event.

2.2. Data

Figure 15 shows the location of the 950105 event (labeled by its origin identification number, *orid*=273228), as well as locations of the ARCESS and KVAR arrays, stations ARU and OBN, and the reference events used in this study. Epicentral distances of the 950105 event to ARCESS, KVAR, ARU and OBN are 1812, 1960, 369, and 1275 km, respectively. Reference events for ARCESS include 3 Novaya Zemlya nuclear explosions (triangles), 24 earthquakes in the Steigen region of Norway (open circles) and 5 earthquakes near Spitsbergen (solid circles). Reference events for WMQ include 16 nuclear explosions in Kazakhstan (triangles), 1 nuclear explosion at the Lop Nor test site in China (triangle), and 23 earthquakes in China and nearby countries (solid circles). In addition, we provide comparisons to 10 Vogtland earthquakes (open circles) recorded by the GERESS array and to 16 PNEs (asterisks) recorded by the NORSAR array. Table 3 provides a summary of these events, their epicentral distances and magnitudes.

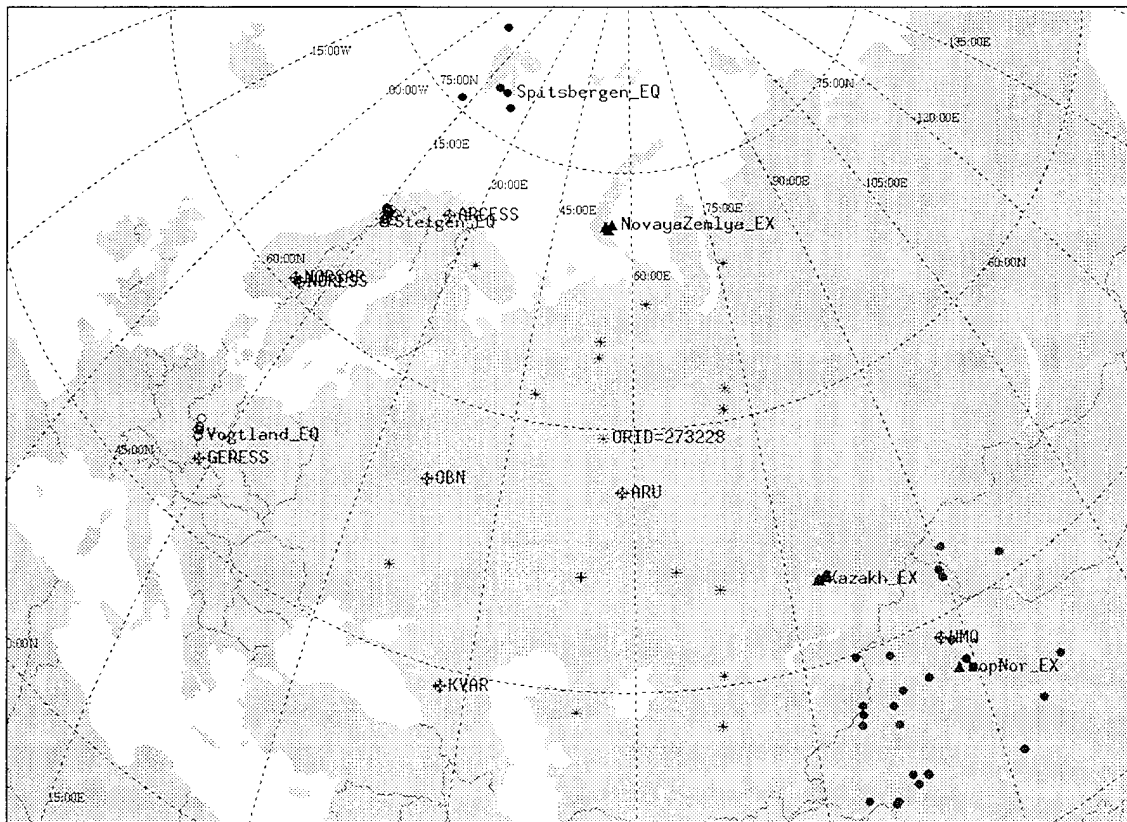


Figure 15. Locations of seismic stations, arrays and events used in our analysis of the 950105 Southern Urals event (ORID=273228).

Table 3. Summary of seismic data sets used in the analysis of the 950105 Urals Event.

Array/Station	Events	Distance (km)	Magnitude
ARCESS	24 Steigen EQs	385-480	1.0-3.2
	5 Spitsbergen EQs	795-1320	1.5-2.9
	3 NZ EXs	1100	>3.9
GERESS	10 Vogtland EQs	140-260	1.4-3.2
WMQ	23 EQs	100-1100	4.2-5.9
	16 Kazakh EXs	950	4.8-6.1
	1 Lop Nor EX	240	4.7
NORSAR	16 PNEs	1320-4210	4.6-6.1

2.2.1. Amplitude Ratios Prior to Applying Distance Corrections

Figure 16 shows Pn/Lg maximum amplitude measurement in the 6-8 Hz band versus distance for the 950105 and reference events. These values are uncorrected for distance effects. Pn/Lg measurements for the 950105 event are provided for the ARU and OBN recordings; no Pn/Lg measurements were obtained for ARCESS and KVAR. The legend associates the marker types to the various events. This figure shows that the Pn/Lg(6-8 Hz) values for the 950105 event are considerably different than those for nuclear explosions and consistent with those for earthquakes.

Figure 17 shows similar results for Pn/Sn(6-8 Hz) measurements, prior to applying distance corrections. In this case, Pn/Sn measurements for the 950105 event are available at ARCESS, KVAR, ARU and OBN. Note that Pn/Sn measurements were obtained for only 1 of the nuclear explosions recorded by WMQ. As for Pn/Lg(6-8 Hz), Pn/Sn(6-8 Hz) values at all four stations or arrays for the 950105 event are more consistent with values for earthquakes.

Figure 18 shows ARCESS Pn/Sn measurements in nine frequency bands on the sz channel, before applying distance corrections, for 3 Novaya Zemlya nuclear explosions, 24 Steigen earthquakes and the 950105 Urals event. The 950105 event compares differently to the earthquakes and explosions in different bands. Note that the 950105 event was over 1800 km from ARCESS and exhibits considerable variation with frequency, likely due to attenuation effects. In Section 2.2.2 we apply distance corrections to make a more meaningful comparison.

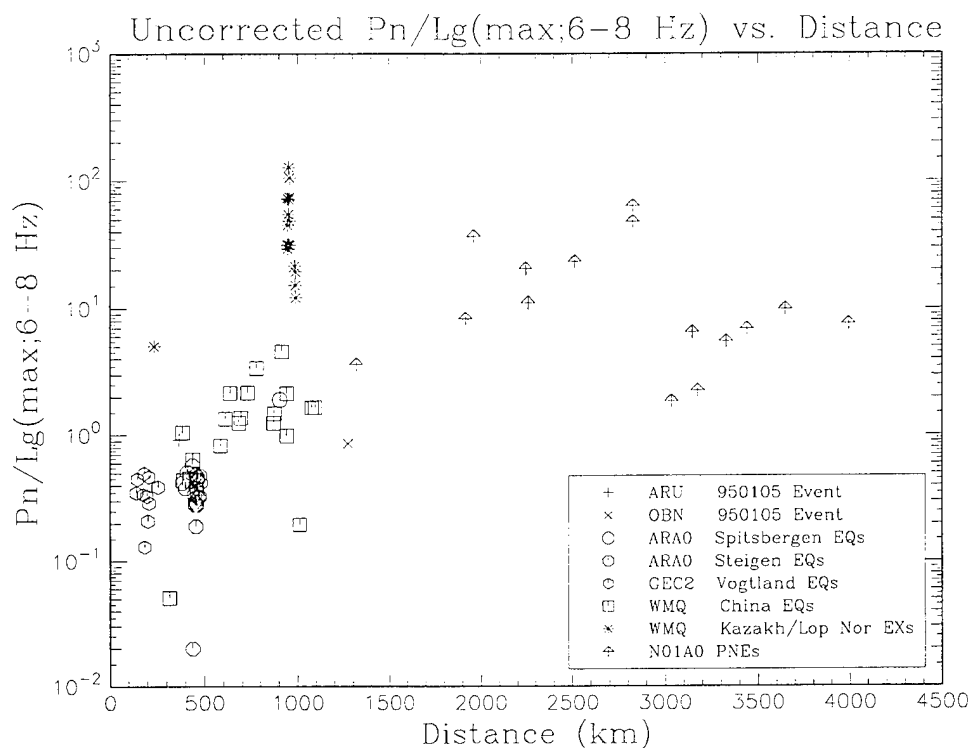


Figure 16. Uncorrected P_n/L_g in the 6-8 Hz band versus distance for earthquakes, nuclear explosions, and the 950105 Urals event.

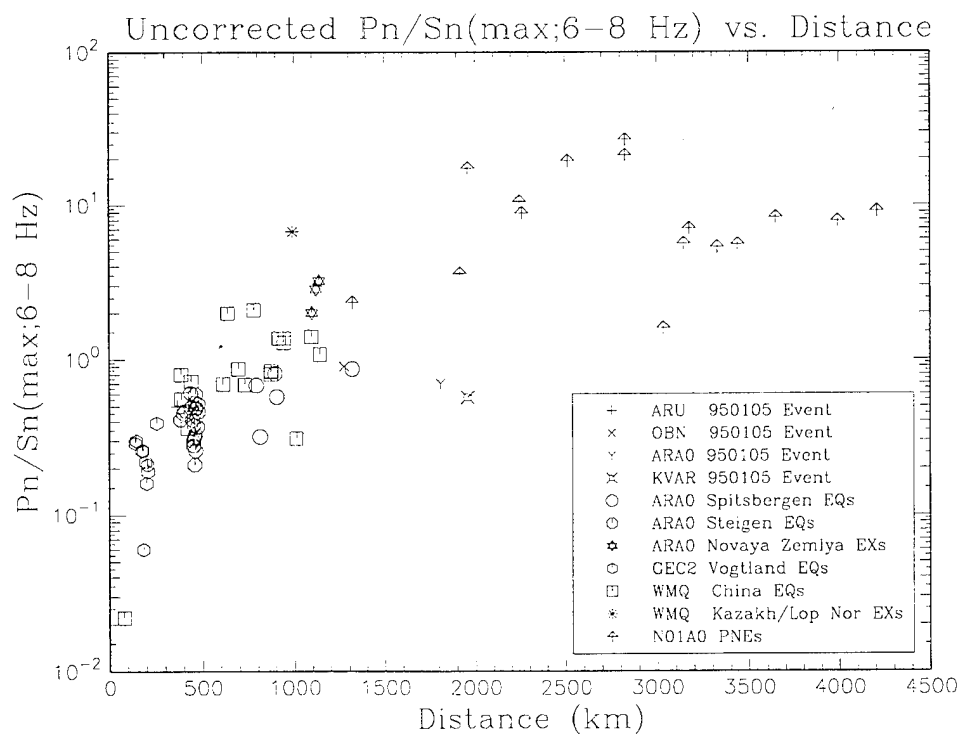


Figure 17. Uncorrected P_n/S_n in the 6-8 Hz band versus distance for earthquakes, nuclear explosions, and the 950105 Urals event.

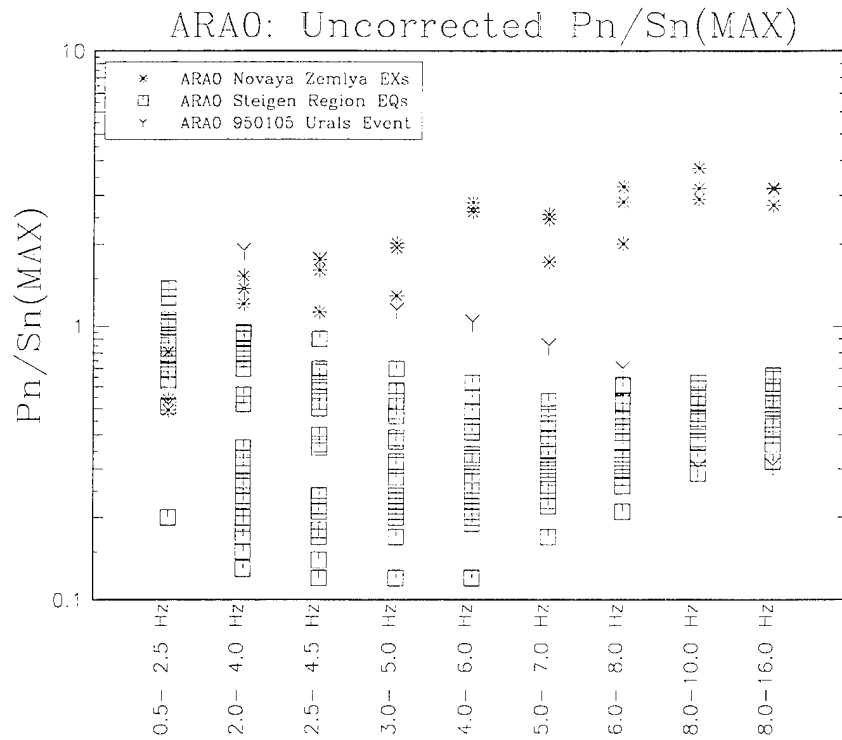


Figure 18. Uncorrected Pn/Sn measurements in nine frequency bands for 3 Novaya Zemlya nuclear explosions, 24 Steigen earthquakes and the 950105 event recorded by ARCESS.

Figure 19 shows Pn/Lg measurements in eight frequency bands on bz channels at stations ARU and OBN for the 950105 event before applying distance corrections. Also shown are Pn/Lg values for 23 earthquakes and 17 nuclear explosions recorded by station WMQ. In all bands above 3 Hz, the Pn/Lg values for the 950105 event are consistent with those for the earthquakes and considerably different than those for the nuclear explosions. Figure 20 shows a similar plot for Pn/Sn measurements. There were no Pn/Sn measurements for the nuclear explosion recorded by WMQ on the bz channel. Figure 20 shows that the Pn/Sn values for the 950105 event are, however, consistent with those for the earthquakes in all frequency bands.

2.2.2. Amplitude Ratios After Applying Distance Corrections

Figure 21 shows distance-corrected Pn/Sn in nine frequency bands for 3 Novaya Zemlya nuclear explosions, 24 Steigen earthquakes and the 950105 event, from ARCESS recordings. Distance corrections applied are from Sereno (1990) for Fennoscandia. Since these corrections do not necessarily apply to the Urals event, we corrected the Novaya Zemlya explosions and Steigen earthquakes relative to the distance at which the 950105 event occurred from ARCESS. Figure 21 shows that corrected Pn/Sn values for the 950105 event are consistent with those for earthquakes above 3 Hz. Pn/Sn values for the 950105 event are significantly attenuated above 8 Hz.

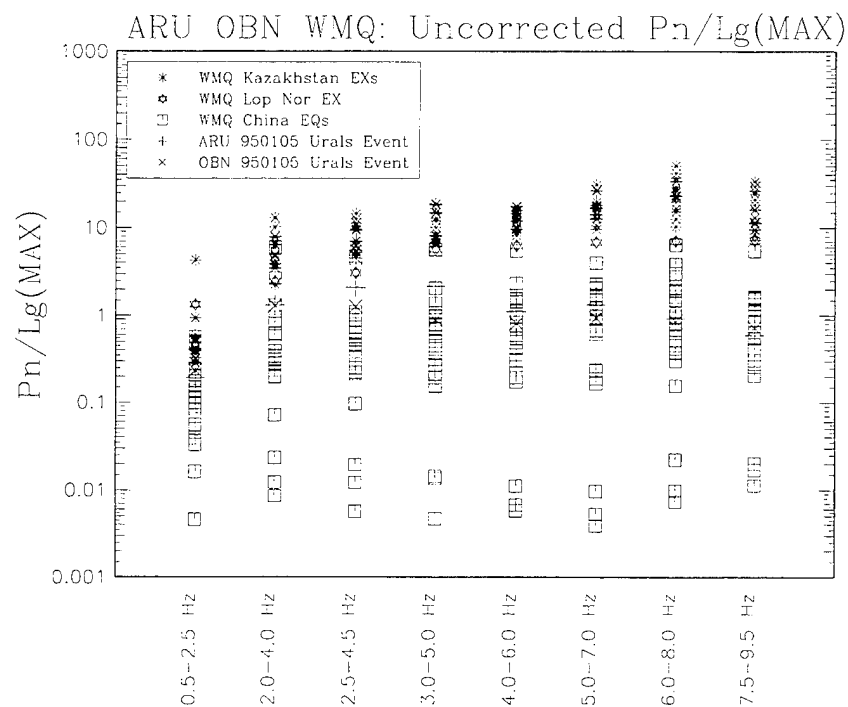


Figure 19. Uncorrected P_n/L_g measurements in eight frequency bands for the 950105 event recorded by ARU and OBN and earthquakes and nuclear explosions recorded by WMQ.

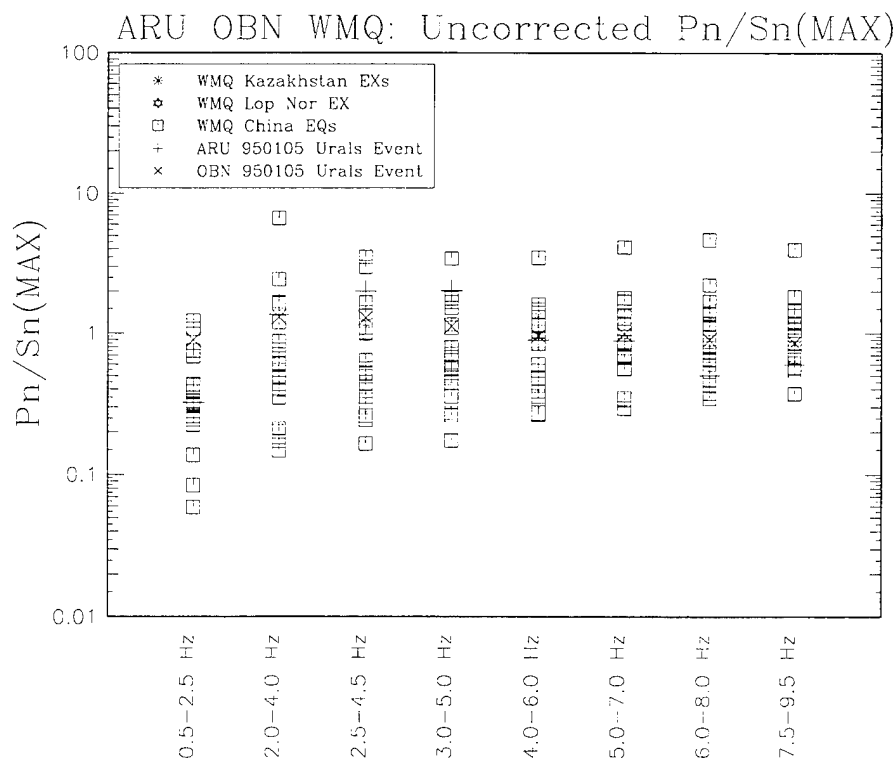


Figure 20. Same as Figure 19, but for uncorrected P_n/S_n .

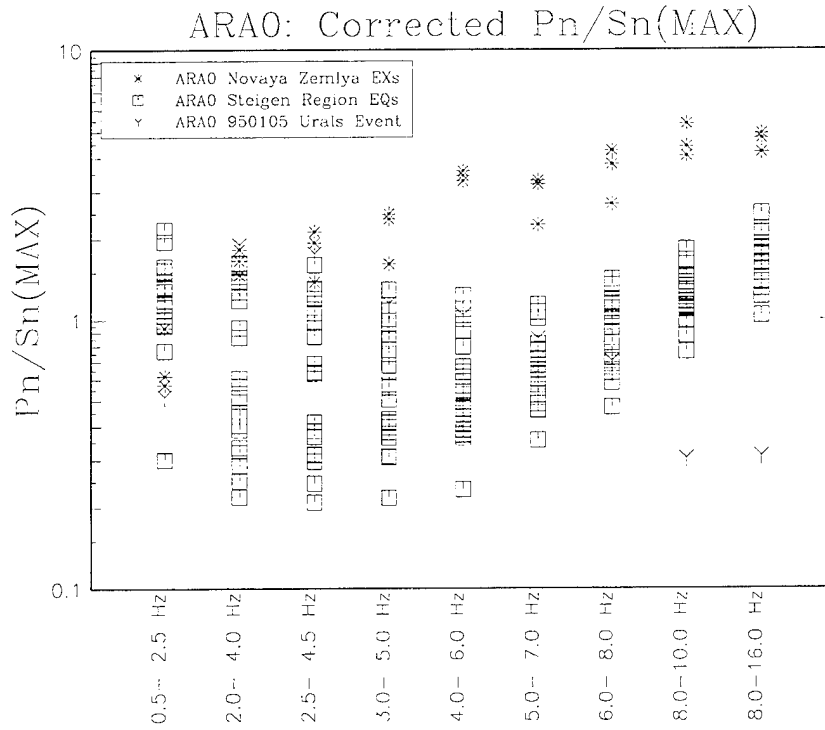


Figure 21. Distance-corrected Pn/Sn values in nine frequency bands for events recorded by ARCESS.

Figure 22 shows distance-corrected Pn/Lg in eight frequency bands for the 950105 event seen at OBN, and 17 nuclear explosions and 23 earthquakes recorded by WMQ. Distance corrections were obtained by performing a least squares fit to Pn/Lg as a function of distance in each frequency band using the earthquakes recorded by WMQ. The reference distance in this case was set at 1275 km to correspond to the distance of the 950105 event from OBN. Figure 22 shows that distance-corrected Pn/Lg values for the 950105 event are consistent with those for earthquakes above 2 Hz and considerably different than those for the nuclear explosions. Figure 23 shows a similar plot of distance-corrected Pn/Sn measurements. Pn/Sn values in all bands at OBN for the 950105 event are also consistent with those for earthquakes seen at WMQ.

We also performed comparisons of Pn/Lg and Pn/Sn measurements at ARU for the 950105 event to those for earthquakes and explosions seen at WMQ. In this case, WMQ events were distance-corrected relative to the 370 km distance of the 950105 event from ARU. At this distance range the corrections vary rapidly as a function of distance and there were only a few WMQ events in this range with which to estimate the corrections. Thus, until further data is obtained, these corrections are suspect for distances less than 400 km and we do not present comparisons here.

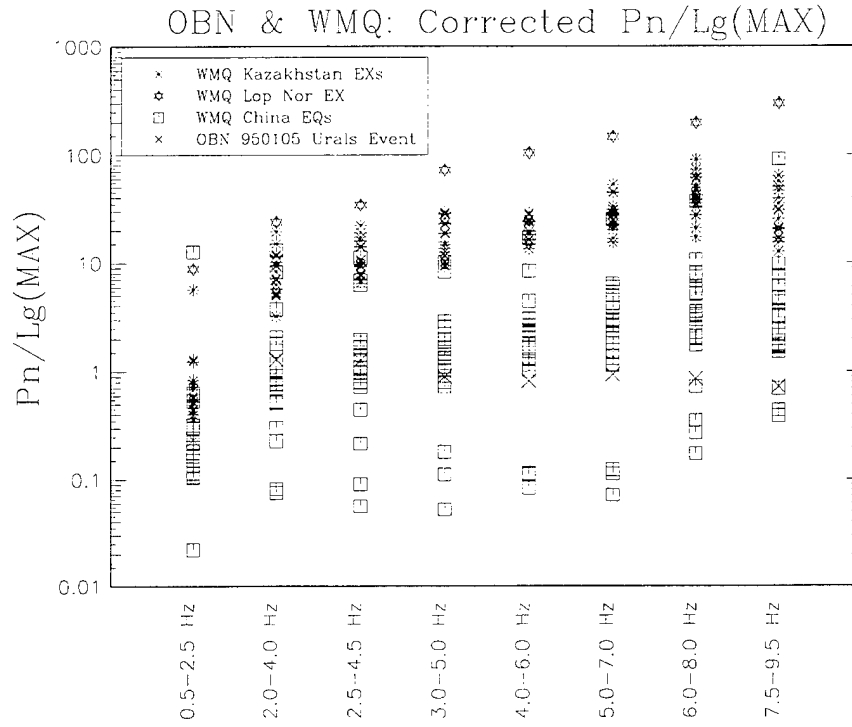


Figure 22. Distance-corrected Pn/Lg measurements in eight frequency bands for the 950105 event recorded by OBN and earthquakes and nuclear explosions recorded by WMQ.

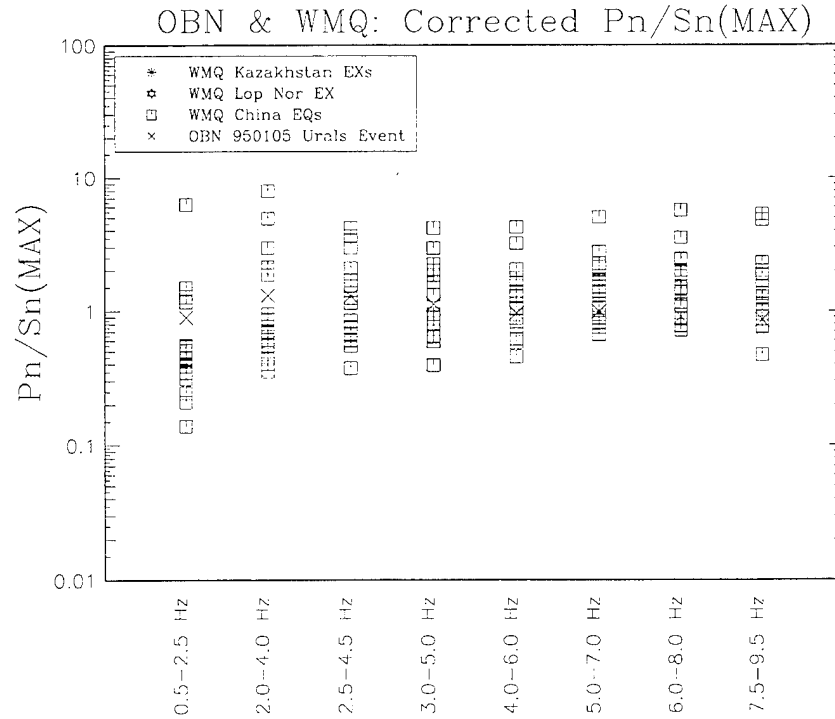


Figure 23. Same as Figure 22, but for distance-corrected Pn/Sn.

2.3. Categorization Results for the 950105 Event

Here we categorize the 950105 Urals event using the procedure described in Section 1. Since the 950105 event was onshore, not deeper than 10 km and the CMR did not have an M_s measurement, this event could not be placed in Category 1. Thus, it was processed further using the multivariate population analysis. Since ARCESS is the only common station or array for which we currently have data for this event and other reference events, we applied the outlier method to the 950105 event using P_n/S_n maximum amplitude measurements in the 3-5, 4-6, 5-7, and 6-8 Hz bands, and using the 24 Steigen and 5 Spitsbergen earthquakes to train the algorithm.

Figure 24 shows categorization results for the 950105 event (orid=273228). Also shown are categorization results for the 3 Novaya Zemlya nuclear explosions (orids shown in black) and the 29 Steigen and Spitsbergen earthquakes (orids shown in white) which were recorded by ARCESS. This figure shows that the 950105 event falls in Category 4 which contains 5 of the 29 earthquakes, while the nuclear explosions fall in Category 10. The probability that an earthquake would fall in Category 4 or lower, based on the outlier likelihood ratio statistic, is 50%, while the probability that an earthquake would fall in Category 10 is 0.0001%. Thus, the 950105 event would not be considered an outlier of the earthquake group unless we are also willing to identify up to 50% of the earthquakes as outliers of the same group to which they actually belong.

2.4. Conclusions and Future Plans

Preliminary comparisons show that the 950105 event is consistent with regional earthquakes seen at station WMQ and the ARCESS array, based on high-frequency P_n/L_g and P_n/S_n measurements. The results further show that this event is considerably different than previous nuclear explosions seen at either WMQ or ARCESS, particularly after applying distance corrections and above 3 Hz, at which frequencies P_n/L_g and P_n/S_n are expected to discriminate explosions from earthquakes. Results presented in Section 2.3 show that this event falls in Category 4, consistent with regional earthquakes seen at ARCESS. In addition, this event is not identified as an outlier of the earthquake group at WMQ, while it is identified as an outlier of the explosion groups at both ARCESS and WMQ. This event is also classified as an earthquake rather than an nuclear explosion using our classification test based also on the likelihood ratio.

These results are provided with the caveats that comparisons of ARU and OBN measurements to those at WMQ may be subject to station and path differences and the propagation distance of the 950105 event to ARCESS is considerably greater than those for the ARCESS reference events. Figures 19 and 21 shows strong frequency dependence of P_n/S_n for the 950105 event, which is likely due to significant attenuation effects over a far regional propagation path (1800 km).

Training Set: Steigen/Spitsbergen_ARA0_EQ
 Test Set 1: Steigen/Spitsbergen_ARA0_EQ
 Test Set 2: NovayaZemlya_ARA0_EX
 Test Set 3: Urals_ARA0_RU

Discriminant(s):
 $P_n/S_n(\max; 3-5\text{Hz})$
 $P_n/S_n(\max; 4-6\text{Hz})$
 $P_n/S_n(\max; 5-7\text{Hz})$
 $P_n/S_n(\max; 6-8\text{Hz})$

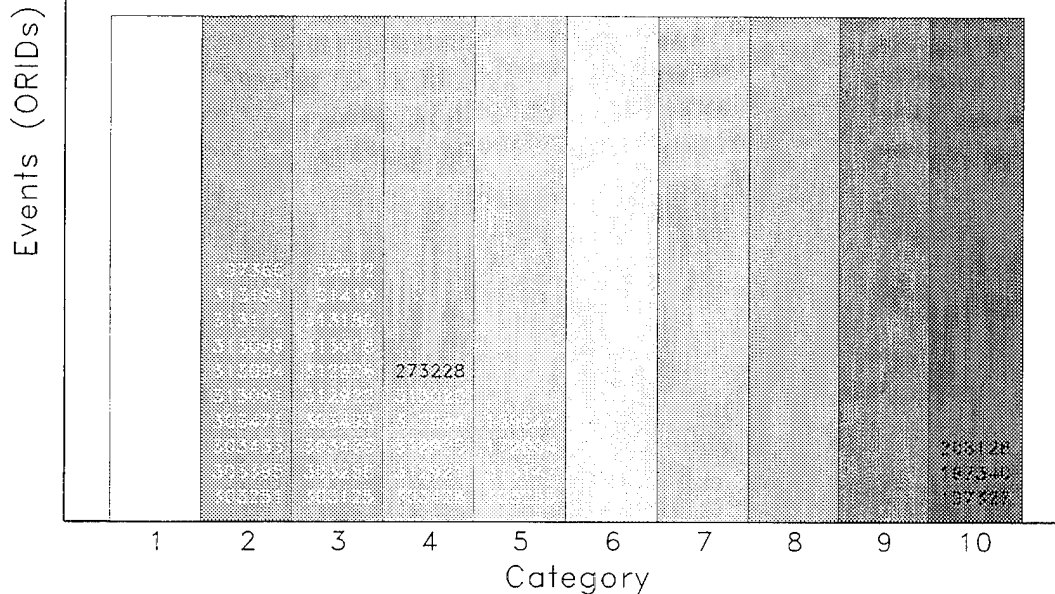


Figure 24. Categorization results for the 950105 event, 29 earthquakes in the Steigen and Spitsbergen regions, and 3 nuclear explosions at the Novaya Zemlya test site.

To circumvent the two stated caveats, we are trying to obtain seismic data for 16 PNEs which occurred in the same region as the 950105 event and were recorded by some of the same stations and arrays. We also plan to analyze seismic data for earthquakes in the same region and seen at the same stations (ARU and OBN) and the KVAR array. Given these data, we will be able to make further direct comparisons.

Further work may also be needed to better understand why high-frequency regional discriminants for this event are consistent with identification as an earthquake, while teleseismic Ms:mb is reportedly inconsistent with identification as an earthquake for such a shallow event. A simulation study by Walter (1995) suggests that the 950105 event can be modeled as a mine collapse. To study this further, we have been trying to obtain an Ms measurement for the 950105 event. We plan to report on the results and an approach to treat such anomalous events in the near future.

3. Assessment of Current Event Characterization Capability using GSETT-3 Alpha Network Data

3.1. Introduction

Here we compile various statistics regarding 1786 seismic events which occurred between 11 January 1995 and 12 February 1995 and were detected by a set of 30 Alpha stations as part of GSETT-3 (Group of Scientific Experts Technical Test-3). Seismic data from these stations were transmitted to the CMR (Center for Monitoring Research) where the records were analyzed. The objective of this study is to assess the numbers and characteristics of events that can be expected to be observed by the Alpha stations during a given period, including the availability and utility of event characterization parameters that can be used to identify them. High-frequency regional phase amplitudes and M_S were computed for the events during this period, as well as location, depth and mb parameters. Specifically, we compute the number or distribution of:

- Overall and regional ($\Delta < 20^\circ$) events detected at each station;
- Events versus mb, M_L and M_S ;
- Events versus area of 90% confidence location error ellipse;
- Events with location error ellipses entirely offshore;
- Events versus hypocentral depth estimate
- Events versus the number of depth phases detected;
- Events with M_S and mb measurements;
- Regional events for which high-frequency Pn/Sn, Pn/Lg, Pg/Sn or Pg/Lg were computed;
- Detecting stations per event for which regional discriminants are available.

We examine how many events can be screened with high confidence as due to natural seismicity, based on teleseismic measures of depth, location and M_S :mb. Of the remaining events, we examine how many have useful regional discriminants such that they could potentially be identified, considering primarily high-frequency regional P/S and P/Lg amplitude ratios. We also assess their utility with respect to signal-to-noise ratios. Last, we evaluate the number of remaining ambiguous events lacking adequate event characterization data to identify them, based on the Alpha network which existed at the time of this study.

In Section 3.2 we describe the data set and results of statistical compilations. In Section 3.3 we discuss the utility of event characterization parameters. In Section 3.4 we provide some conclusions and recommendations regarding current and future event identification performance.

3.2. GSETT-3 Data

Figure 25 shows locations of 30 Alpha stations, as well as epicentral locations of 1786 events which occurred between 11 January 1995 and 12 February 1995 and were reviewed by seismic analysts. Origin, association and event characterization data for these events were retrieved from the *origin*, *origerr*, *assoc* and *originamp* tables in the IDCWDB (International Data Center Working Data Base) at the CMR. Table 4 summarizes the names, locations, types (single station or array) and dates on which each Alpha station began operating (but not necessarily transmitting data to the CMR). Of the 30 Alpha stations, 11 are arrays and the remainder are single 3-component stations.

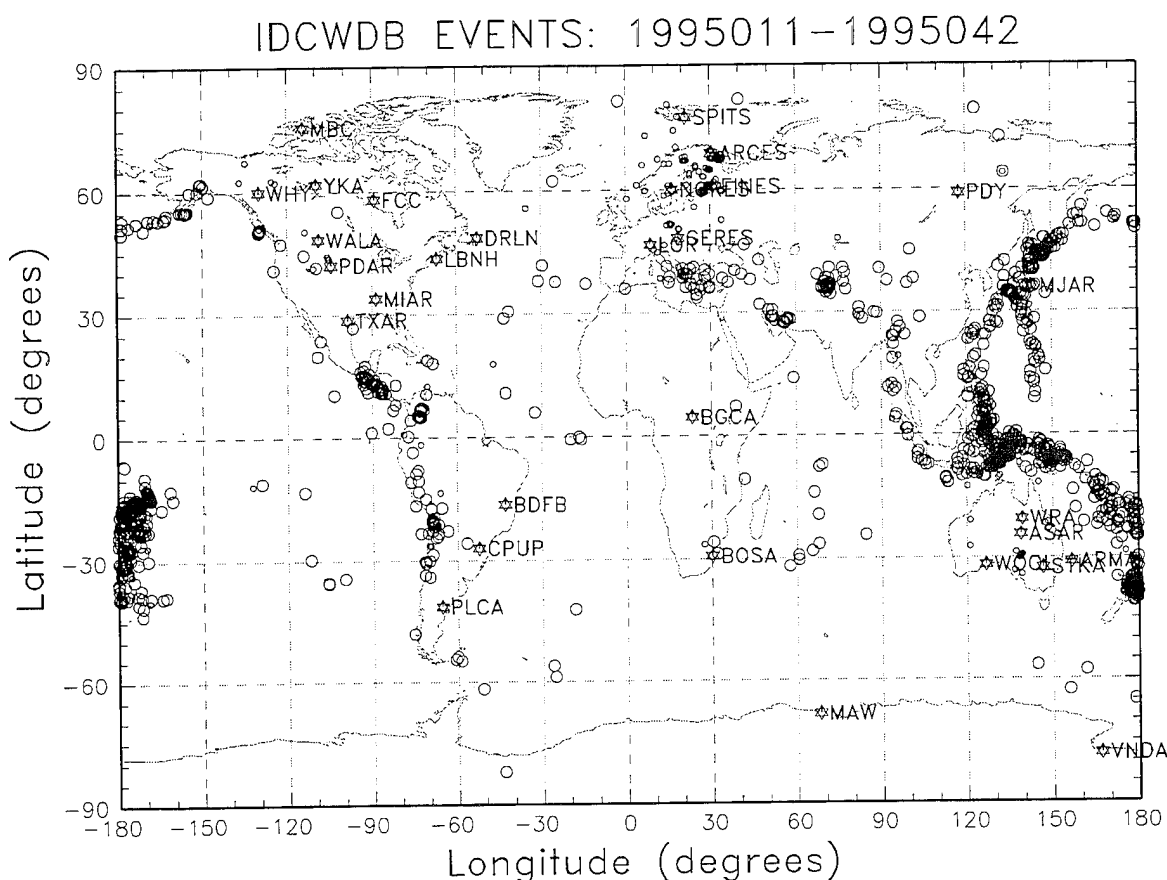


Figure 25. Locations of 30 Alpha stations and 1786 seismic events recorded by them between 11 January and 12 February 1995.

3.2.1. Events Per Alpha Station

Figure 26 shows the numbers of overall and regional events that were detected by each Alpha station. Of the 1786 events during this period, there were a total of 634 events within regional distance ($\Delta < 20^\circ$) of at least one of the 30 Alpha station.

Table 4. Alpha station names, operation start dates, locations, and types.

Station/Array	On Date	Latitude	Longitude	Station/Array Name	Type
ARCES	1987273	69.5349	25.5058	ARCESS Array, Norway	ar
ARMA	1994175	-30.4198	151.6280	Armidale, Australia	ss
ASAR	1987001	-23.6664	133.9044	Alice Springs Array, Australia	ar
BDFB	1993189	-15.6418	-48.0148	Brasilia, Brazil	ss
BGCA	1994256	5.1761	18.4242	Bogoin, Central African Republic	ss
BOSA	1993056	-28.6140	25.2555	Boshof, South Africa	ss
CPUP	1994001	-26.3306	-57.3292	Villa Florida, Paraguay	ss
DRLN	1993348	49.2560	-57.5042	Deer Lake, Canada	ss
FCC	1967175	58.7610	-94.0870	Fort Churchill, Canada	ss
FINES	1993322	61.4436	26.0771	FINESS Array, Finland	ar
GERES	1990067	48.8451	13.7016	GERESS Array, Germany	ar
LBNH	1993226	44.2401	-71.9259	Lisbon, New Hampshire	ss
LOR	1963001	47.2683	3.8589	Lormes, France	ss
MAW	1956181	-67.6039	62.8706	Mawson, Antarctica	ss
MBC	1961291	76.2420	-119.3600	Mould Bay, Canada	ss
MIAR	1992267	34.5457	-93.5730	Mount Ida, Arkansas	ss
MJAR	1984092	36.5427	138.2070	Matsushiro Array, Japan	ar
NORES	1984277	60.7353	11.5414	NORESS Array, Norway	ar
PDAR	1991001	42.7667	-109.5579	Pinedale Array, Wyoming	ar
PDY	1993218	59.6333	112.7003	Peleduy, Russia	ss
PLCA	1992300	-40.7283	-70.5500	Paso Flores, Argentina	ss
SPITS	1992311	78.1777	16.3700	Spitsbergen Array, Norway	ar
STKA	1991263	-31.8769	141.5952	Stephens Creek, Australia	ss
TXAR	1993244	29.3338	-103.6670	TXAR Array, Texas	ar
VNDA	1993362	-77.5139	161.8456	Vanda, Antarctica	ss
WALA	1992136	49.0586	-113.9115	Waterton Lakes, Canada	ss
WHY	1993239	60.6597	-134.8806	Whitehorse, Canada	ss
WOOL	1994157	-31.0730	121.6780	Woolibar, Australia	ss
WRA	1965274	-19.9426	134.3394	Warramunga Array, Australia	ar
YKA	1963273	62.4932	-114.6053	Yellowknife Array, Canada	ar

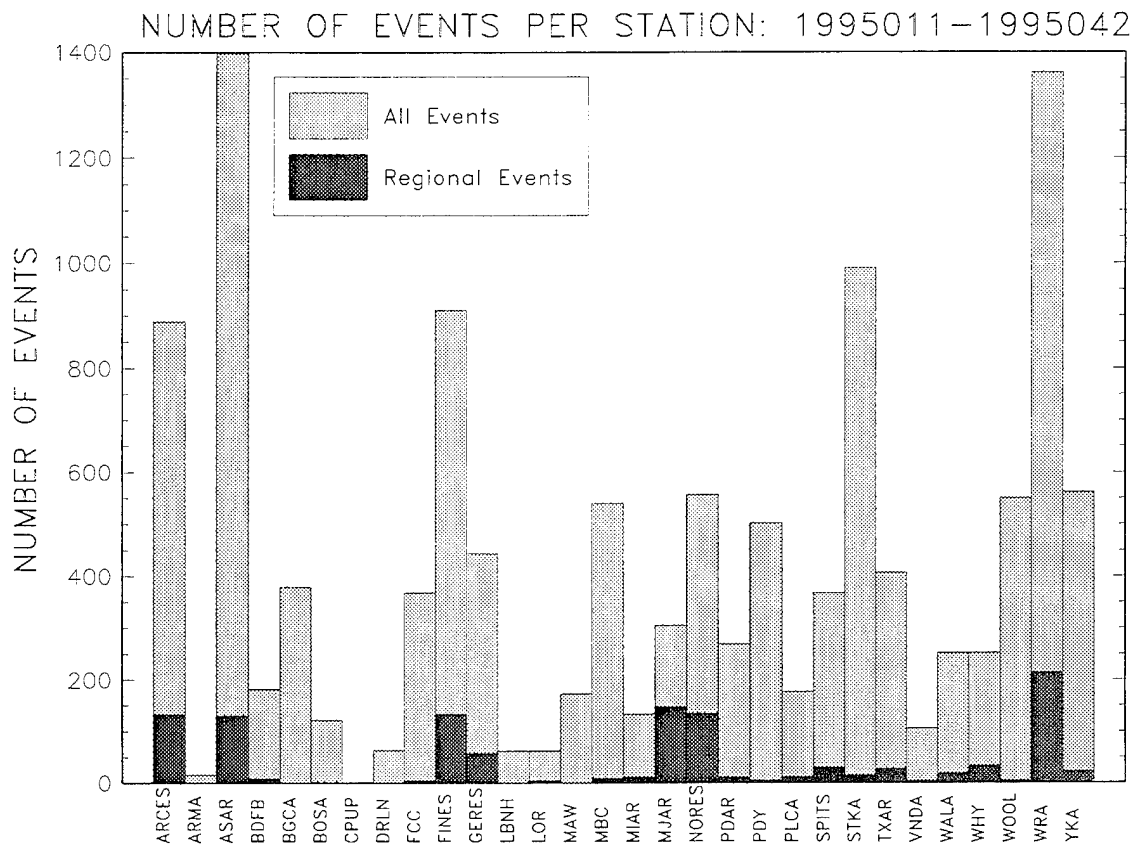


Figure 26. Number of overall and regional events per Alpha station.

3.2.2. Events Versus Location and Location Uncertainty

Figure 27 shows the distribution of events versus the area of their 90% confidence location error ellipses. Roughly half of the events have 90% location error ellipses with areas greater than 10,000 km². Figure 28 shows a scatter plot of location error ellipse area versus mb. The areas exhibit relatively little dependence on mb. It is expected that future use of Beta and Gamma station data, as well as data from additional planned Alpha stations, will help to reduce the size of the location error ellipses.

Comparisons by North (1995) of event locations in Canada, based on Alpha station data, to Canadian NDC locations using Beta and Gamma station data indicate that a significant percentage (11/16) of the 90% confidence location ellipses do not contain the Canadian NDC locations, accounting for their uncertainties as well. This may indicate that there are significant biases in location estimates which are not treated in the location uncertainty analysis.

Note that of the 1786 events during this period, 609 have 90% confidence location error ellipses entirely offshore.

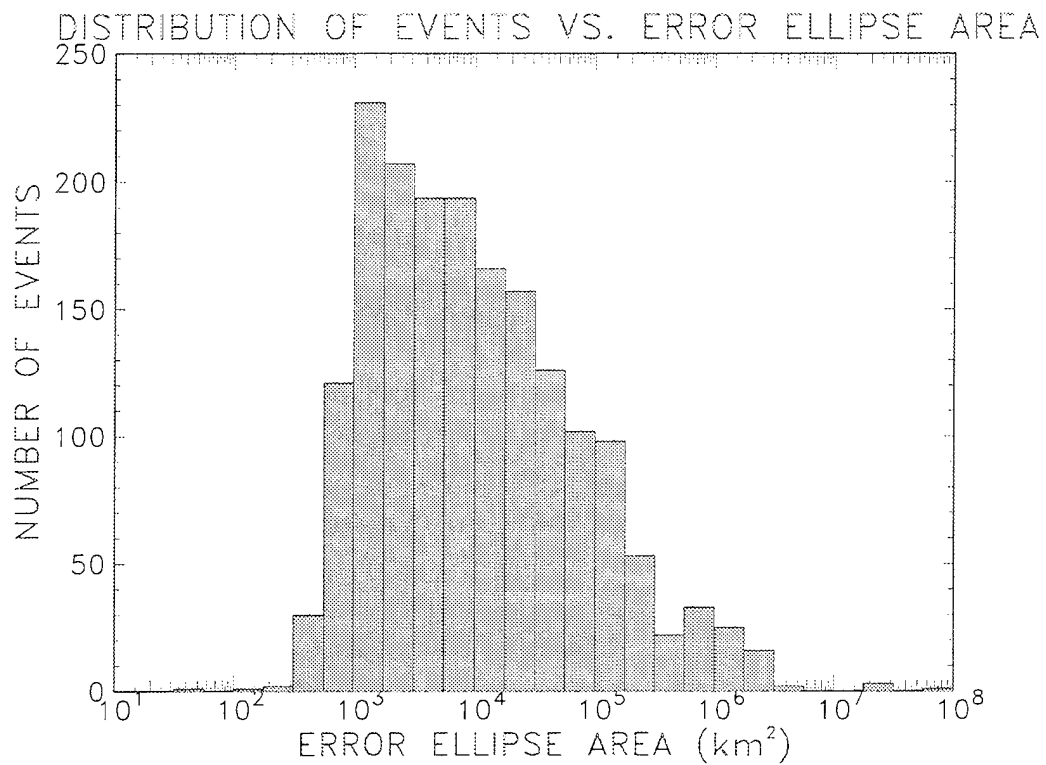


Figure 27. Distribution of events versus 90% confidence location error ellipse area.

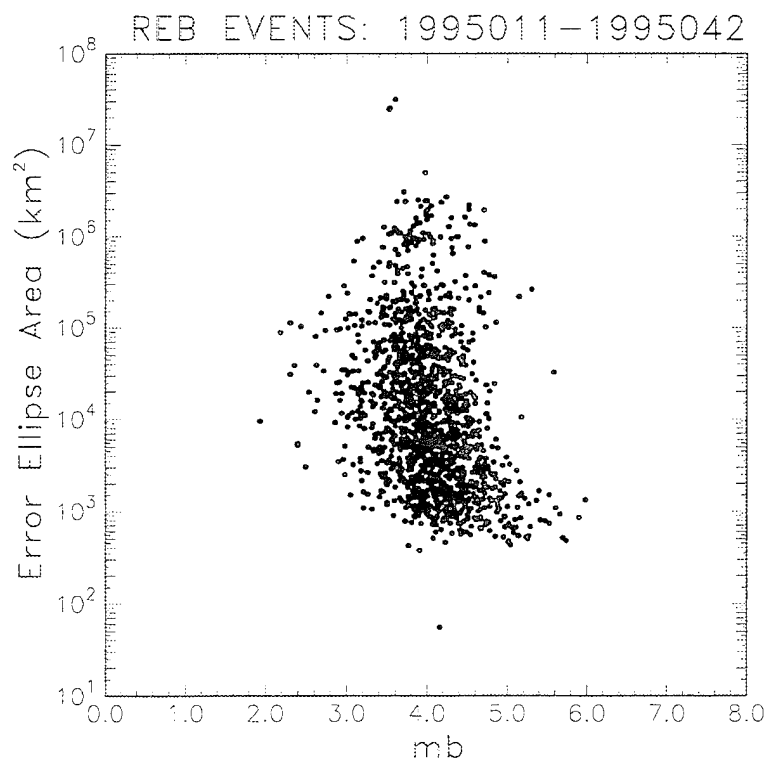


Figure 28. Scatter plot of 90% confidence location error ellipse area versus mb.

3.2.3. Events Versus Depth and Detected Depth Phases

Figure 29 shows the distribution of events versus their hypocentral depth estimates. There are 1201 of 1786 events (67%) whose depth estimates are less than 10 km deep or undetermined. Figure 30 shows the distribution of events versus the number of depth phases detected. There are only 59 events for which at least one depth phase was detected. Figure 31 shows the cumulative distribution of events, with or without at least one detected depth phase, versus the upper bound of the 95% depth confidence interval. There are 292 of 1786 events during this period with 95% depth confidence intervals deeper than 10 km, of which there are 58 with at least one detected depth phase. Thus, using a 95% confidence interval for depth, roughly 16% of the events can be classified as deep natural events. If we also require that at least one depth phase be detected¹, only 3% of the events can be classified as deep natural events with high confidence.

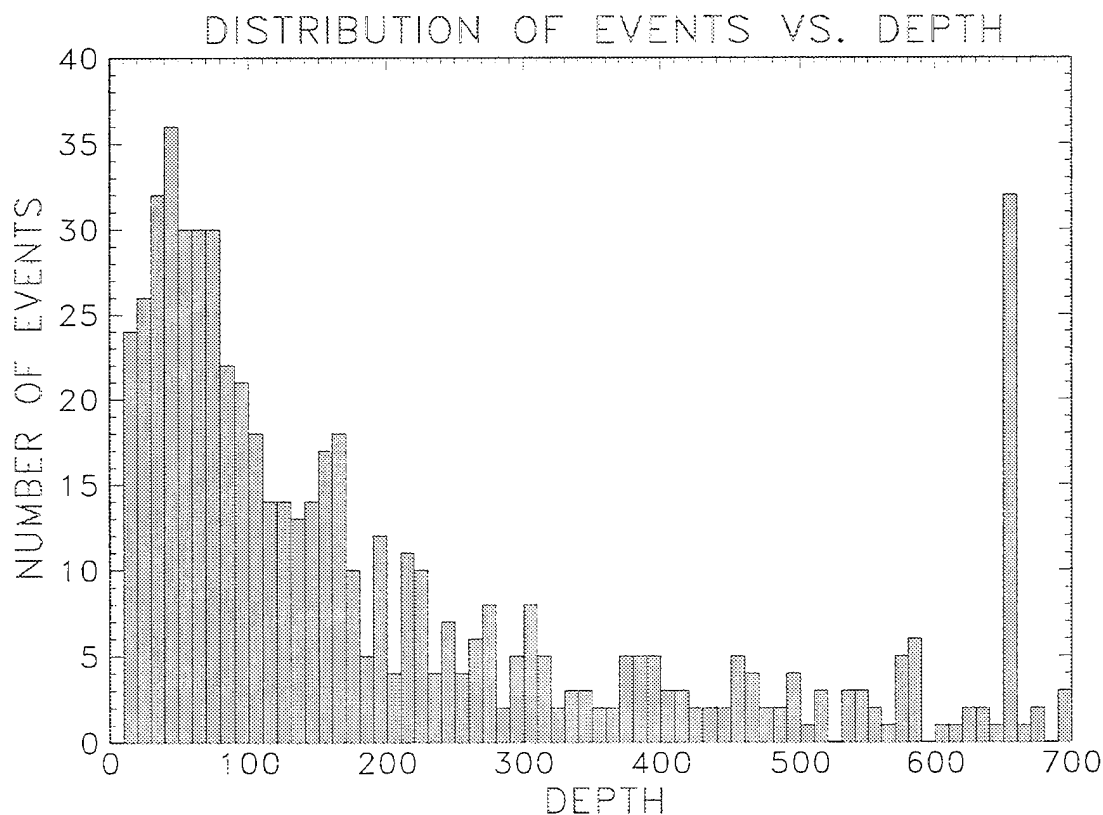


Figure 29. Distribution of events vs. hypocentral depth estimate.

1. The additional requirement that at least one depth phase be detected is motivated by the fact that potential biases in depth and location estimates may exist which are not treated when simultaneously computing depth confidence intervals and location error ellipses.

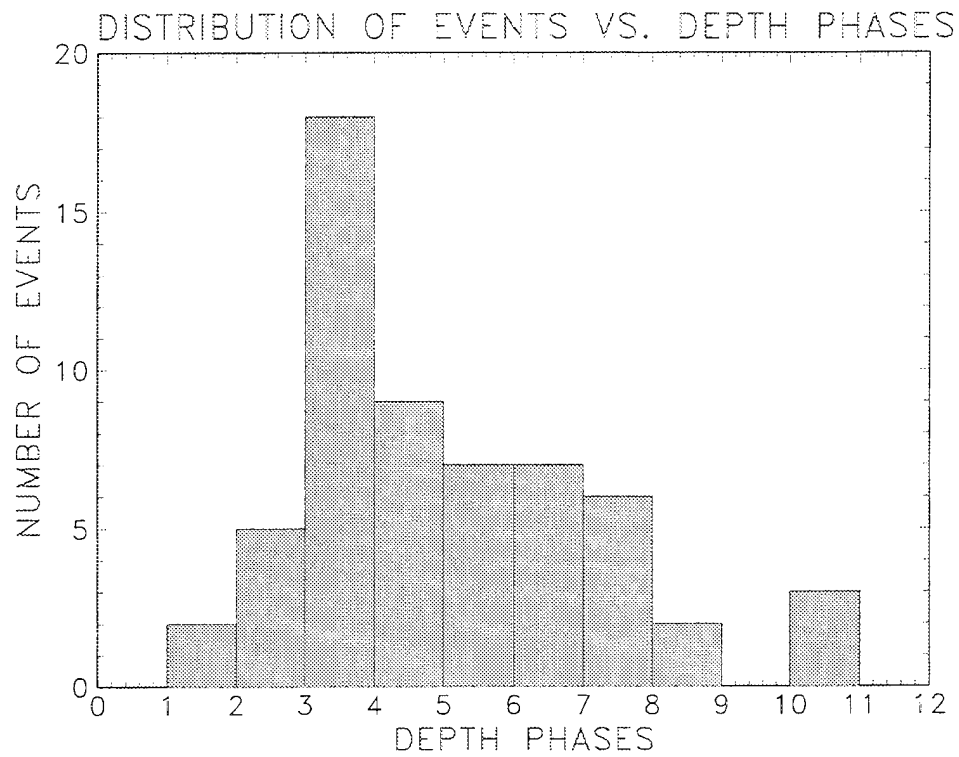


Figure 30. Distribution of events vs. number of depth phases per event.

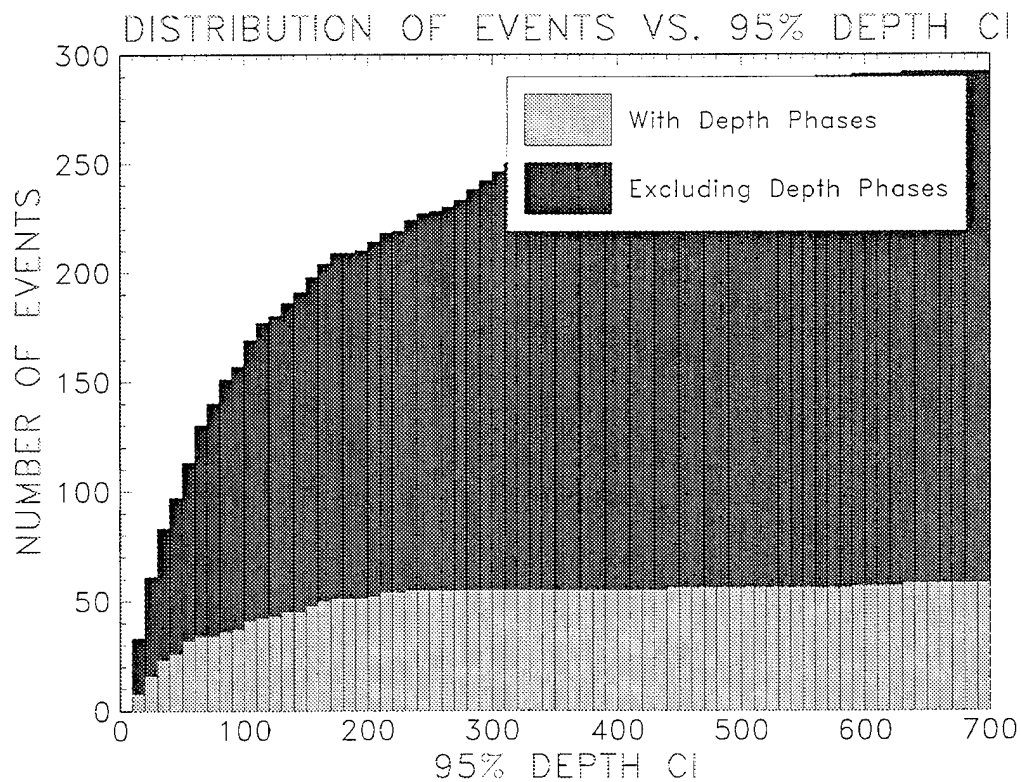


Figure 31. Cumulative distribution of events, with or without one or more detected depth phases, versus the upper bound of the 95% confidence interval for depth.

3.2.4. Events Versus Magnitude

Figure 32 shows distributions of the events as functions of m_b , M_S and M_L . Note that of the 1786 events, there are 327, 1643 and 1388 events for which m_b , M_S and M_L , respectively, were not measured. Of the remaining 1459 events for which m_b was measured, all but 35 (roughly 2%) were above m_b 3. Comparisons of IDC m_b values to those from the QED (Quick Epicentre Determination) of the U.S.G.S. National Earthquake Information Center found that the IDC m_b values are about 0.3 units smaller than the QED magnitudes (IDC Performance Report, 3 February 1995). This suggests that roughly 98% of the events are above m_b 3.3 and, thus, there are relatively few mining blasts to contend with for now.

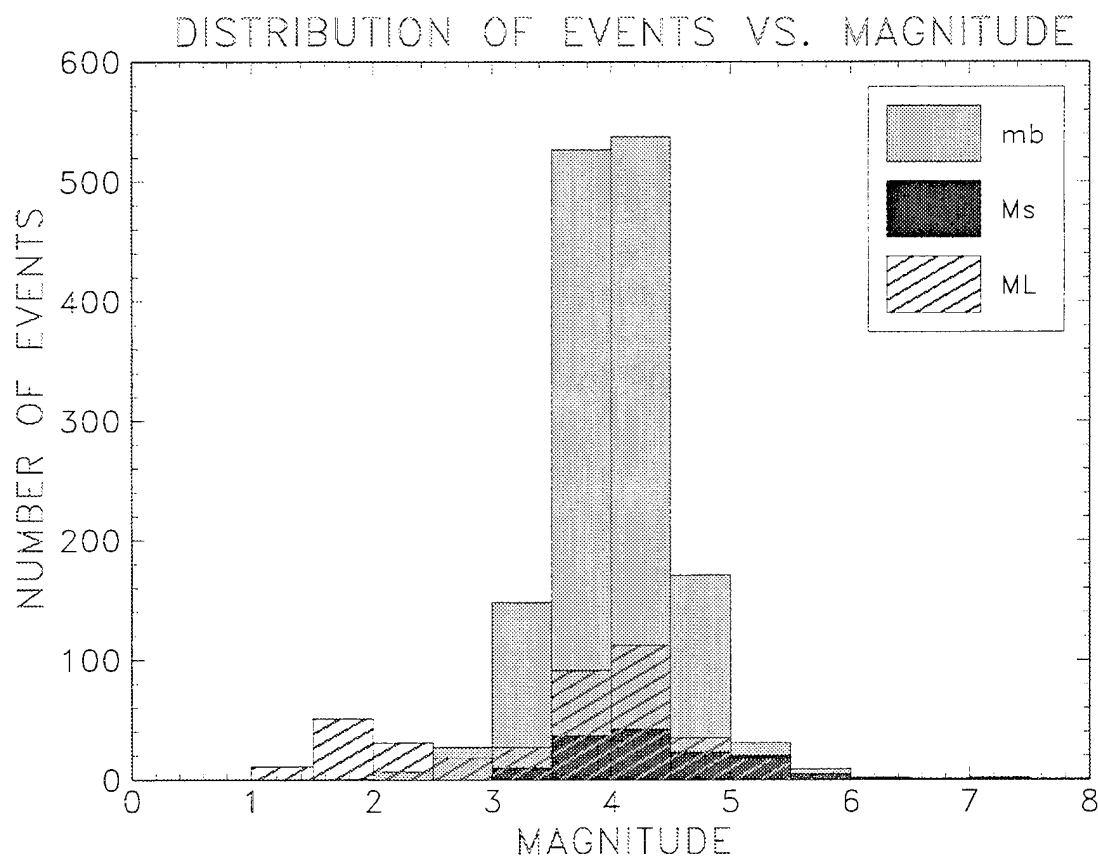


Figure 32. Distributions of events versus m_b , M_S and M_L .

Figure 33 shows a scatter plot of M_S versus m_b for 143 events for which both m_b and M_S were measured. All but 3 of these 143 events fall above the line defined by $m_b - M_S = 1.2$. Figure 34 shows a similar plot of M_L versus m_b . The scatter about the linear trend is greater than one magnitude unit. This has serious implications regarding the usefulness of M_L as an accurate or consistent measure of source size, and will likely require regional calibration.

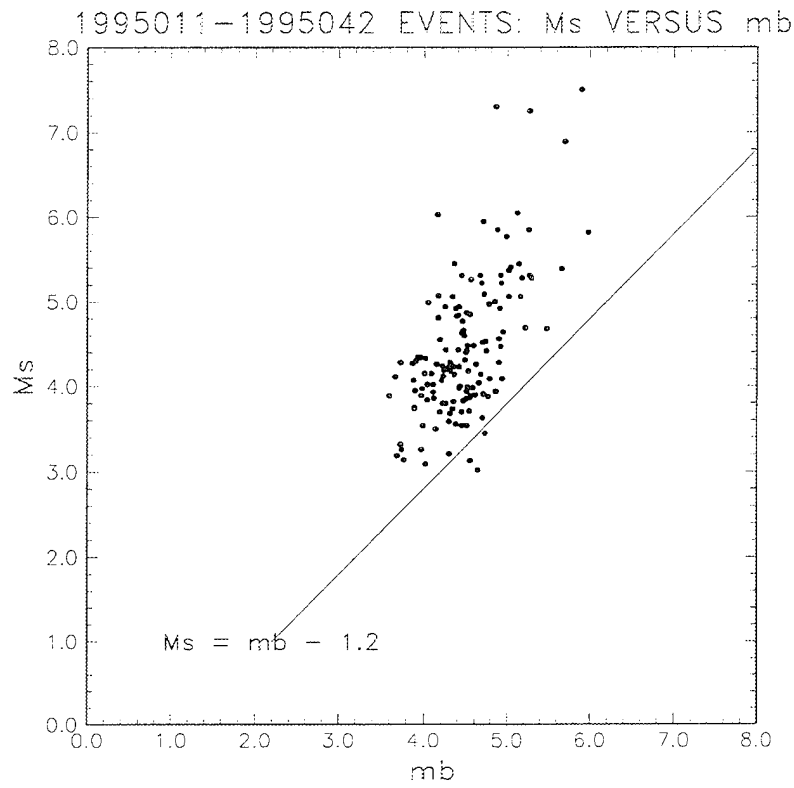


Figure 33. Scatter plot of M_s versus m_b .

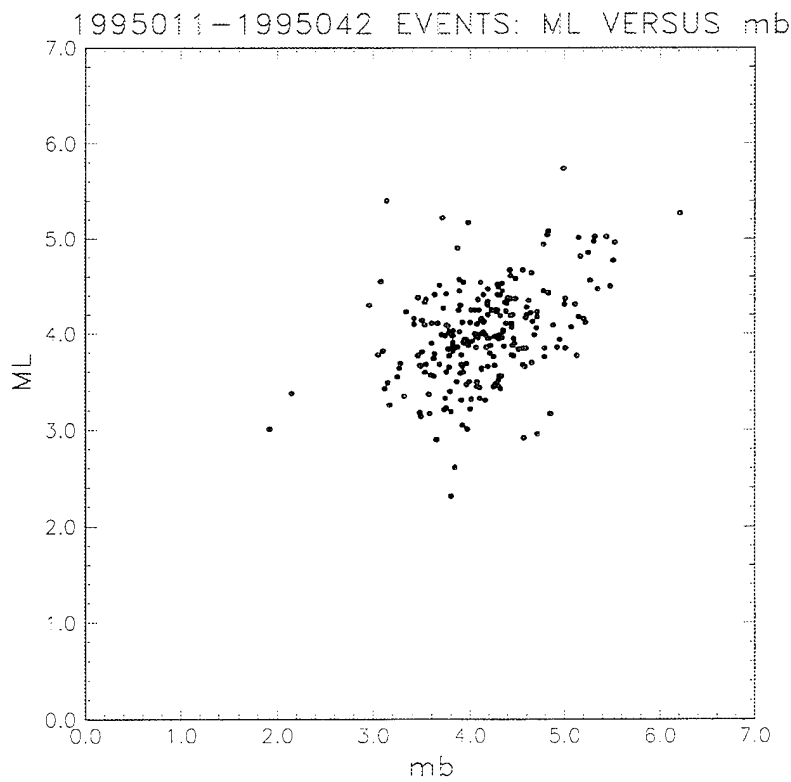


Figure 34. Scatter plot of M_L versus m_b .

3.2.5. Regional High-Frequency Amplitude Ratios

Regional phase amplitudes for the events during this period were computed by automated software at the CMR. Absolute maximum amplitudes were measured on 2-4, 4-6, 6-8 and 8-10 Hz rms beams within predicted group velocity or time windows defined in Table 2 for Pn, Pg, Sn and Lg. Similar measurements were made of noise amplitudes in predicted pre-Pn, pre-Pg, pre-Sn and pre-Lg windows, which are also summarized in Table 5. Note that the eight windows for predicted theoretical arrivals are used for all regions and stations.

Table 5. Description of regional phase amplitude measurements.

Phase	Window Starts	Window Ends
Pn	3 sec before Pn	6.4 km/sec
Pg	6.3 km/sec	6.0 km/sec
Sn	4.8 km/sec	4.2 km/sec
Lg	3.6 km/sec	3.0 km/sec
Pre-Pn noise	8 sec before Pn	3 sec before Pn
Pre-Pg noise	6.4 km/sec	6.3 km/sec
Pre-Sn noise	4.9 km/sec	4.8 km/sec
Pre-Lg noise	3.7 km/sec	3.6 km/sec

Figure 35 shows the number of regional events associated by each Alpha station, those for which Pn/Sn, Pn/Lg, Pg/Sn and/or Pg/Lg were computed, and the subset of these with signal-to-noise ratios (SNR) greater than 2 for Pn or Pg and Sn or Lg. (The legend associates the hatch patterns to these three cases.) There are a total of 634 events within regional distance ($\Delta < 20^\circ$) of at least one Alpha station. Except for MJAR, regional phase amplitudes were computed for most (487 of 634) regional events. For ARCES, FINES, GERES, LOR, MJAR, PDAR, PLCA, SPITS, WALA, WHY and WOOL, the number of events for which regional phase amplitudes were computed (given in the *originamp* table) exceeds the number of associated regional events in the *assoc* table. (This is because the regional phase amplitudes were based on automated time windows, not on explicit phase picks.) Only 249 of the 487 events had SNR greater than 2 for at least one regional P phase and Sn or Lg. Thus, less than 40% of the events detected within regional distances have useful high-frequency regional amplitude ratios.

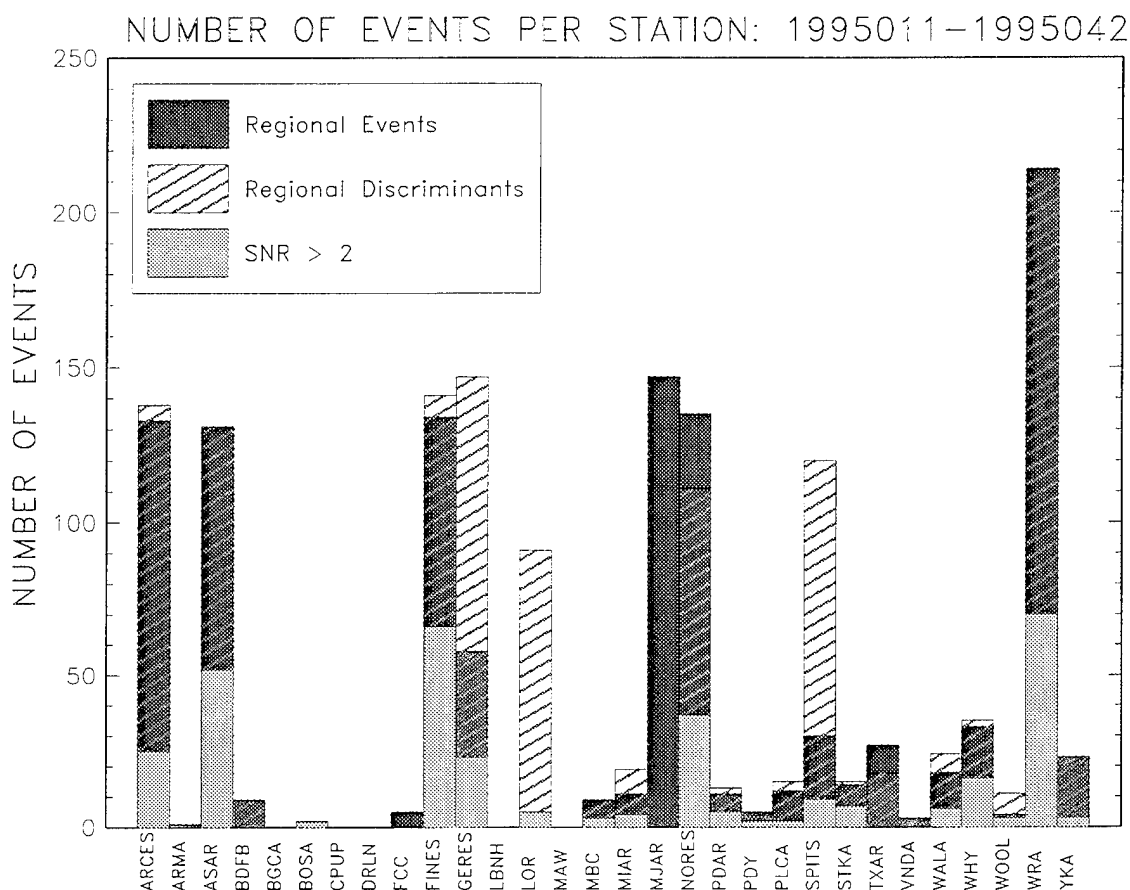


Figure 35. Number of regional events per Alpha station.

Figure 36 shows distributions of events versus the number of detecting regional stations in the *assoc* table per event, those for which regional discriminants were computed and those for which the regional discriminants have SNR > 2. There were 1152 events which were not associated by any station within regional distances. All but 5 of the 634 events in the *assoc* table, were associated by four or fewer stations. Regional amplitudes were computed for some events at as many as six stations. (Note that associations for some of these regional stations were missing in the *assoc* table.) However, of the events with SNR > 2 for both numerator and denominator of at least one regional amplitude ratio, there were only 9 events detected by three or more stations. Thus, events which cannot be identified by teleseismic discriminants will likely be analyzed using regional discriminant data from one to three, or possibly four, Alpha stations, at least until the density of the Alpha network changes. Supplemental regional data from Beta stations may also be used to improve identification performance for regional events.

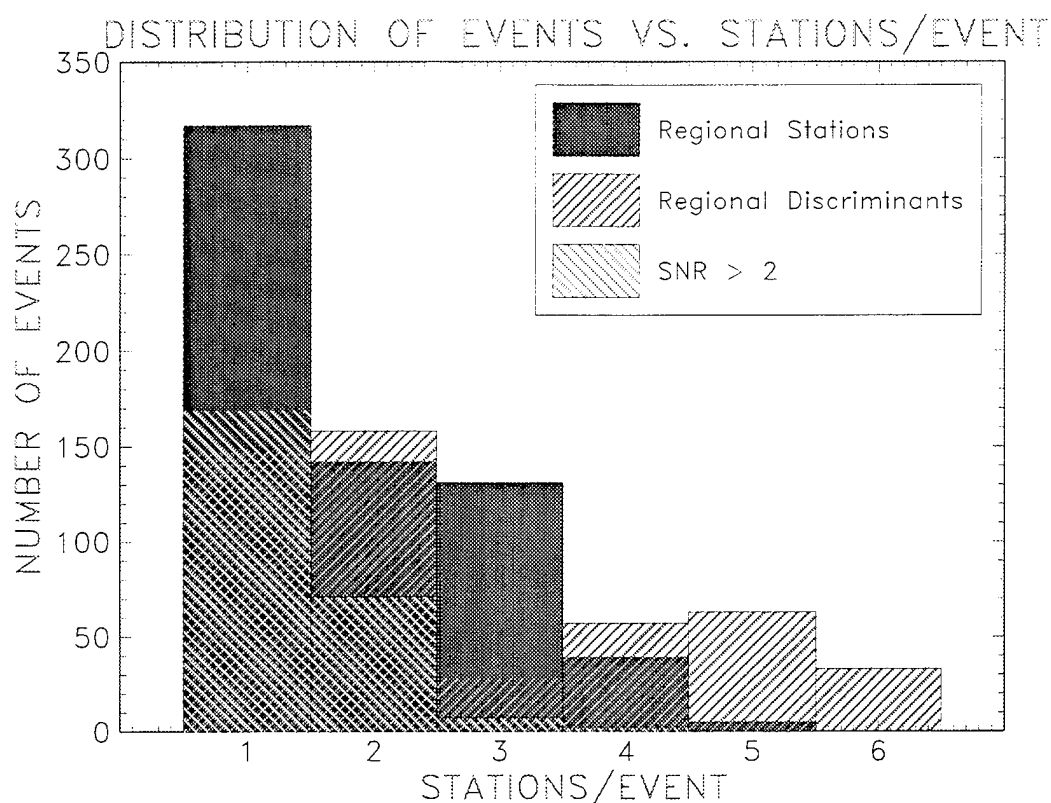


Figure 36. Distribution of regional events versus the number of stations per event.

Figures 37-40 show plots of P_n/S_n , P_n/L_g , P_g/S_n and P_g/L_g amplitude ratios, respectively, computed in four frequency bands (2-4, 4-6, 6-8 and 8-10 Hz), for each Alpha station. The markers are coded based on SNR: circles indicate SNR below 2 for either numerator or denominator, while asterisks indicate SNR greater than 2 for both numerator and denominator. Note that the majority of amplitude ratios are plotted as circles, indicating that most amplitude ratios do not satisfy a criteria of $SNR > 2$ for both numerator and denominator. Examination of the amplitude ratios also indicates that there are a very wide range in values (e.g., from 10^{-4} to 10^{+4} at station WRA) for events which are predominantly earthquakes.

Figures 41 and 42 show similar plots of P_n/S_n and P_n/L_g , respectively, in the same four frequency bands versus distance for the regional events and for all Alpha stations. Markers are defined as in Figures 37-40. There are a significant number of amplitude ratios in the 4-6, 6-8 and 8-10 Hz bands which are identically equal to 1.0 due to treating the amplitudes to only one significant digit. Most events fall along typical attenuation curves, but there is considerable scatter.

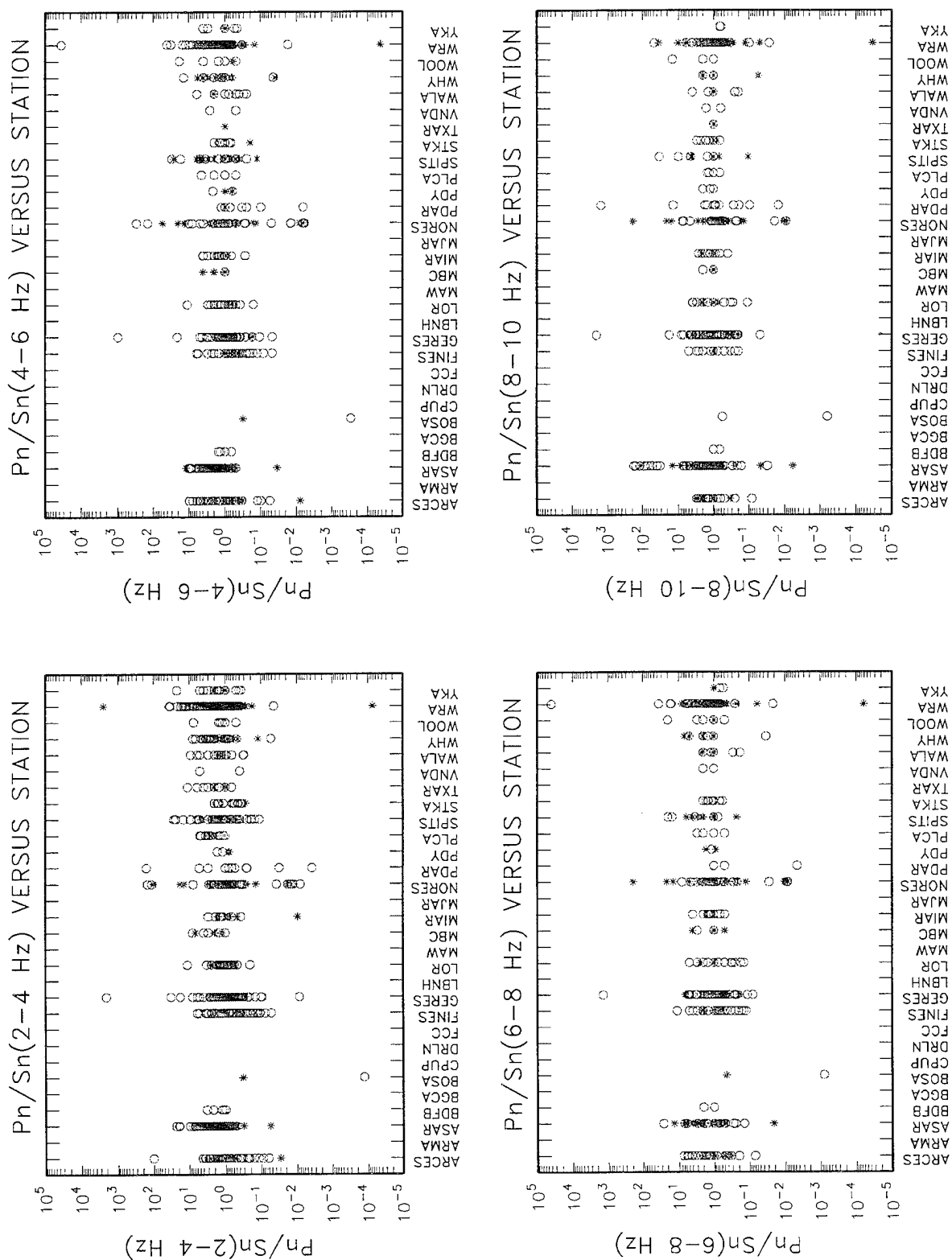


Figure 37. P_n/S_n in 4 frequency bands versus Alpha station. Circles indicate $\text{SNR} < 2$ for either numerator or denominator, while asterisks indicate $\text{SNR} > 2$ for both numerator and denominator.

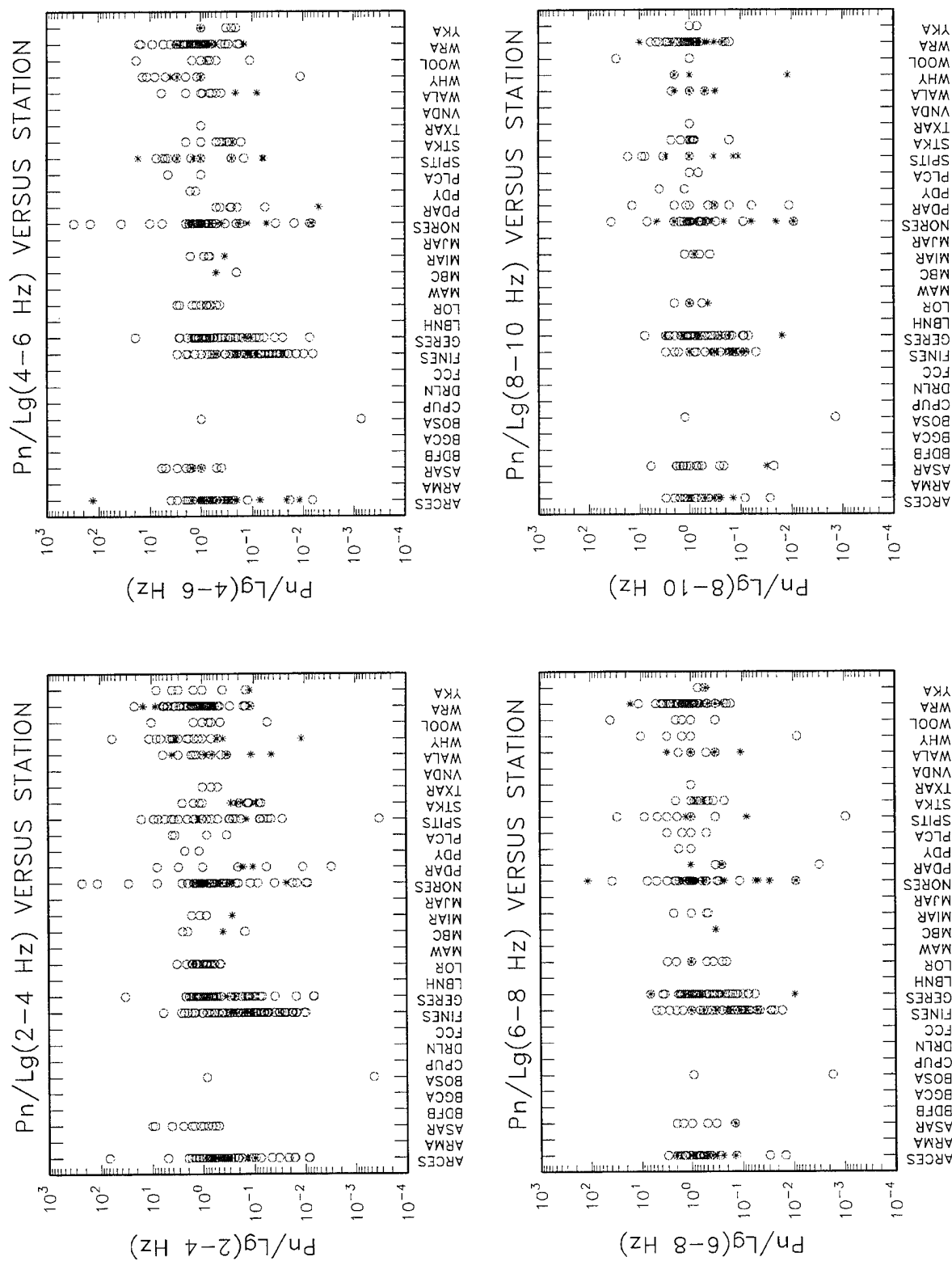


Figure 38. Same as Figure 37, but for P_n/L_g .

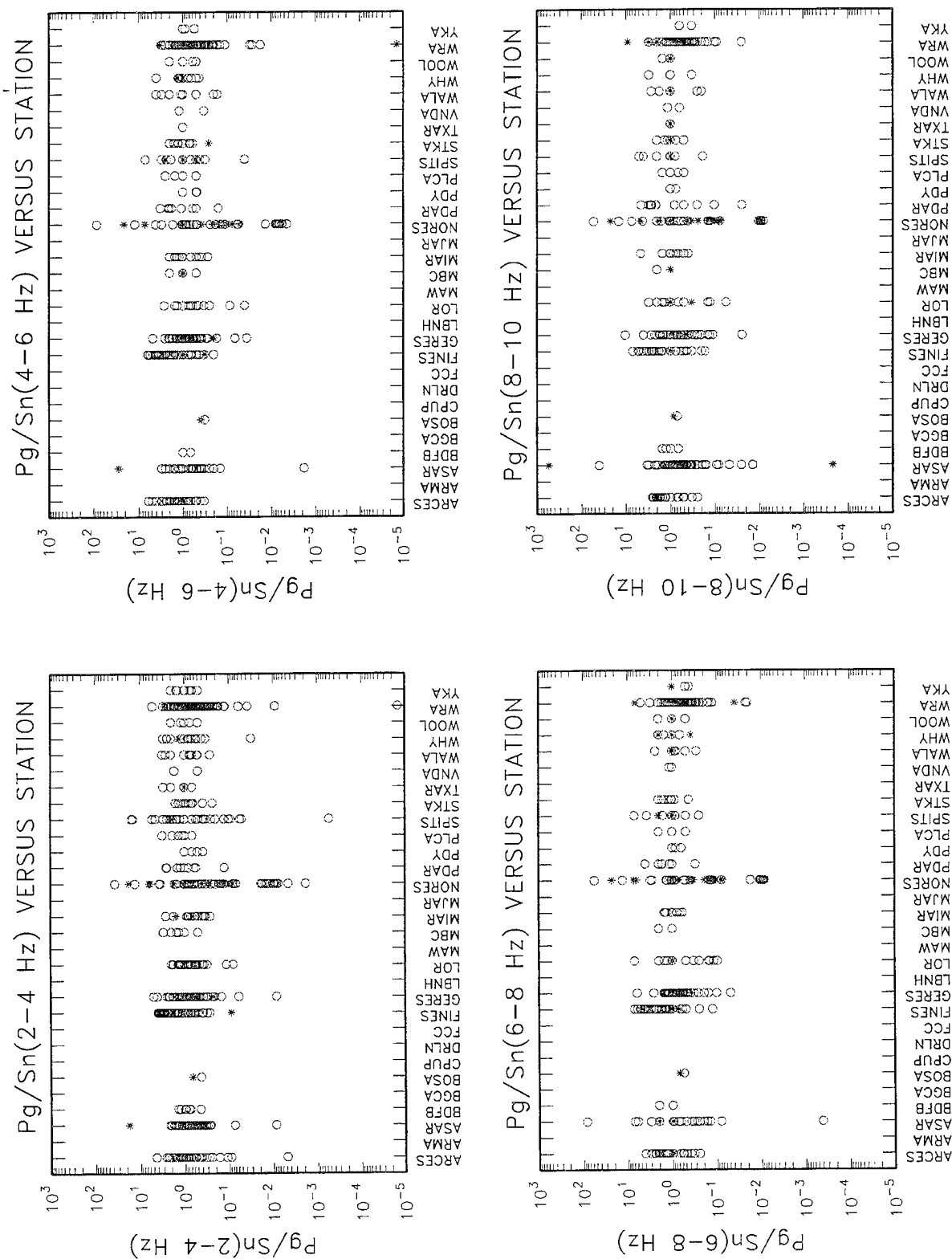


Figure 39. Same as Figure 37, but for Pg/Sn .

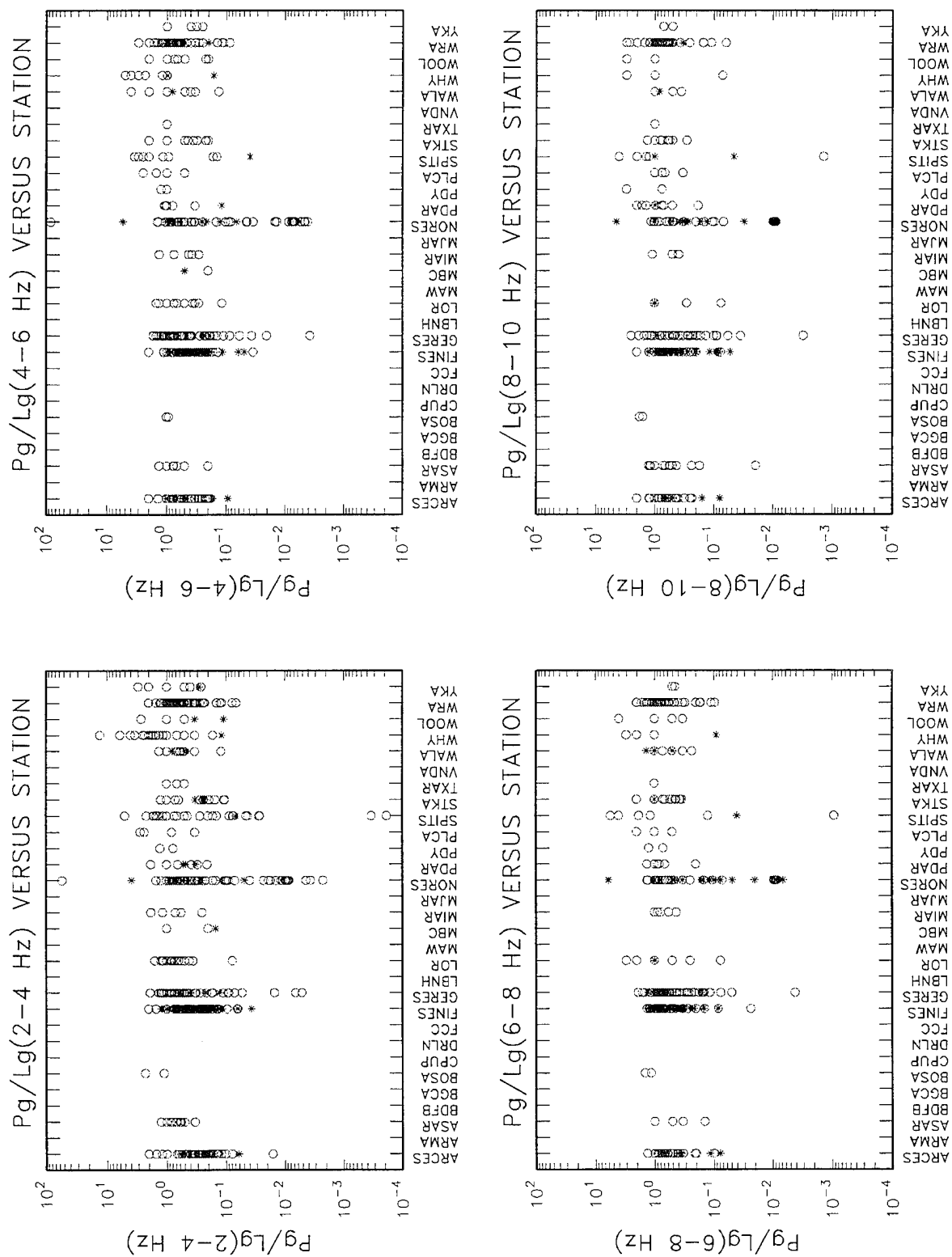


Figure 40. Same as Figure 37, but for Pg/Lg .

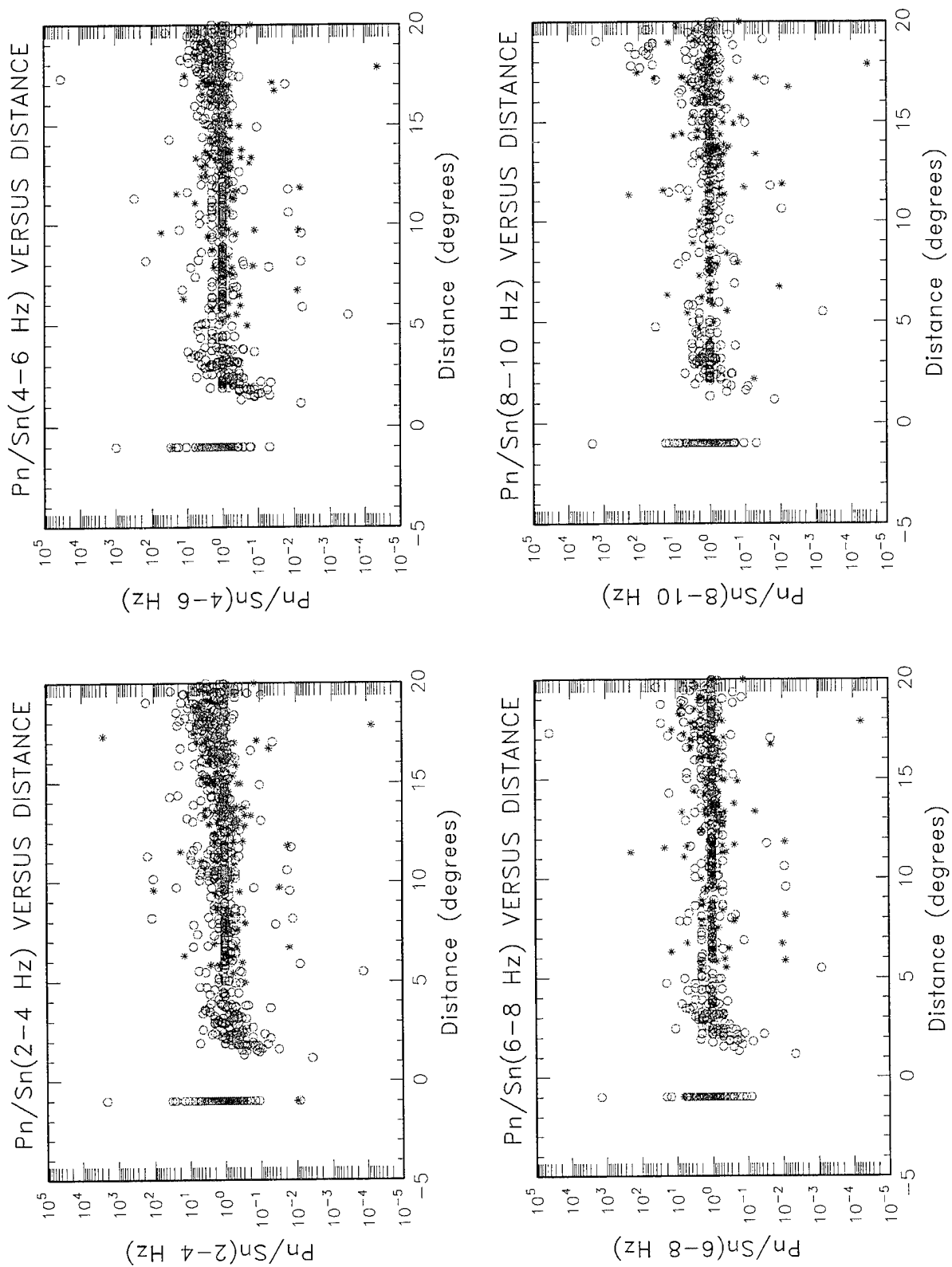


Figure 41. P_n/S_n in 4 frequency bands versus distance. Markers are defined as in Figure 37.

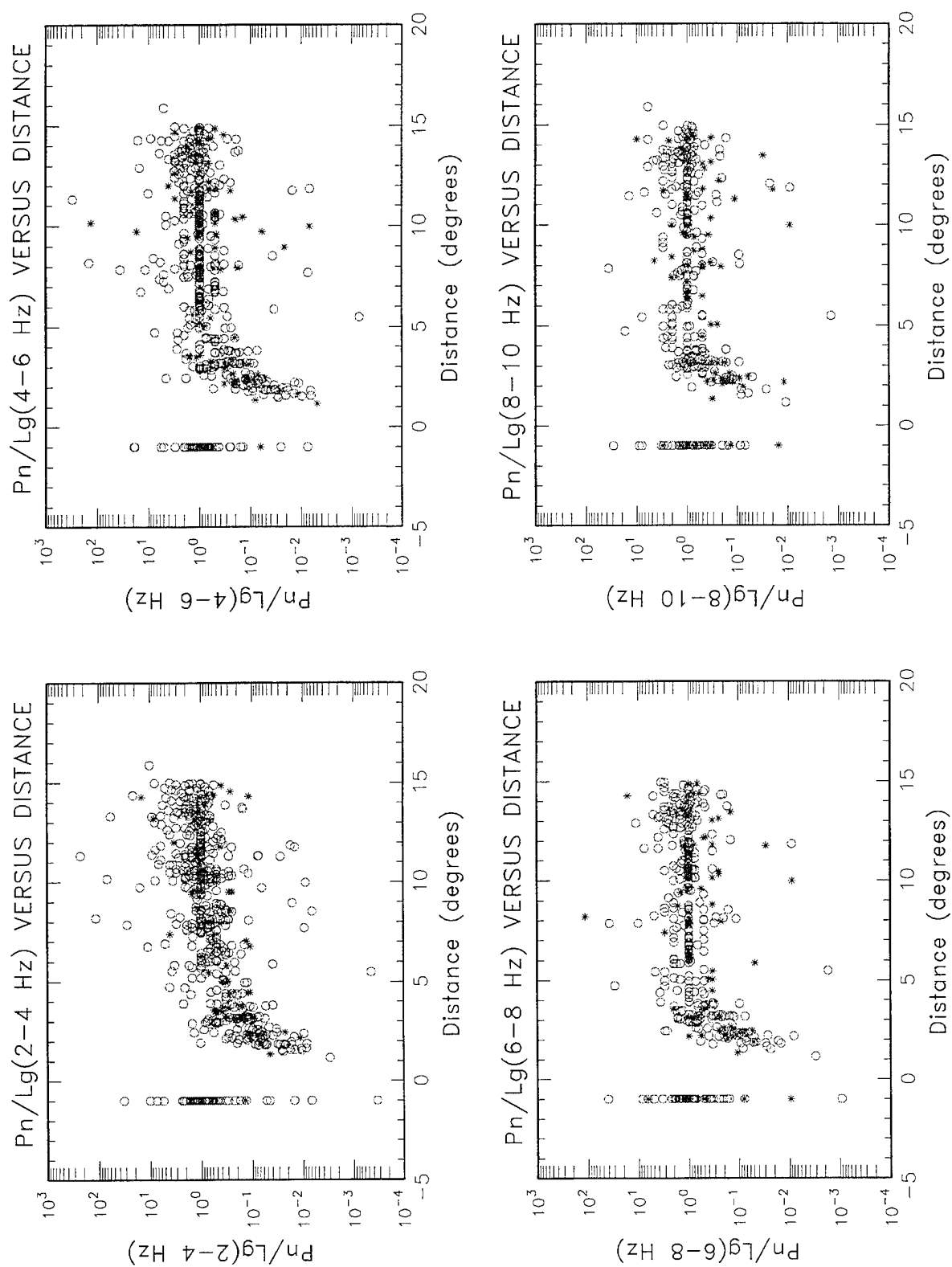


Figure 42. Same as Figure 41, but for Pn/Lg.

Some obvious questions arise regarding these measurements. First, why are there such a broad range of amplitude ratios, including some abnormally high values? Second, why are there cases in which the phase amplitudes are greater than 100 nm but the SNR is less than 2? Third, how robust are the phase windows to regional variations in crustal velocities? That is, do the fixed theoretical windows contain the true expected arrivals for some, most or all of the regional events? Fourth, how robust are these windows to hypocentral depth? Some of these questions are clearly related. By comparing the *originamp* table to the REB for 12 events with very high amplitude ratios (greater than 100), F. Ryall (1995) found the following peculiarities associated with the regional phase amplitude measurements.

1. Sn times in the *originamp* table are inconsistent with arrival times in the REB for events seen at the Australian and European arrays.
2. Most later phases for the 12 events have very small amplitudes (e.g., less than 1.0) and are close to or smaller than the “noise” amplitudes. Almost all are much smaller than “Pn” (e.g., by two orders of magnitude). For example, orid 286620 was an mb 5.2 event, 17.3 degrees from WRA. The WRA “Pn” amplitude for this event is 6272.0, while the “Pg” amplitude, which is only 20 sec after “Pn,” measures 1.9, i.e., 3300 times smaller. For the same event, the “Sn” amplitude is 0.2, while the “pre-Pn noise” amplitude is 0.1.
2. The automated program measured amplitudes for crustal phases (e.g., “Pg”) for events which were deep and for which the REB arrivals were P and S. Examples are orids 277917 and 292133, for which the depths were 244 and 195 km, respectively. (Note that the depth confidence intervals were too large, however, to classify these events as deeper than 10 km at a 95% confidence level.)
3. The high-frequency bandpass (8-10 Hz) gives amplitudes at stations ASAR and PDAR that are 12 to 50 times larger than the other bands, for all 12 events. This does not seem reasonable since ASAR is 17-18 degrees from the events. Thus, it should be expected that high-frequency content would be attenuated. Also, for orid 299937, PDAR has an 8-10 Hz “Pn” that is 20 times larger than 2-4 Hz “Pn” for a Gulf of California event (typically low-frequency), with a low-Q path of 19 degrees entirely in the tectonically active western North America.
4. Amplitudes are calculated for phases that were not associated (i.e., not listed in the REB *assoc* table) - Pg and Lg for all 12 events, as well as Sn for orids 284853, 299937, 300444.
5. Amplitudes are given for one station that was not listed in the REB and could not have recorded the event. For orid 298017, GERES is not listed in the REB, but has very large “Pn” and “pre-Pn noise” values in the *originamp* table. This event was in Russia and was probably a mine blast.

Amplitudes at the three Scandinavian arrays are quite small (less than 10). The high amplitudes listed for GERES (423.0-1963.0) were possibly for a noise spike or another event near the array.

Further investigation of the data (including the seismic waveforms) by D. Jepsen (1995) provided the following conclusions. First, there are numerous cases for which large noise spikes were not masked before computing the high-frequency amplitudes. Figure 43 shows an example of seismic waveforms for an event recorded by the Pinedale array. Large amplitude noise spikes were present on two of the channels.

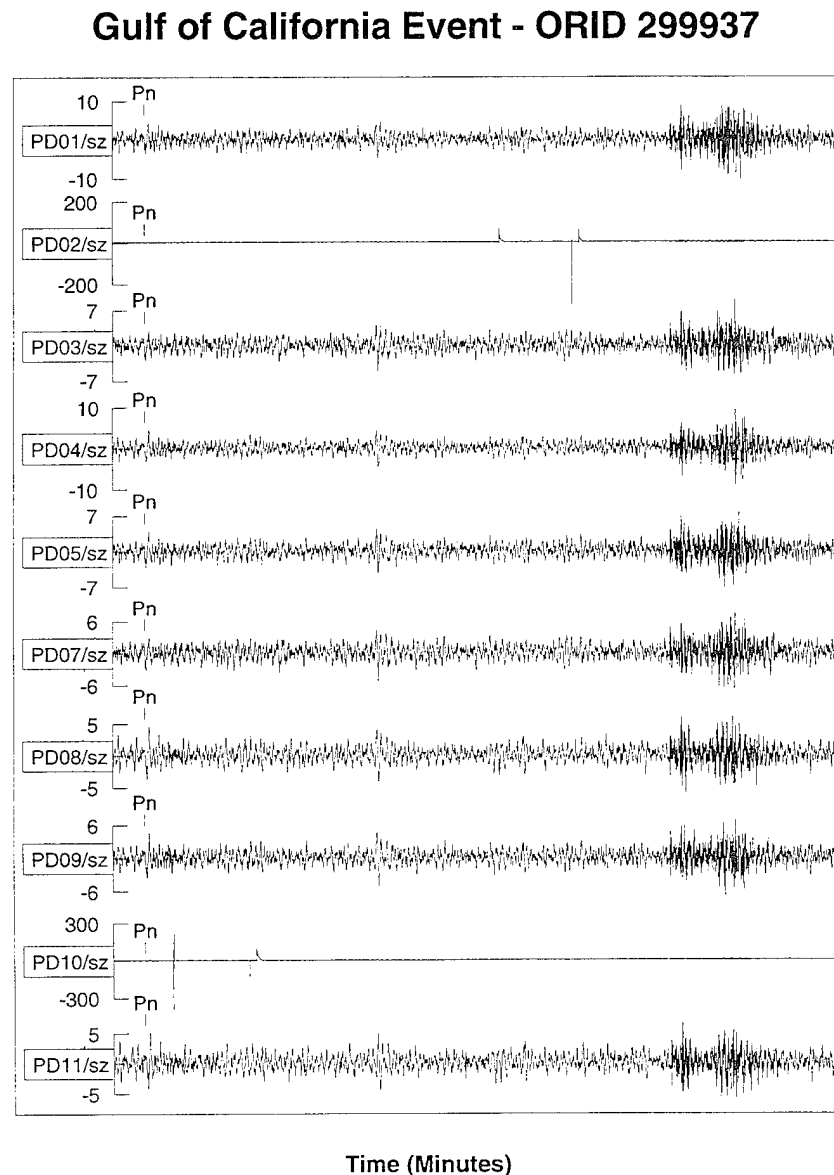


Figure 43. Seismic waveforms for a Gulf of California event which was recorded by the Pinedale array. Large amplitude noise spikes were present on two of the channels.

Second, the theoretical Sn velocity window does not contain the actual Sn arrivals, picked by seismic analysts, for the majority of events within ten degrees from an Alpha station (Figure 44). The window (dashed curves) in most cases was prior to the actual Sn arrivals, leading to unusually small Sn values. The solid line depicts the IASPEI91 travel time curve for Sn which is more consistent with the analyst's picks. Thus, although the Sn measurements are currently erroneous, the problem appears to have a simple solution.

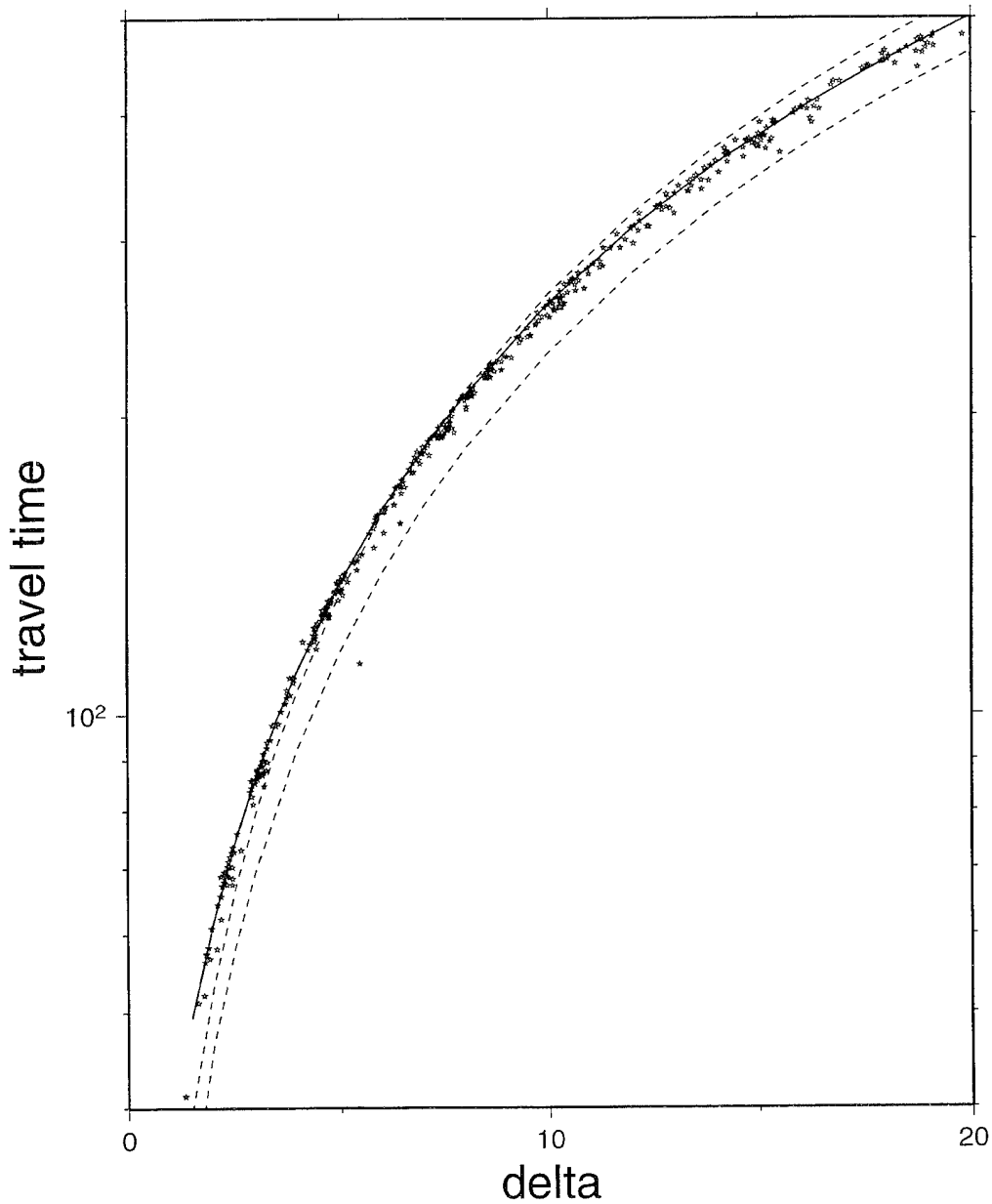


Figure 44. Sn travel times versus distance (stars) based on analyst picks for the one-month data set. Also plotted are the IASPEI91 Sn travel time curve (solid line) and the theoretical velocity window (dashed lines) used to make automated Sn measurements. (Courtesy of D. Jepsen.)

Third, the abnormally large 8-10 Hz amplitudes for some events is due to applying instrument response corrections in a frequency band near the Nyquist frequency for some stations or arrays where the instrument response falls off sharply. That is, most of the seismic energy in this band is at 8 Hz, while the correction applied is based on the instrument response at 9 Hz, which leads to a significant over-correction. Thus, amplitudes in the 8-10 Hz band, at stations with a Nyquist frequency of 10 Hz or less, should not be used and, possibly, not included in the database at all.

Although there are several significant problems with the high-frequency phase amplitude measurements, virtually all of the problems found have straightforward solutions. Current work by SAIC includes developing software to better mask noise spikes and modifying the predicted S_n time window to include the actual arrivals. Cross-checking the *originamp* table with the *assoc* table in the REB database is also expected to alleviate problems with interfering events, etc.

3.3. Utility of Event Characterization Parameters

Here we discuss the utility of teleseismic and regional event characterization parameters. We focus on determining how many events can be characterized as due to natural seismicity and on assessing how many ambiguous events remain due to a lack of any useful discriminants. Using depth, M_S :mb, location (offshore versus onshore), and high-frequency regional P/S and P/Lg discriminants to characterize the events, we obtain the following results for the 1786 events:

- 292 events have 95% depth confidence intervals deeper than 10 km and are thus classified as deep natural events.
- 143 events have M_S and mb measurements, of which all but 3 satisfy $mb - M_S < 1.2$. Data to compute M_S :mb confidence intervals were unavailable. (Only 6 of the 143 events were also classified as deep.)
- 454 remaining events (609 total) have 90% location error ellipses entirely offshore but there are no hydroacoustic data available to verify that these events were not offshore explosions.
- 324 remaining events (487 total) have high-frequency regional amplitude ratios available. Only 166 remaining events (249 total) have SNR greater than 2 for both numerator and denominator of at least one amplitude ratio for at least one regional station.
- Overall, 883 of 1786 events (49%) can potentially be identified, based on depth, location (plus hydroacoustic data eventually), and M_S :mb. Including high-frequency regional phase amplitude ratios with $SNR > 2$, a total of 1049 events (59%) can potentially be identified¹.

1. Note that peculiarities regarding the regional amplitude measurements must be resolved before a definitive assessment of their utility for event characterization can be obtained.

Thus, at best, there are still 511 teleseismic and 226 regional events which cannot be identified based on available information considered. That is, there are 737 of the 1786 events (41%) during the period 1955011-1995042 which cannot be classified as deep or offshore, and do not have M_S :mb or high-frequency regional discriminants with adequate SNR. Figure 45 summarizes these results. The bars indicate the numbers of: (1) total events; (2) offshore events; (3) deep events; (4) events with M_S :mb; (5) events with regional amplitude ratios (total and those with SNR>2); (6) teleseismic (T) and regional (R) events with one or more of the considered discriminants; and (7) teleseismic and regional events with none of the considered discriminants.

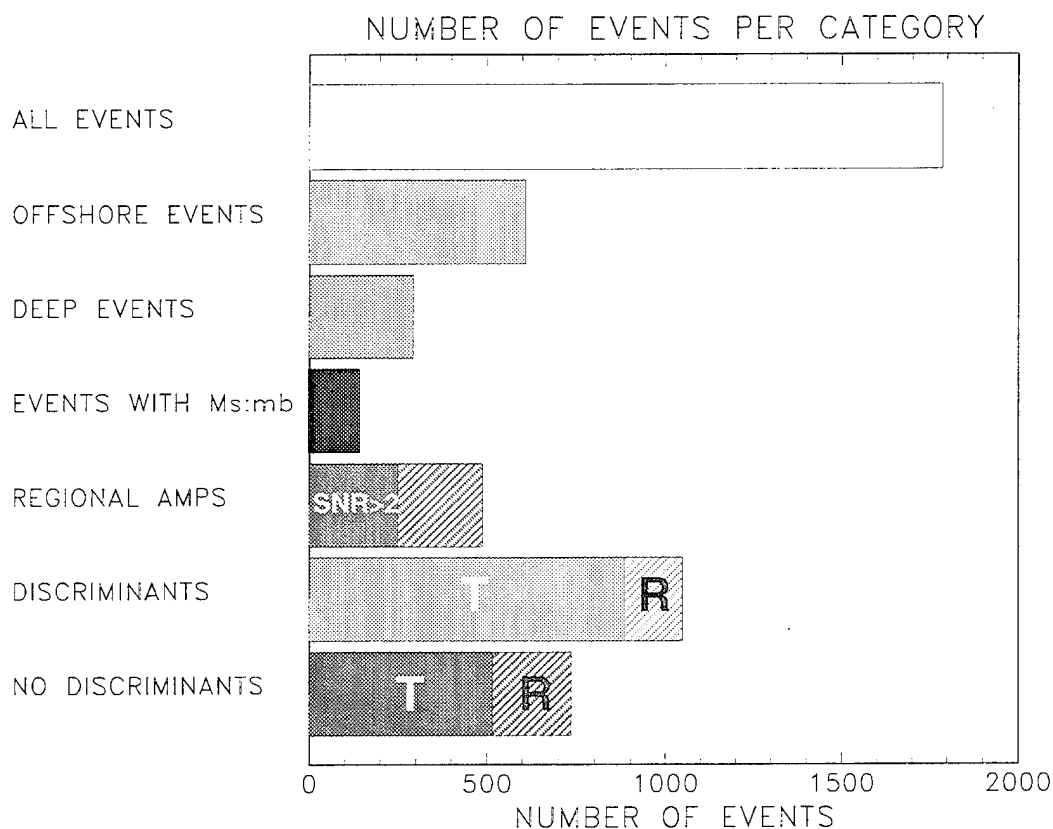


Figure 45. Distribution of events with various available discriminants.

Figure 46 shows locations of the 1049 events which are deep, offshore, have M_S :mb, and/or have at least one regional high-frequency amplitude ratio. Events for which regional amplitudes were computed occurred primarily in northern Europe and Scandinavia, in or near Australia, and in Alaska and Canada. Figure 47 shows locations (asterisks) and 90% error ellipses of the 511 teleseismic events which cannot be classified as deep or offshore, do not have M_S :mb, and do not have any regional P/S or P/Lg discriminants. The diamonds indicate the locations of the 226 regional events which do have at least one regional P/S or P/Lg discriminant, but with SNR less

than 2 for either numerator or denominator (or both). Alpha stations transmitting data to the CMR at the time of this study are shown in black, while projected Alpha stations are shown in light gray. Note that many of these events are at far regional to teleseismic distances from existing Alpha stations, but would be well within regional distances of future Alpha stations. Thus, additional planned Alpha stations will greatly help to reduce the number of events for which none of the considered discriminants are available or regional amplitude ratios have insufficient SNR.

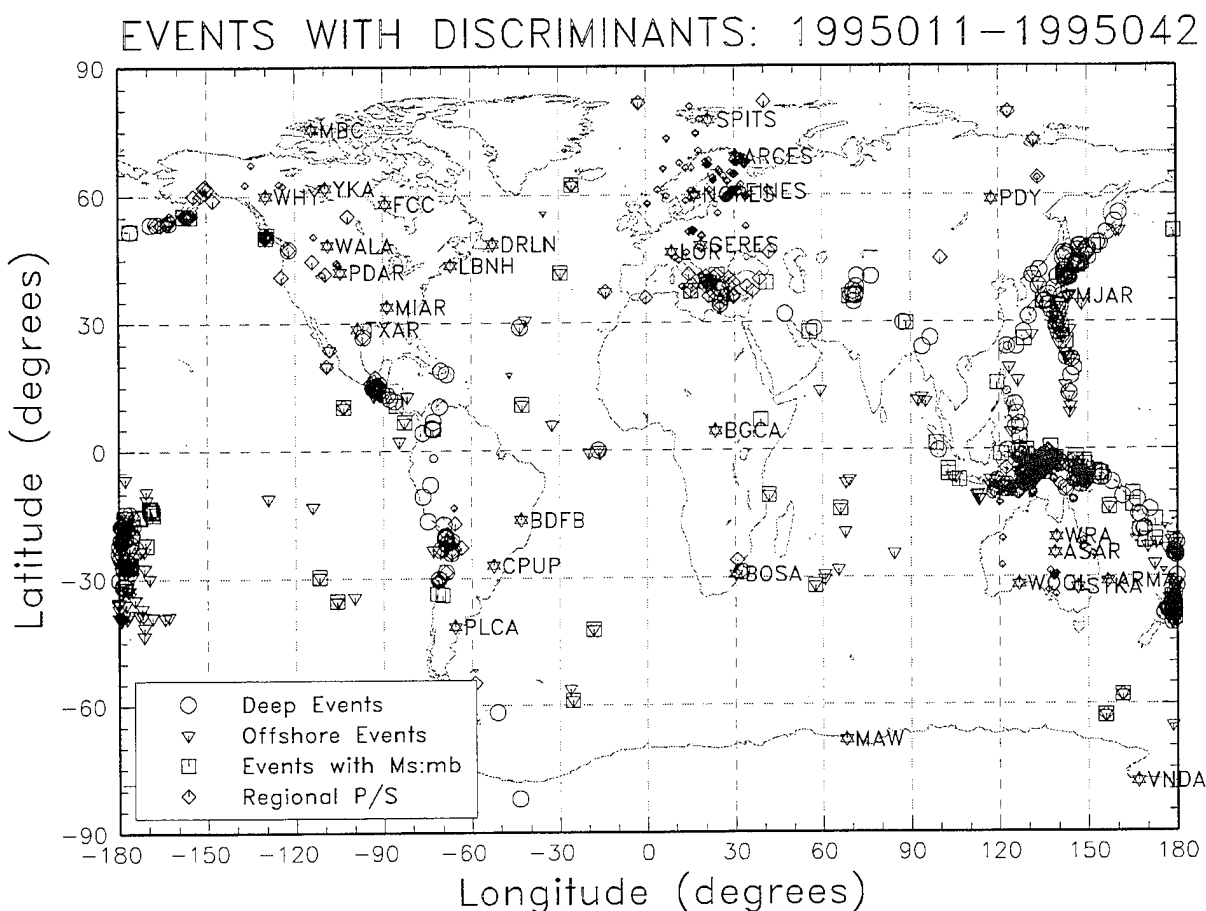


Figure 46. Locations of events which can be classified as deep, offshore, with $mb-M_S < 1.2$, or with at least one high-frequency regional amplitude ratio. Markers are coded by category.

There are, however, a significant number of events within regional distances of existing Alpha stations (e.g., from MJAR in Japan) for which no regional phases were associated, even after analyst review. For events which occurred between 1995001 to 1995027, there were only 158 of 444 events within regional distances for which Pn or Pg and Sn or Lg were among the associated phases. Possible explanations for this include (1) regional phase attenuation for events at far regional distances; (2) regional phase blockage (e.g., for events southeast of GERES); (3) deep

regional events (e.g., near MJAR) which do not produce crustal phases but whose 95% depth confidence intervals were not deeper than 10 km; and (4) possible phase association errors by the automated system which were not corrected after analyst review. Examples supporting the first three explanations have been found. Study of relevant waveforms is needed to determine whether additional regional phases could be identified based on further inspection by a seismic analyst.

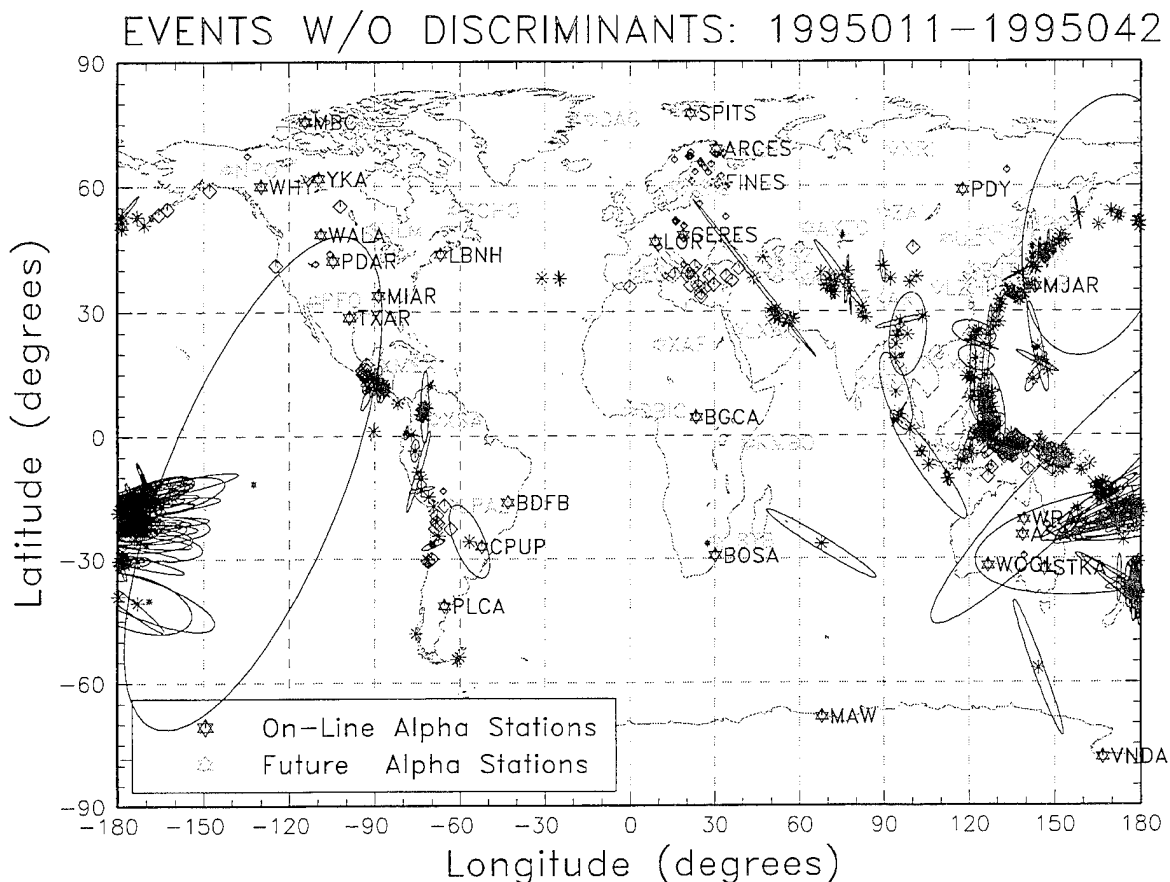


Figure 47. Locations of events for which none of the considered teleseismic and regional discriminants are available.

Last, Figure 47 shows epicentral location estimates of at least five events which appear to be clearly offshore, e.g., two in the north Atlantic Ocean, one in the south Pacific Ocean, and two in the Indian Ocean (one south and one west of Australia). The two in the north Atlantic are actually in the Azores Island region, while the two in the Indian Ocean and the one in the south Pacific have 90% error ellipses which overlap either Antarctica, Madagascar or North America. Jepsen (1995) found that several of the events with extremely large error ellipses had only one or two arrivals, on which these location estimates were based, and the events were subsequently omitted from the REB.

3.4. Conclusions and Recommendations

Based on the analyses described above for events which occurred between 11 January 1995 and 12 February 1995 of GSETT-3, we now provide some conclusions regarding the current capability to screen seismic events based on available information. We also provide some recommendations to make necessary improvements and to study unresolved issues.

First, requiring that the 95% confidence interval for depth be deeper than 10 km, 292 of the 1786 events (16%) are classified as deep natural events. If we also require that at least one depth phase be detected (since there may be potential biases in location and depth estimates), only 58 events are classified as deep. Thus, it is important to resolve the issue of biases in location and depth estimates, and to assess whether improvements in identifying depth phases can be made.

Second, there are 143 events (8%) with M_S :mb measurements. This low percentage is due to the fact that M_S measurements are currently made only for long-period instruments which are limited in number. Future work by S-Cubed includes array processing for broadband instruments, which should lead to a much higher percentage of events with M_S measurements. All but 3 of the 143 events satisfy $mb - M_S < 1.2$; however, the effect of magnitude biases has yet to be resolved and parameters to compute appropriate confidence intervals are still needed.

Third, 609 events have 90% location error ellipses entirely offshore, but there were no hydro-acoustic (HA) data available to verify that they were not offshore explosions. Future plans by ARPA include collection of HA data and implementation of algorithms to compute relevant event characterization parameters. Incorporating seismic data from Beta stations could lead to smaller error ellipses, thereby improving the capability to classify offshore events with high confidence.

Fourth, there were 487 events for which regional phase amplitudes were computed. Of these, 249 have at least one Pn or Pg phase and one Sn or Lg phase with SNR greater than 2. We found, however, numerous discrepancies in these measurements, specifically, some very large amplitude ratios (e.g., greater than 100) for events which are presumed earthquakes. Many of the anomalous values are due, in part, to large unfiltered noise spikes in the waveforms. The amplitude ratios also need to be distance-corrected. Theoretical windows used in computing Sn amplitudes often do not coincide with the actual Sn arrivals. Work to resolve these discrepancies is under way and appears promising. Further quality control is needed, however, before these regional discriminants can be used with confidence.

Overall, there were 883 events which can be identified by teleseismic measures of depth, offshore location and/or M_S :mb. An additional 166 events have regional discriminants with adequate SNR,

although further work is needed to recompute and validate these measurements. At best there are still 511 teleseismic and 226 regional events which cannot be identified based on available information considered. That is, there are 737 of the 1786 events (41%) during the period 1955011-1995042 which cannot be classified as deep or offshore, and do not have M_S :mb or high-frequency regional amplitude ratios with adequate SNR.

These results indicate that better global coverage is needed, which should be provided when additional Alpha and Beta stations come on-line. ARPA contractors are also implementing new discriminants and working on regional calibration issues that will improve magnitude, location and depth estimation. We are implementing a subsystem for event characterization/screening which will be used to objectively assess the combined utility of proposed discriminants.

Among the algorithms to be integrated is the multivariate population (i.e., outlier) analysis described in Section 1. In this approach, it is assumed that events above mb 3 are predominantly earthquakes with potentially one or at least a small number of nuclear explosions. That is, we assume that there will be very few chemical mining blast above mb 3. Note that of the 1459 events with mb measurements, there were only 35 below mb 3. Accounting for the bias of 0.3 units in the IDC mb values relative to QED mb values implies that roughly 98% of the events during this period were actually above mb 3.3. This suggests that the majority of events will fall in the regime where application of the outlier analysis is valid.

Since events may be observed by several (e.g., 2 to 5) stations within regional distances, we have also been addressing the problem of how to best combine regional event characterization data from multiple stations in the population analysis. We describe the solution to this problem in the following section.

Among future issues that need to be addressed are:

- The adequacy of hydroacoustic data for identifying offshore events;
- The adequacy of infrasonic data for identifying atmospheric or shallow-buried events;
- The accuracy of location and depth estimates (i.e., are there significant untreated biases which require extensive regional calibration?);
- The performance of our multivariate event characterization system once a more complete set of event characterization parameters becomes available.

4. Optimizing Multivariate Network Evidence for Outlier Detection

4.1. Introduction

Fisk et al. (1993, 1994) have presented and applied to seismic data a multivariate approach, based on the likelihood ratio, to test for outliers. In general, there are numerous types of regional measurements that can be used as discriminants, which may be available at multiple (e.g., 2 to 5) Alpha stations and it is not clear from the outset how to best combine this information in a test for outliers. Here we address a fundamental problem of how to utilize multivariate discriminant data from multiple stations in order to optimize the power of the outlier test for fixed false alarm rate.

There are at least three approaches to this problem. The first is to simply insert all available features that are thought to discriminate into the likelihood ratio. The second is to perform an optimal weighting of some or all of the discriminants first and then insert the weighted combinations into the likelihood ratio. The third is to perform separate tests, based on the likelihood ratio and subsets of discriminants, calling an event an outlier if it is found to be an outlier by any of the individual tests. The significance levels of the individual tests, in this case, must be appropriately modified to maintain the overall false alarm rate of the combined results.

In Section 4.2, analytic expressions are derived for the power of each of these tests. In Section 4.3, a parametric study is presented in which the power of the three tests are compared in order to determine conditions for which a particular test is favored over the others. In Section 4.4, some conclusions and recommendations are provided for operational application to seismic monitoring.

4.2. Technical Approach

Suppose there are two populations of events π_1 and π_2 (e.g., earthquakes and explosions) and that a p -dimensional vector of discriminants, $X' = \left(X^{(1)}, \dots, X^{(p)} \right)$, is used to characterize the event type for each event. Given n previous observations from π_1 only, x_j for $j = 1, \dots, n$, allocation of a new observation, x , as an outlier or not is accomplished by testing the hypothesis

$$H_0: x_1, x_2, \dots, x_n, x \in \pi_1 \quad \text{versus} \quad H_1: x_1, x_2, \dots, x_n \in \pi_1, x \notin \pi_1. \quad (\text{EQ 1})$$

The likelihood ratio can be used to test whether the new event is an outlier of the first population or not. Under the assumption¹ that $X \sim N(\mu^{(i)}, \Sigma)$ if $X \in \pi_i$, it can be shown (e.g., Anderson, 1984, Chapter 5) that the likelihood ratio statistic to test a new observation, x , is given by

1. Note that if the discriminant data do not have a multivariate normal distribution, the Box-Cox transformation (Box and Cox, 1964) can be used to transform the data to approximate normality.

$$\lambda = \left(1 + \frac{1}{n+1} (x - \bar{x})' \hat{\Sigma}^{-1} (x - \bar{x}) \right)^{-\frac{n+1}{2}} = \left(1 + \frac{1}{n-1} T^2 \right)^{-\frac{n+1}{2}}, \quad (\text{EQ 2})$$

where

$$\bar{x} = \frac{1}{n} \sum_{j=1}^n x_j \text{ and } \hat{\Sigma} = \frac{1}{n} \sum_{j=1}^n (x_j - \bar{x}) (x_j - \bar{x})' \quad (\text{EQ 3})$$

are maximum likelihood estimates of $\mu^{(1)}$ and Σ , respectively. It can further be shown that

$$\frac{n-p}{p(n-1)} T^2 \sim F_{p, n-p}(\delta), \quad (\text{EQ 4})$$

where $F_{p, n-p}(\delta)$ is the noncentral F-distribution with p and $n-p$ degrees of freedom and noncentrality parameter $\delta = \frac{n}{n+1} \Delta\mu' \Sigma^{-1} \Delta\mu$, where $\Delta\mu = \mu^{(i)} - \mu^{(1)}$ if $x \in \pi_i$. Note that if the new event is from π_1 , the noncentrality parameter is zero, yielding a central F-distribution.

Small values of λ provide evidence against H_0 . Thus, the outlier test is: reject H_0 if $\lambda < \lambda_\alpha$ where λ_α is the critical value such that the test has α significance level. That is, λ_α or, equivalently, $F_{p, n-p}^{(\alpha)}$ is set such that $P[\lambda < \lambda_\alpha | H_0] = P[F_{p, n-p} > F_{p, n-p}^{(\alpha)}] = \alpha$, using the central F-distribution. The power of the test is the probability of rightfully rejecting H_0 when $x \notin \pi_1$, and is given by $P[\lambda > \lambda_\alpha | H_1] = P[F_{p, n-p}(\delta) < F_{p, n-p}^{(\alpha)}]$, using the noncentral F-distribution. Note that if the sample size n is sufficiently large, the noncentral F-distribution becomes the noncentral χ^2 -distribution with p degrees of freedom and noncentrality parameter $\delta = \Delta\mu' \Sigma^{-1} \Delta\mu$.

Now consider three separate hypothesis tests which differ by how the p -dimensional discriminant vector is used as input into the likelihood ratio. We assume for now that the sample size is sufficiently large so that the χ^2 -distribution may be used. The three tests are defined as follows:

Test 1: Full Vector Case: Insert the full p -dimensional vector for the training data and new event into the expression for λ . Using the central χ^2 -distribution with p degrees of freedom, set critical value so that the test has α significance level. Compute the power using a noncentral χ^2 -distribution with p degrees of freedom and noncentrality parameter given by $\Delta\mu' \Sigma^{-1} \Delta\mu$.

Test 2: Minimum Variance Weighting Case: Compute the linear combination of the p discriminants, $z = a'x$, where $a' = (a_1, a_2, \dots, a_p)$ minimizes the variance of z , subject to the constraint that $a'\beta = 1$ for $\beta = (1, 1, \dots, 1)$. It may be shown that the mean and variance of z are given by $\mu_z = a'\mu$ and $\sigma_z^2 = a'\Sigma a$. The vector a which minimizes σ_z^2 is given by

$a = \Sigma^{-1}\beta/\beta'\Sigma^{-1}\beta$. Hence, $\sigma_z^2 = 1/\beta'\Sigma^{-1}\beta$. (Note that if the correlations are zero, this procedure is equivalent to inverse variance weighting of the p discriminants.) Insert values of the scalar z for the training data and new event into the expression for λ . Using the central χ^2 -distribution with I degree of freedom, set critical value so that test has α significance level. Compute the power using a noncentral χ^2 -squared distribution with 1 degree of freedom and noncentrality parameter given by $\Delta\mu_z^2/\sigma_z^2 = \left(\beta'\Sigma^{-1}\Delta\mu\right)^2/\beta'\Sigma^{-1}\beta$.

We also examine two variations of Test 2. In the first, we use inverse variance weighting where $a = \Sigma^{-1}\beta/\beta'\Sigma^{-1}\beta$ as above, but with the correlations set to zero. Alternatively, we consider the minimum variance combination with the further restriction that all components of a are positive. These two variations of Test 2 are referred to as Tests 4 and 5, respectively. As we show below, neither of these alternatives provide an improvement in power under the assumptions considered.

Test 3: "At Least One" Case: Insert each component of the p -dimensional discriminant vector into separate expressions for λ . Using the central χ^2 -distribution with I degree of freedom, set the critical values so that each test has α/p significance level. (An event is considered an outlier of π_1 if it is found to be an outlier by any of the individual tests. Note that setting the significance level of each test to α/p yields an overall significance level less than or equal to α .) Compute the overall power of the test by simulating new observations from π_2 and determining the percentage of events for which either discriminant value violates the respective threshold.

4.3. Parametric Power Comparison

We performed a parametric study to assess the conditions for which a particular test is preferred over the other two, based on its relative power. Assume for now that $p = 2$, i.e., that there are two scalar components of the discriminant vector. For example, the two components could be Pn/Lg and Pn/Sn or Pn/Lg in two different frequency bands at a single station, or Pn/Lg in the same band at two different stations. (In Section 4.4, we will discuss how these results relate to the general case of p discriminants.) In the following, we set the significance level at $\alpha = 0.01$. Also setting $\sigma_1 = 1$ without loss of generality, the free parameters are $\sigma_2, \rho, \Delta\mu_1, \Delta\mu_2$.

Figure 48 shows a comparison of tabulated power of each of the three tests for $\sigma_2 = 1$ and various values of the correlation coefficient from -0.6 to +0.9. Each plot shows values of the power for fixed ρ and various values of $\Delta\mu_1, \Delta\mu_2$ from 0 to 4. The numbers for each parametric case are ordered by test number, i.e., upper, middle and lower values are for Tests 1, 2 and 3, respectively. Figure 49 is similar to Figure 48, except that $\sigma_2 = 2$. Examination of the tables in Figures 48 and 49 indicates that there is no single test which provides the greatest power under all parametric conditions. This is further illustrated in Figures 50 and 51 which show power curves

for the three tests versus correlation for various values of $\Delta\mu_1$ and $\Delta\mu_2$. The solid, dashed and dotted curves represent the powers of Tests 1, 2 and 3, respectively. Note that the power of Test 3 typically decreases as the correlation increases, although this test is the least sensitive to correlation as might be expected. The power of Test 2 decreases monotonically with increasing correlation if the variances are equal since $\Delta\mu_z$ is independent of the correlation for this case, while σ_z^2 increases monotonically with increasing correlation. The power of Test 1 also decreases monotonically with increasing correlation until the correlation becomes relatively high, provided $\Delta\mu_1$ and $\Delta\mu_2$ are different. This occurs because Test 1 detects outliers with inconsistencies in the correlation structure.

Note that Test 2 has the greatest power if the correlation is sufficiently small, depending on $\Delta\mu_1$ and $\Delta\mu_2$. Test 3 can have the greatest power if the correlation is in a particular range, which also depends on $\Delta\mu_1$ and $\Delta\mu_2$. This observation makes it tempting to establish a rule whereby we use a particular test if the correlation is in a particular range. Unfortunately, the danger associated with doing this lies in the fact that we will not know $\Delta\mu_1$ and $\Delta\mu_2$ in most situations. Thus, it is not clear how to establish a criterion on the correlation which is valid for all possible values of $\Delta\mu_1$ and $\Delta\mu_2$. For example, Test 2 can yield extremely poor power if $\Delta\mu_1$ and $\Delta\mu_2$ are considerably different.

If we are, however, confident that $\Delta\mu_1$ and $\Delta\mu_2$ are not dramatically different, such a rule can be established of the form:

- If σ_1 and σ_2 are significantly different, use Test 2.
- If σ_1 and σ_2 are similar and $\rho < 0$, use Test 2.
- If σ_1 and σ_2 are similar and $\rho > 0$, use Test 1 (or possibly Test 3 if $0 < \rho < 0.6$).

Note that while there are ranges of the parameters for which Test 2 or Test 3 have the greatest power, Test 1 generally has comparable or greater power than the other two tests over all parameters and there are no situations in which using Test 1 yields dramatically poor results. To illustrate this further, Figures 52 and 53 show the difference in the powers of Tests 2 and 1 and Tests 3 and 1, respectively, versus correlation for various values of $\Delta\mu_1$ and $\Delta\mu_2$ between 0 and 4. Figure 52 shows that while there are cases for which Test 2 can provide roughly a 10% increase in power over Test 1, there are many cases for which Test 2 can provide dramatically poorer power, particularly if $\sigma_1 = \sigma_2$. Figure 53 shows that while there are also cases for which Test 3 can provide roughly a 5% to 10% increase in power over Test 1, there are many cases for which Test 2 can provide dramatically poorer power than Test 1 (e.g., by as much as 90%), depending primarily on the correlation and the values of $\Delta\mu_1$ and $\Delta\mu_2$.

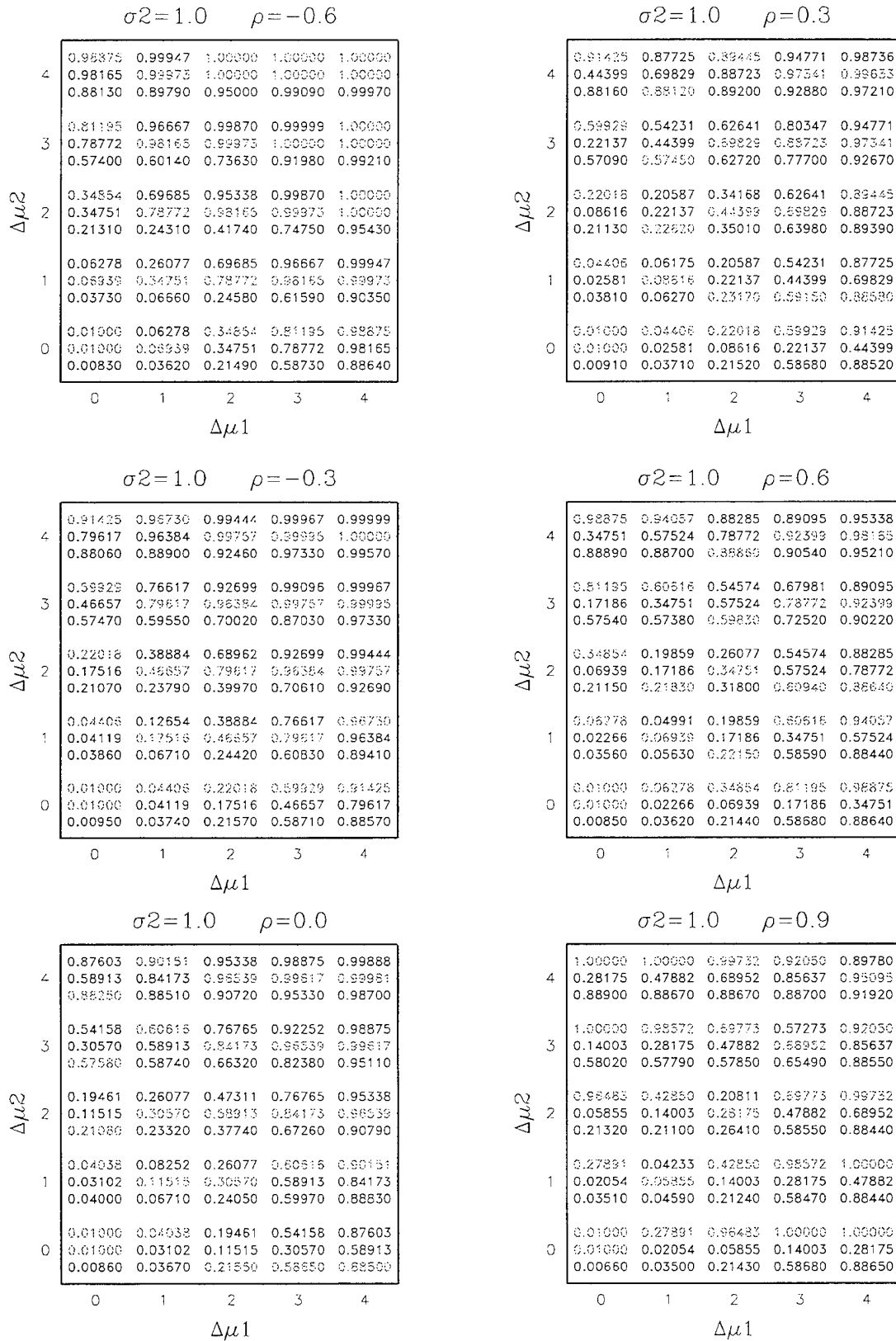


Figure 48. Power comparison of the three tests for $\sigma_1 = \sigma_2 = 1$.

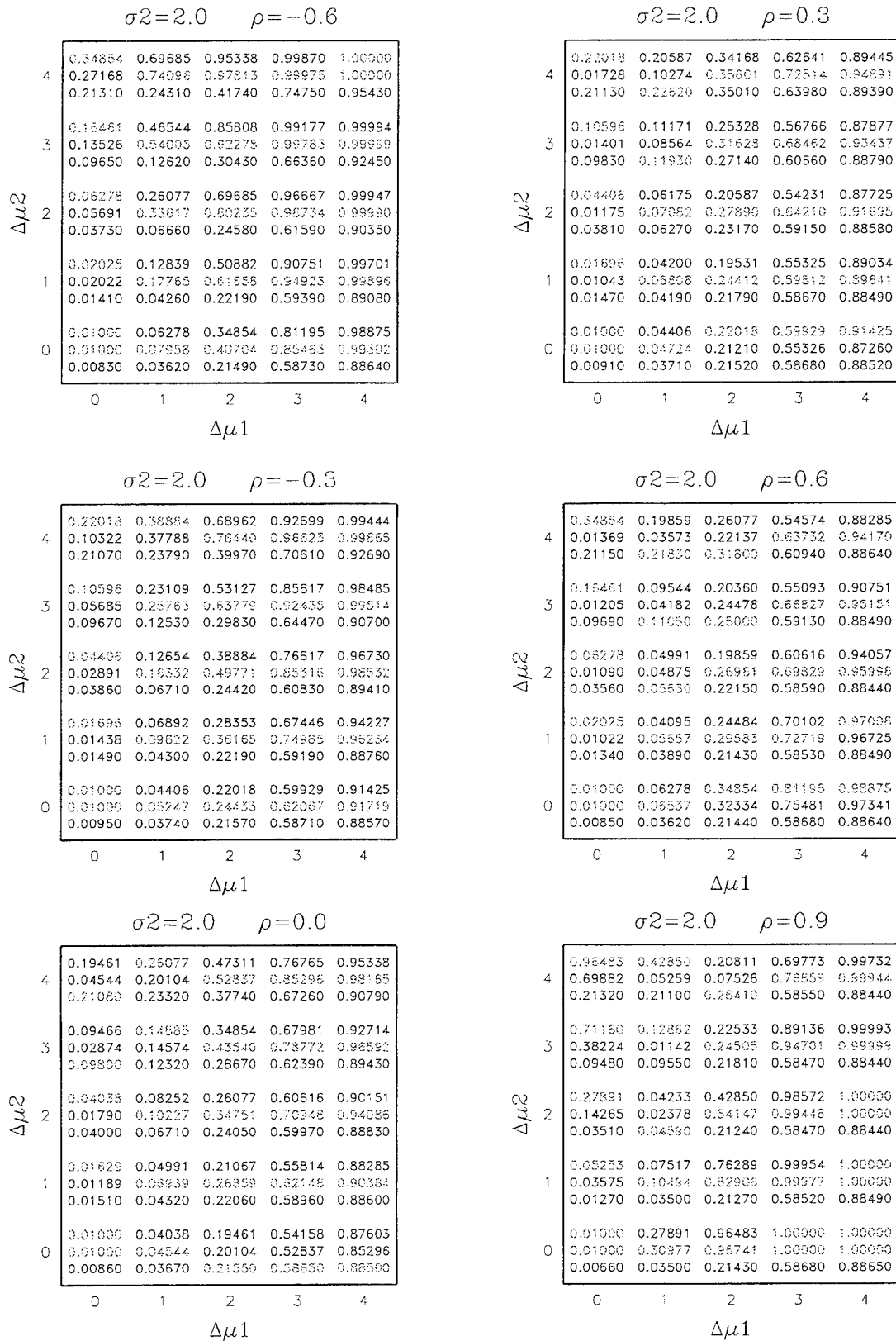


Figure 49. Power comparison of the three tests for $\sigma_1 = 1$ and $\sigma_2 = 2$.

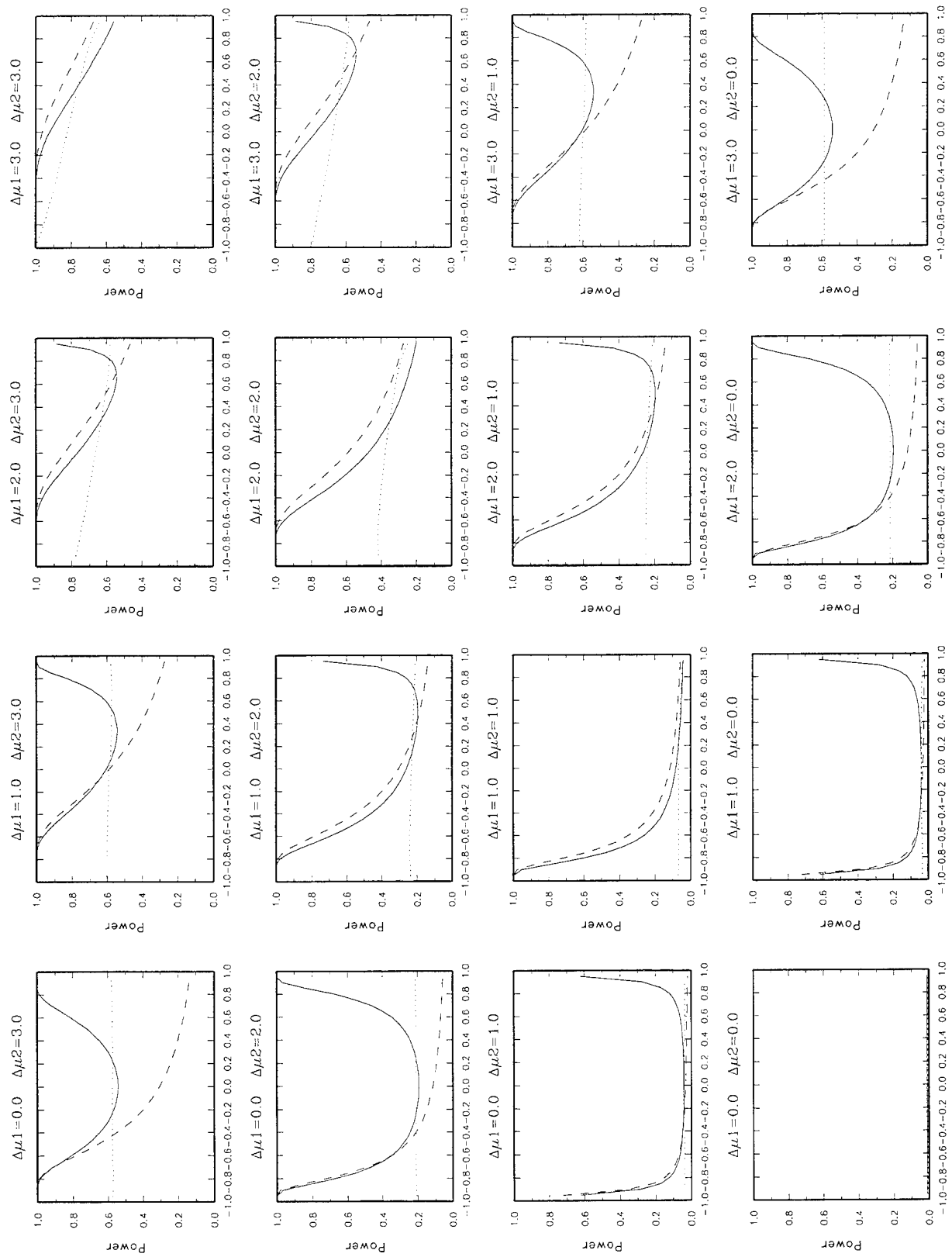


Figure 50. Power of Tests 1 (solid), 2 (dashed) and 3 (dotted) versus ρ for $\sigma_1 = \sigma_2 = 1$ and various values of $\Delta\mu_1$ and $\Delta\mu_2$ from 0 to 3.

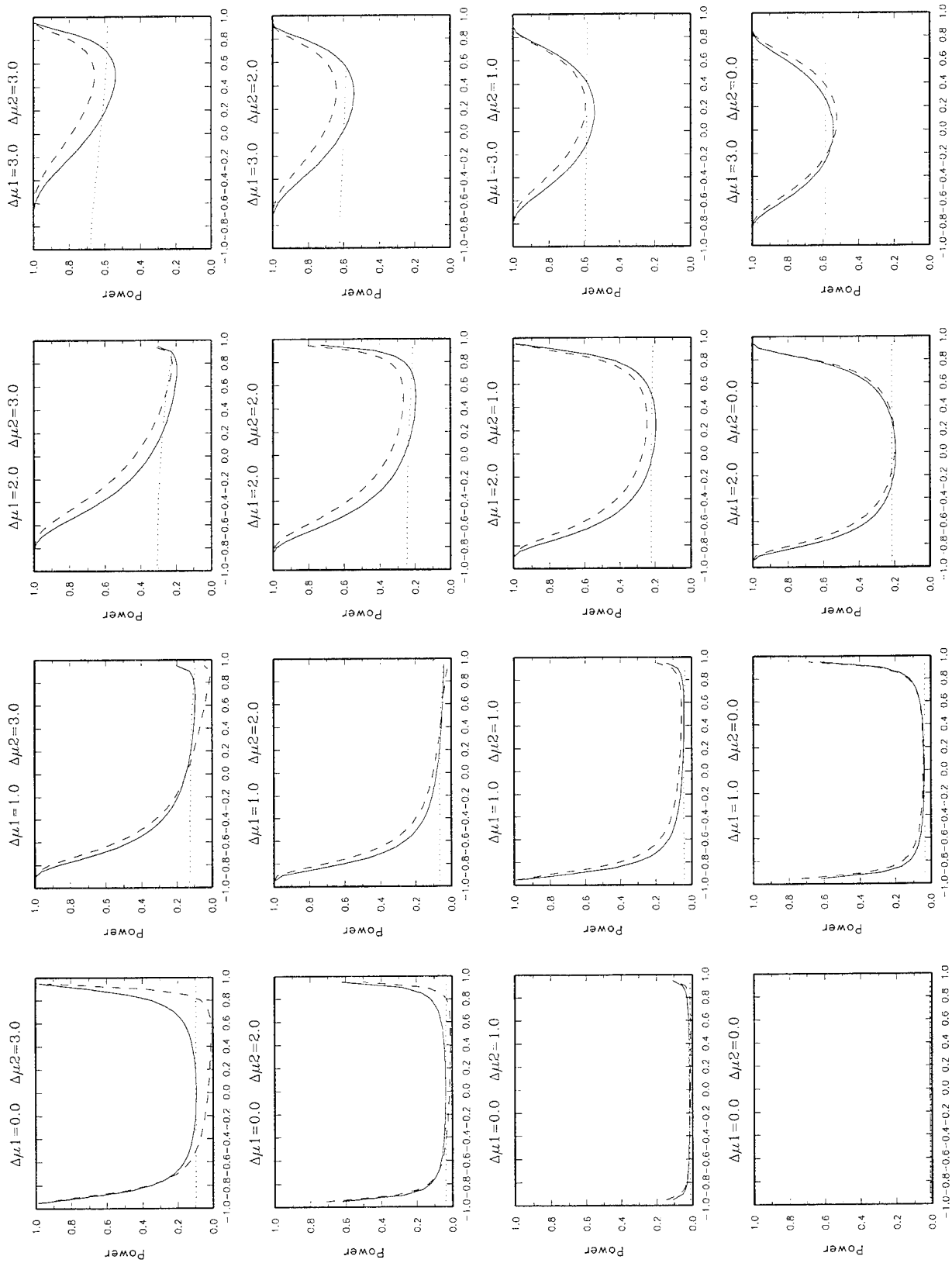


Figure 51. Same as Figure 50, except that $\sigma_2 = 2$.

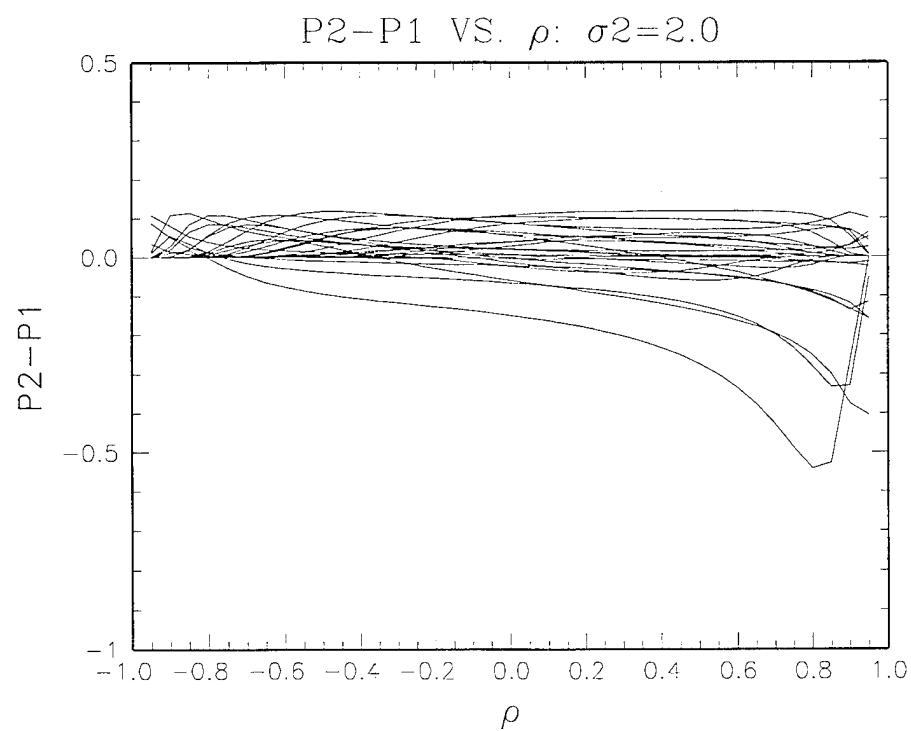
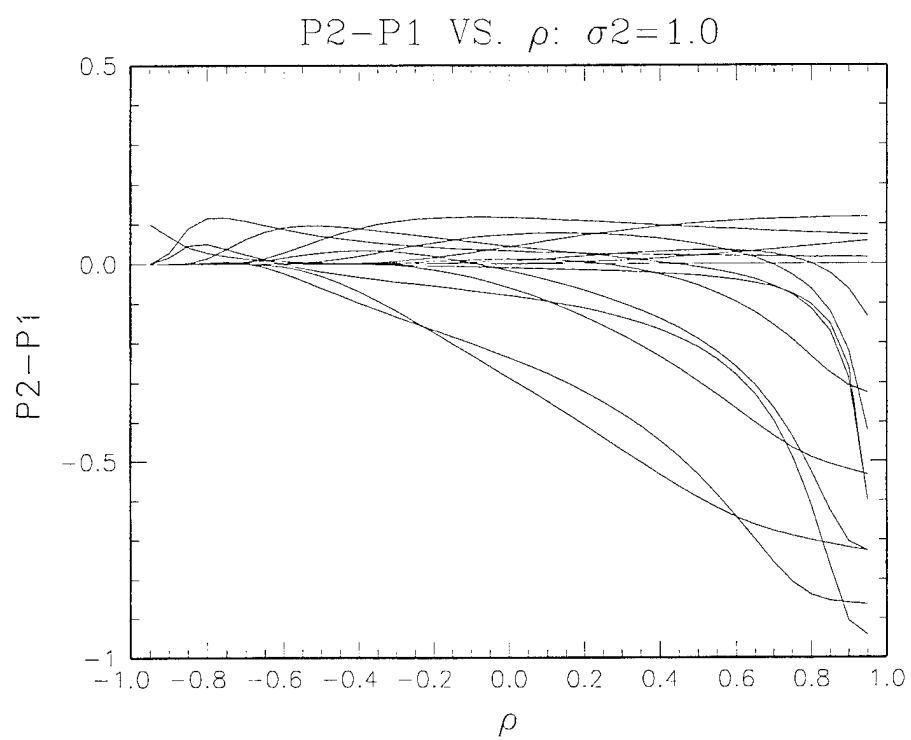


Figure 52. Difference in the power of Test 2 and Test 1 versus correlation for various values of $\Delta\mu_1$ and $\Delta\mu_2$ from 0 to 4.

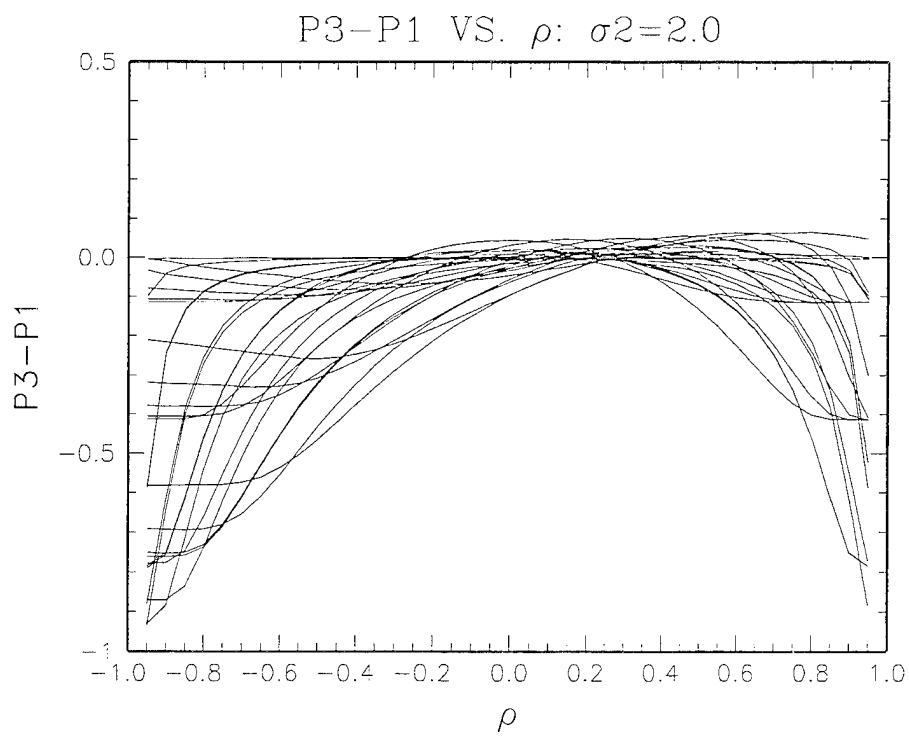
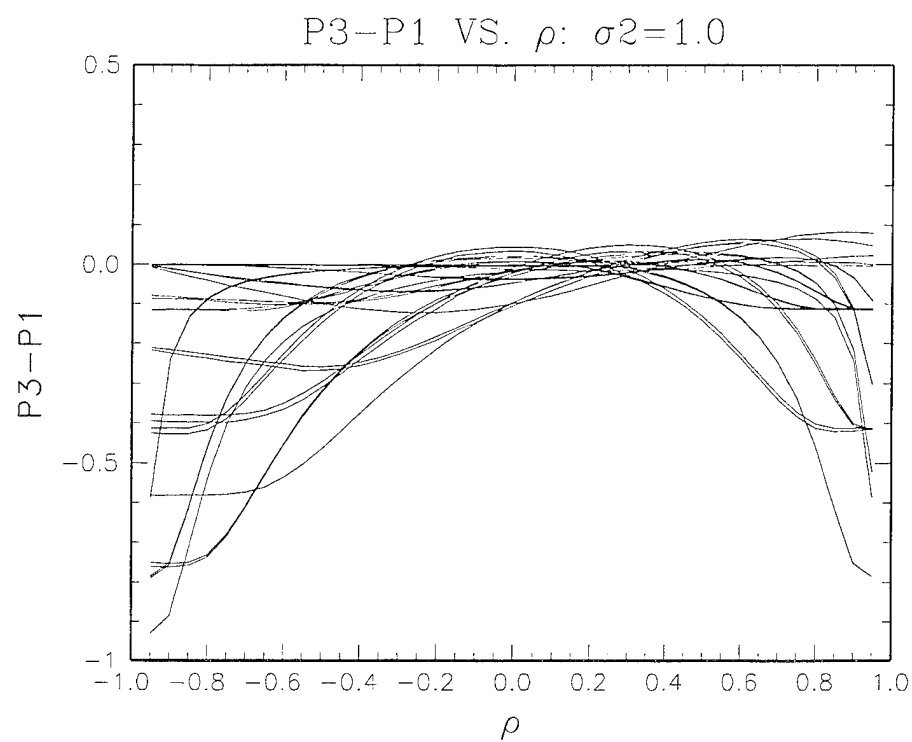


Figure 53. Difference in the power of Test 3 and Test 1 versus correlation for various values of $\Delta\mu_1$ and $\Delta\mu_2$ from 0 to 4.

Although we will eventually have a considerable amount of information from earthquake data regarding the covariance matrix, we will not know $\Delta\mu_1$ and $\Delta\mu_2$ in most situations. Hence, we will not know which of the curves in Figures 52 and 53 apply. Thus, the most robust procedure is to use Test 1 in which the full vector of discriminants is inserted into the likelihood ratio.

To illustrate how the powers of the three tests compare for a real situation, we now present results based on Pn/Lg measurements in the 6-8 Hz band at stations KNB and MNV for 35 earthquakes and 69 nuclear explosions on the Nevada Test Site. In this case, $\rho = 0.228$, $\hat{\sigma}_1 = 0.485$, $\hat{\sigma}_2 = 0.416 = 0.856\hat{\sigma}_1$, $\Delta\hat{\mu}_1 = 1.104 = 2.276\hat{\sigma}_1$, and $\Delta\hat{\mu}_2 = 1.662 = 3.427\hat{\sigma}_1$. Treating these estimates as approximately equal to the corresponding true parameter values and setting the significance level $\alpha = 0.01$, the powers of Tests 1, 2 and 3 are 0.922, 0.954 and 0.926, respectively. All three tests have comparable power in this case. However, since $\Delta\mu_1$ and $\Delta\mu_2$ are not dramatically different and the correlation is relatively small, it should be expected that Test 2 would have the greatest power.

For comparison, the power of the tests at 0.01 significance level using either one of the stations is 0.363 for KNB and 0.938 for MNV. Thus, combining data from the two stations has comparable power to using only the best station and does not require that we know which station provides greater power which, in practice, we will not know in most situations.

Thus, for cases in which we know $\Delta\mu_1$ and $\Delta\mu_2$, criteria may be established to select a particular outlier test with the highest power. Note, however, that since we have this information, we could perform a statistical classification test, which has greater power than any of these outlier tests, using fixed criteria or training data for both event types.

We now consider two final cases which are variations of Test 2. In the first, we use inverse variance weighting, rather than the minimum variance combination. In the second, we use the minimum variance combination with the further restriction that all components of a are positive. We compare the power of these tests (Tests 4 and 5, respectively) to the power of Test 2. Note that if $\sigma_1 = \sigma_2$, all three of these tests are equivalent. Hence, we set $\sigma_1 = 1$ and $\sigma_2 = 2$.

Figure 54 shows power curves for Tests 2, 4 and 5 versus correlation for various values of $\Delta\mu_1$ and $\Delta\mu_2$ from 0 to 3. Here the solid, dashed and dotted curves represent the powers of Tests 2, 4 and 5, respectively. Figure 54 illustrates that Test 2 generally has the greatest power of these three tests. Test 2 provides considerably greater power for cases in which the correlation is particularly high and $\Delta\mu_1$ is greater than $\Delta\mu_2$. Note that if the correlation is greater than $\sigma_1/\sigma_2 = 0.5$, the power of Test 5 is independent of the correlation since only the first discriminant (with the smallest variance) is being used in these cases.

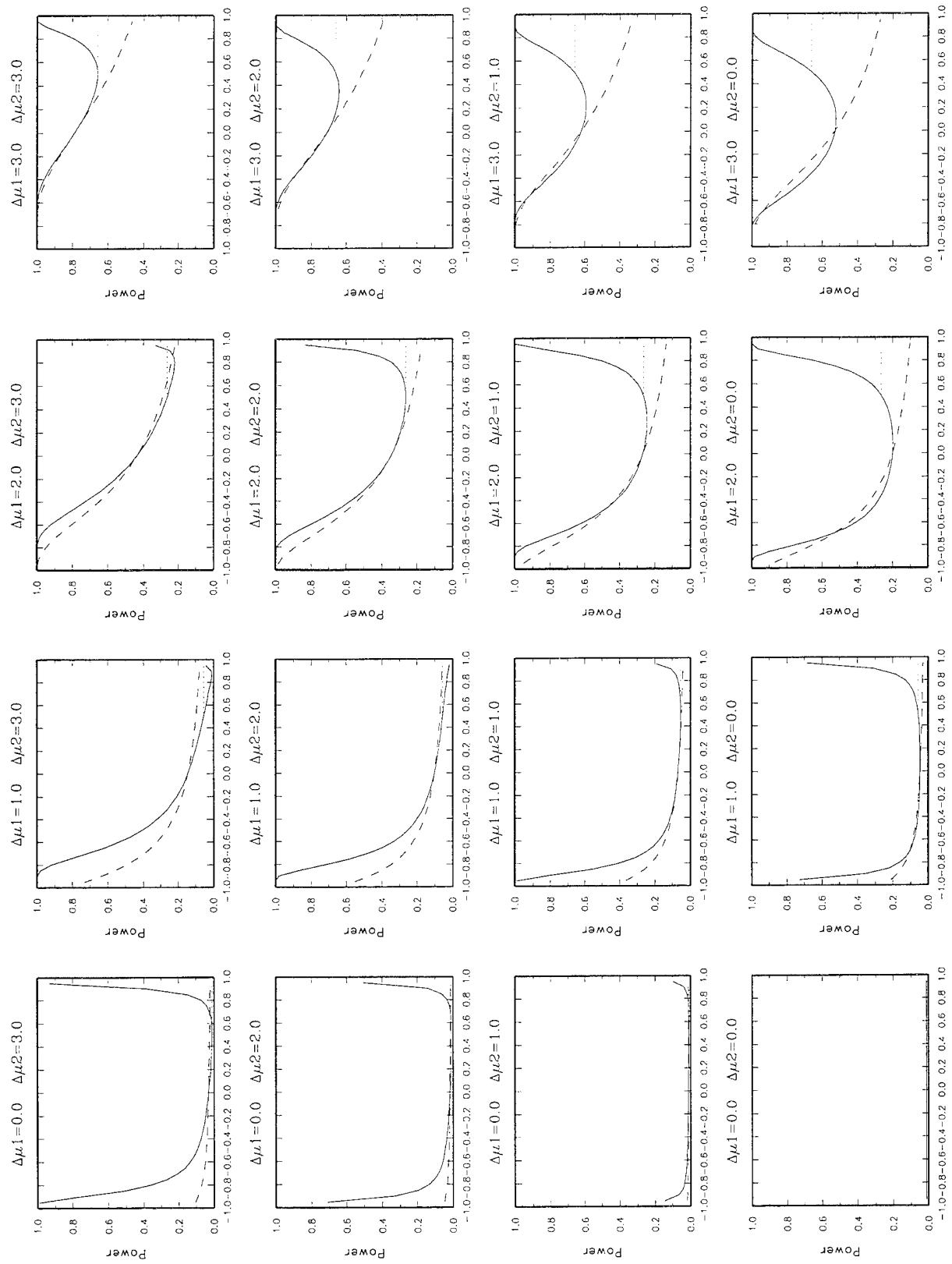


Figure 54. Power of Tests 2 (solid), 4 (dashed) and 5 (dotted) versus ρ for $\sigma_1 = 1, \sigma_2 = 2$ and various values of $\Delta\mu_1$ and $\Delta\mu_2$ from 0 to 3.

To further illustrate these points, Figure 55 shows the difference in the powers of Tests 4 and 2 versus correlation for various values of $\Delta\mu_1$ and $\Delta\mu_2$ between 0 and 4. While there are cases for which Test 4 provides a slight improvement in power over Test 2, there are many cases for which Test 4 provides dramatically poorer power, particularly if ρ is negative and large and $\Delta\mu_2$ is greater than $\Delta\mu_1$ or if ρ is positive and large and $\Delta\mu_1$ is greater than $\Delta\mu_2$. Thus, Test 2 is more robust than Test 4 under the assumptions considered.

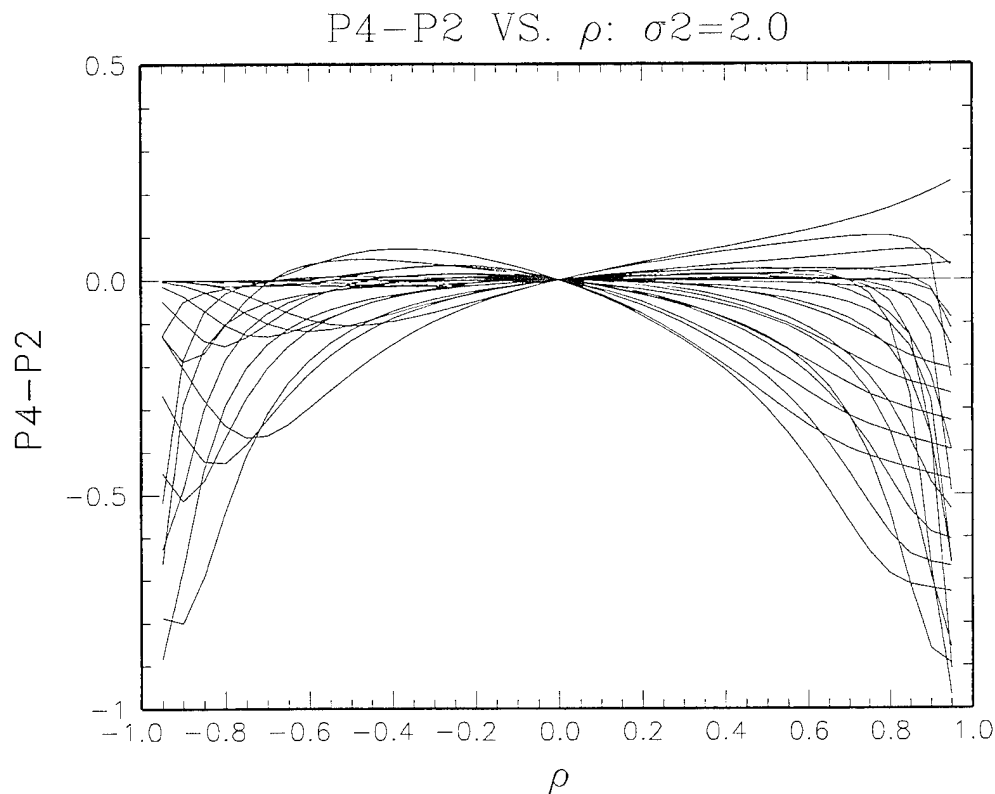


Figure 55. Difference in the power of Test 4 and Test 2 versus correlation for various values of $\Delta\mu_1$ and $\Delta\mu_2$ from 0 to 4.

Figure 56 shows a similar plot comparing the powers of Tests 5 and 2 versus correlation for various values of $\Delta\mu_1$ and $\Delta\mu_2$ between 0 and 4. Note that these two tests provide equivalent power unless the correlation is greater than $\sigma_1/\sigma_2 = 0.5$. While there are cases for which Test 5 provides greater power than Test 2, there are many cases for which Test 5 provides dramatically poorer power, particularly if ρ and $\Delta\mu_1$ (corresponding to the discriminant with the smallest variance) are large. Thus, Test 2 is also more robust than Test 5 under the assumptions considered. Hence, consideration of these two variations of Test 2 do no impact our previous conclusion that Test 1 is the most robust outlier test to use under the widest range of reasonable assumptions.

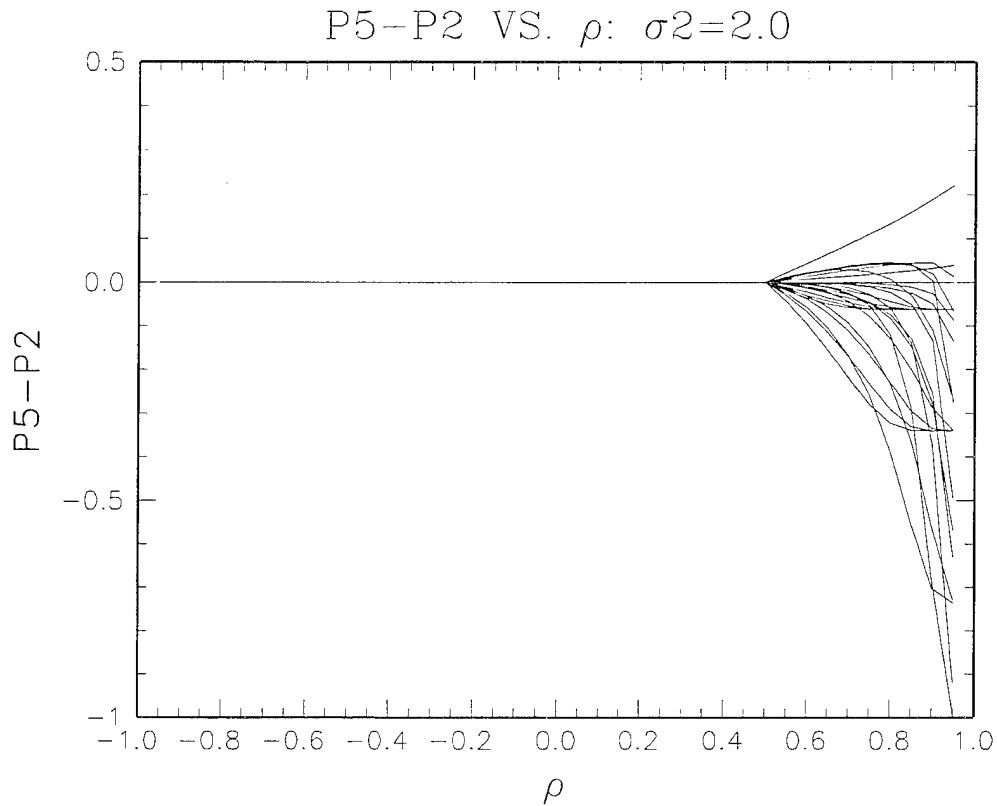


Figure 56. Difference in the power of Test 5 and Test 2 versus correlation for various values of $\Delta\mu_1$ and $\Delta\mu_2$ from 0 to 4.

4.4. Conclusions and Recommendations

In Section 4.2, we presented three outlier tests, all based on the likelihood ratio, which utilize input data in different forms. Based on the parametric study presented in Section 4.3, it is apparent that there is no single test which provides the greatest power under all conditions. In practical monitoring situations, one of three cases will apply: (1) we will know (or at least be able to estimate) all of the parameters if we have sufficient training data for both earthquakes and nuclear explosions; (2) we will know (or at least be able to estimate) the covariance matrix if we have sufficient training data for one event type (e.g., earthquakes), and we may be able to infer a range of reasonable values for $\Delta\mu_1$ and $\Delta\mu_2$ from previous experience in other similar regions; (3) we will know (or at least be able to estimate) the covariance matrix, but we will not have sufficient information regarding $\Delta\mu_1$ and $\Delta\mu_2$.

Under the first scenario, we could select the outlier test with the greatest power. Alternatively, we could perform a statistical classification test, with even greater power, using training data for both

event types. In this case, it can be shown that if the discriminant vector has a multivariate normal distribution and the covariance matrices for the earthquakes and explosions are equal, the classification test with the greatest power is based on the linear discriminant function (e.g., Anderson, 1984, p. 205) using the full vector (i.e., with no prior weighting of the discriminants).

Under the second scenario, there may be sufficient information to select the best outlier test if $\Delta\mu_1$ and $\Delta\mu_2$ can be inferred reasonably well and if $\Delta\mu_1$ is not dramatically different than $\Delta\mu_2$.

Under the third scenario, which will also be the most common, we will not know $\Delta\mu_1$, $\Delta\mu_2$ and, hence, we should use the outlier hypothesis test in the form of Test 1, using the full discriminant vector as input into the outlier likelihood ratio. The practical difficulty with using Test 1 is that unless there is a lot of data, it may be difficult to get a good estimate of the covariance matrix for cases in which we have a large number of discriminants. This limitation should become irrelevant since, after a sufficient period of time, a large earthquake database will be established with which to estimate the covariance matrix for all discriminants at all combinations of stations that will observe any regional event.

As a final note, there will generally be far more than two discriminants used in an operational setting. Although the same three monitoring scenarios still apply, the parameter space for which one outlier test is chosen over the others becomes far more complicated under the second scenario and may require substantial a priori knowledge regarding discriminant means for explosions. Thus, we recommend using Outlier Test 1 for all cases in which we do not have regional training data for nuclear explosions and we recommend using a multivariate classification test for cases in which we do.

References

- Anderson, T.W. (1984). *An Introduction to Multivariate Analysis*, Second Edition, John Wiley and Sons, Inc., New York.
- Baek, J., H.L. Gray, and W.A. Woodward (1992). A Generalized Likelihood Ratio Test in Outlier Detection or Script Matching, Technical Report, Department of Statistical Science, Southern Methodist University, Dallas, TX.
- Baumgardt, D.R. (1993). Private Communication.
- Baumgardt, D.R., J. Carney, M. Maxson and S. Carter (1992). Evaluation of Regional Discriminants using the Intelligent Seismic Event Identification System, Semi-Annual Technical Report SAS-TR-93-38, ENSCO, Inc., Springfield, VA.
- Blandford, R.R., A. Dainty, R. Lacoss, R. Maxion, A. Ryall, B. Stump, C. Thurber, and T. Wallace (1992). Report on the DARPA Seismic Identification Workshop, Center for Seismic Studies, Arlington, VA, 18-19 May 1992.
- Box, G.E.P. and D.R. Cox (1964). An Analysis of Transformations, *J. R. Stat. Soc.*, 26, 211-252.
- Carter, J. (1995). Private Communication.
- Efron, B. (1979). Bootstrap methods: another look at the jackknife, *Ann. Stat.*, 7, 1-26.
- Fisk, M.D. (1993). Event Identification Analysis of the 31 December 1992 Novaya Zemlya Event with Attenuation Corrections, MRC-R-1459, Mission Research Corp., Santa Barbara, CA.
- Fisk, M.D. and H.L. Gray (1993). Event Identification Analysis of the Novaya Zemlya Event on 31 December 1992 using Outlier and Classification Likelihood Ratio Tests, Paper in volume compiled by Ryall (1993), MRC-R-1449, Mission Research Corp., Santa Barbara, CA.
- Fisk, M.D., H.L. Gray and G.D. McCartor (1995). Regional event discrimination without transporting thresholds, submitted to *Bull. Seism. Soc. Am.*
- Fisk, M.D., H.L. Gray and G.D. McCartor (1994). Preliminary Assessment of CTBT/NPT Monitoring Capability, PL-TR-94-2300, Phillips Laboratory, Hanscom AFB, MA, ADA293188.
- Fisk, M.D., H.L. Gray and G.D. McCartor (1993). Applications of Generalized Likelihood Ratio Tests to Seismic Event Identification, PL-TR-93-2221, Phillips Laboratory, Hanscom AFB, MA, ADA279479.
- Gray, H.L., W. Woodward, M.D. Fisk and G.D. McCartor (1994). A hypothesis testing approach to discriminant analysis with mixed categorical and continuous variables when data are missing, *Paper in Proceeding of the 16th Annual Seismic Research Symposium*, 7-9 September 1994, Thornwood, NY, Phillips Laboratory, Hanscom AFB, MA, PL-TR-94-2217, ADA284667.
- IDC Performance Report - January 15-28, 1995 (February 3, 1995). Available through the Center for Monitoring Research, Arlington, VA.
- Jepsen, D. (1995). Private Communication.

- Lilwall, R.C, and A. Douglas (1985). AWRE Report O 23/84 (U.K. Atomic Weapons Research Establishment).
- North, R. (1995). GSETT-3 - Experience and Lessons Learned So Far, paper in *Proceedings of the CTBT Monitoring Technologies Conference*, 15-18 May 1995, Chantilly, VA, Sponsored by ARPA/NMRO, Arlington, VA.
- Patton, H. and W. Walter (1994). Private Communication.
- Ringdal, F. (1984). in *The VELA Program: A Twenty-Five Year Review of Basic Research* (Ed. A.U. Kerr, Executive Graphic Services), p. 611.
- Ryall, F. (1995). Private Communication.
- Sereno, T.J. (1990). Attenuation of Regional Phases in Fennoscandia and Estimates of Arrival Time and Azimuth Uncertainty using Data Recorded by Regional Arrays, SAIC-90/1472, Science Applications International Corp., San Diego, CA.
- Walter, W.R. (1995). Private Communication.
- Walter, W.R., K.M. Mayeda and H.J. Patton (1994). Phase and spectral ratio discrimination between NTS earthquakes and explosions Part I: Empirical observations, LLNL Preprint UCRL-JC-118551, submitted to *Bull. Seism. Soc. Am.*

Prof. Thomas Ahrens
Seismological Lab, 252-21
Division of Geological & Planetary Sciences
California Institute of Technology
Pasadena, CA 91125

• Prof. Keiiti Aki
Center for Earth Sciences
University of Southern California
• University Park
Los Angeles, CA 90089-0741

Prof. Shelton Alexander
Geosciences Department
403 Deike Building
The Pennsylvania State University
University Park, PA 16802

Dr. Thomas C. Bache, Jr.
Science Applications Int'l Corp.
10260 Campus Point Drive
San Diego, CA 92121 (2 copies)

Prof. Muawia Barazangi
Cornell University
Institute for the Study of the Continent
3126 SNEE Hall
Ithaca, NY 14853

Dr. Douglas R. Baumgardt
ENSCO, Inc
5400 Port Royal Road
Springfield, VA 22151-2388

Dr. T.J. Bennett
S-CUBED
A Division of Maxwell Laboratories
11800 Sunrise Valley Drive, Suite 1212
Reston, VA 22091

Dr. Robert Blandford
AFTAC/TT, Center for Seismic Studies
1300 North 17th Street
Suite 1450
Arlington, VA 22209-2308

• Dr. Stephen Bratt
• ARPA/NMRO
• 3701 North Fairfax Drive
Arlington, VA 22203-1714

Mr. Dale Breeding
Sandia National Laboratories
Organization 9236, MS 0655
Albuquerque, NM 87185

Dr. Jerry Carter
Center for Seismic Studies
1300 North 17th Street
Suite 1450
Arlington, VA 22209-2308

Mr Robert Cockerham
Arms Control & Disarmament Agency
320 21st Street North West
Room 5741
Washington, DC 20451,

Dr. Zoltan Der
ENSCO, Inc.
5400 Port Royal Road
Springfield, VA 22151-2388

Dr. Stanley K. Dickinson
AFOSR/NM
110 Duncan Avenue
Suite B115
Bolling AFB, DC 20332-6448

Dr. Petr Firbas
Institute of Physics of the Earth
Masaryk University Brno
Jecna 29a
612 46 Brno, Czech Republic

Dr. Mark D. Fisk
Mission Research Corporation
735 State Street
P.O. Drawer 719
Santa Barbara, CA 93102

Dr. Cliff Frolich
Institute of Geophysics
8701 North Mopac
Austin, TX 78759

Dr. Holly Given
IGPP, A-025
Scripps Institute of Oceanography
University of California, San Diego
La Jolla, CA 92093

Dr. Jeffrey W. Given
SAIC
10260 Campus Point Drive
San Diego, CA 92121

Dan N. Hagedorn
Pacific Northwest Laboratories
Battelle Boulevard
Richland, WA 99352

Dr. James Hannon
Lawrence Livermore National Laboratory
P.O. Box 808, L-205
Livermore, CA 94550

Dr. Roger Hansen
University of Colorado, JSPC
Campus Box 583
Boulder, CO 80309

Prof. David G. Harkrider
Phillips Laboratory
Earth Sciences Division, PL/GPE
29 Randolph Road
Hanscom AFB, MA 01731-3010

Prof. Danny Harvey
University of Colorado, JSPC
Campus Box 583
Boulder, CO 80309

Prof. Donald V. Helmberger
Division of Geological & Planetary Sciences
California Institute of Technology
Pasadena, CA 91125

Prof. Eugene Herrin
Geophysical Laboratory
Southern Methodist University
Dallas, TX 75275

Prof. Robert B. Herrmann
Department of Earth & Atmospheric Sciences
St. Louis University
St. Louis, MO 63156

Prof. Lane R. Johnson
Seismographic Station
University of California
Berkeley, CA 94720

Prof. Thomas H. Jordan
Department of Earth, Atmospheric &
Planetary Sciences
Massachusetts Institute of Technology
Cambridge, MA 02139

Mr. Robert C. Kemerait
ENSCO, Inc.
445 Pineda Court
Melbourne, FL 32940

U.S. Dept of Energy
Max Koontz, NN-20, GA-033
Office of Research and Develop.
1000 Independence Avenue
Washington, DC 20585

Dr. Richard LaCoss
MIT Lincoln Laboratory, M-200B
P.O. Box 73
Lexington, MA 02173-0073

Prof. Charles A. Langston
Geosciences Department
403 Deike Building
The Pennsylvania State University
University Park, PA 16802

Jim Lawson, Chief Geophysicist
Oklahoma Geological Survey
Oklahoma Geophysical Observatory
P.O. Box 8
Leonard, OK 74043-0008

Prof. Thorne Lay
Institute of Tectonics
Earth Science Board
University of California, Santa Cruz
Santa Cruz, CA 95064

Dr. William Leith
U.S. Geological Survey
Mail Stop 928
Reston, VA 22092

Mr. James F. Lewkowicz
Phillips Laboratory/GPE
29 Randolph Road
Hanscom AFB, MA 01731-3010(2 copies)

Dr. Gary McCartor
Department of Physics
Southern Methodist University
Dallas, TX 75275

Prof. Thomas V. McEvelly
Seismographic Station
University of California
Berkeley, CA 94720

Dr. Keith L. McLaughlin
S-CUBED
A Division of Maxwell Laboratory
P.O. Box 1620
La Jolla, CA 92038-1620

Prof. Bernard Minster
IGPP, A-025
Scripps Institute of Oceanography
University of California, San Diego
La Jolla, CA 92093

Prof. Brian J. Mitchell
Department of Earth & Atmospheric Sciences
St. Louis University
St. Louis, MO 63156

Mr. Jack Murphy
S-CUBED
A Division of Maxwell Laboratory
11800 Sunrise Valley Drive, Suite 1212
Reston, VA 22091 (2 Copies)

Dr. Keith K. Nakanishi
Lawrence Livermore National Laboratory
L-025
P.O. Box 808
Livermore, CA 94550

Prof. John A. Orcutt
IGPP, A-025
Scripps Institute of Oceanography
University of California, San Diego
La Jolla, CA 92093

Dr. Howard Patton
Lawrence Livermore National Laboratory
L-025
P.O. Box 808
Livermore, CA 94550

Dr. Frank Pilotte
HQ AFTAC/TT
1030 South Highway A1A
Patrick AFB, FL 32925-3002

Dr. Jay J. Pulli
Radix Systems, Inc.
6 Taft Court
Rockville, MD 20850

Prof. Paul G. Richards
Lamont-Doherty Earth Observatory
of Columbia University
Palisades, NY 10964

Mr. Wilmer Rivers
Teledyne Geotech
1300 17th St N #1450
Arlington, VA 22209-3803

Dr. Alan S. Ryall, Jr.
Lawrence Livermore National Laboratory
P.O. Box 808, L-205
Livermore, CA 94550

Dr. Chandan K. Saikia
Woodward Clyde- Consultants
566 El Dorado Street
Pasadena, CA 91101

Mr. Dogan Seber
Cornell University
Inst. for the Study of the Continent
3130 SNEE Hall
Ithaca, NY 14853-1504

Secretary of the Air Force
(SAFRD)
Washington, DC 20330

Office of the Secretary of Defense
DDR&E
Washington, DC 20330

Thomas J. Sereno, Jr.
Science Application Int'l Corp.
10260 Campus Point Drive
San Diego, CA 92121

Dr. Michael Shore
Defense Nuclear Agency/SPSS
6801 Telegraph Road
Alexandria, VA 22310

Prof. David G. Simpson
IRIS, Inc.
1616 North Fort Myer Drive
Suite 1050
Arlington, VA 22209

Dr. Jeffrey Stevens
S-CUBED
A Division of Maxwell Laboratory
P.O. Box 1620
La Jolla, CA 92038-1620

Prof. Brian Stump
Los Alamos National Laboratory
EES-3
Mail Stop C-335
Los Alamos, NM 87545

Prof. Tuncay Taymaz
Istanbul Technical University
Dept. of Geophysical Engineering
Mining Faculty
Maslak-80626, Istanbul Turkey

Prof. M. Nafi Toksoz
Earth Resources Lab
Massachusetts Institute of Technology
42 Carleton Street
Cambridge, MA 02142

Dr. Larry Turnbull
CIA-OSWR/NED
Washington, DC 20505

Dr. Karl Veith
EG&G
2341 Jefferson Davis Highway
Suite 801
Arlington, VA 22202-3809

Prof. Terry C. Wallace
Department of Geosciences
Building #77
University of Arizona
Tucson, AZ 85721

Dr. William Wortman
Mission Research Corporation
8560 Cinderbed Road
Suite 700
Newington, VA 22122

ARPA, OASB/Library
3701 North Fairfax Drive
Arlington, VA 22203-1714

HQ DNA
ATTN: Technical Library
Washington, DC 20305

Defense Technical Information Center
8725 John J. Kingman Road
Ft Belvoir, VA 22060-6218
(2 copies)

TACTEC
Battelle Memorial Institute
505 King Avenue
Columbus, OH 43201 (Final Report)

Phillips Laboratory
ATTN: GPE
29 Randolph Road
Hanscom AFB, MA 01731-3010

Phillips Laboratory
ATTN: TSML
5 Wright Street
Hanscom AFB, MA 01731-3004

Phillips Laboratory
ATTN: PL/SUL
3550 Aberdeen Ave SE
Kirtland, NM 87117-5776 (2 copies)

Dr. Michel Campillo
Observatoire de Grenoble
I.R.I.G.M.-B.P. 53
38041 Grenoble, FRANCE

Dr. Kin Yip Chun
Geophysics Division
Physics Department
University of Toronto
Ontario, CANADA

Prof. Hans-Peter Harjes
Institute for Geophysics
Ruhr University/Bochum
P.O. Box 102148
4630 Bochum 1, GERMANY

Prof. Eystein Husebye
IFJF
Jordskjelvstasjonen
Allegaten, 5007 BERGEN NORWAY

David Jepsen
Acting Head, Nuclear Monitoring Section
Bureau of Mineral Resources
Geology and Geophysics
G.P.O. Box 378, Canberra, AUSTRALIA

Ms. Eva Johannisson
Senior Research Officer
FOA
S-172 90 Sundbyberg, SWEDEN

Dr. Peter Marshall
Procurement Executive
Ministry of Defense
Blacknest, Brimpton
Reading FG7-FRS, UNITED KINGDOM

Dr. Bernard Massinon, Dr. Pierre Mechler
Societe Radiomana
27 rue Claude Bernard
75005 Paris, FRANCE (2 Copies)

Dr. Svein Mykkeltveit
NTNT/NORSAR
P.O. Box 51
N-2007 Kjeller, NORWAY (3 Copies)

Dr. Jorg Schlittenhardt
Federal Institute for Geosciences & Nat'l Res.
Postfach 510153
D-30631 Hannover , GERMANY

Dr. Johannes Schweitzer
Institute of Geophysics
Ruhr University/Bochum
P.O. Box 1102148
4360 Bochum 1, GERMANY

Trust & Verify
VERTIC
Carrara House
20 Embankment Place
London WC2N 6NN, ENGLAND